Optical Analysis of Characteristics of Rape-seed Oil Diesel Spray Applied to Direct Injection Diesel Engine

A thesis submitted in fulfillment of the
requirement for the award of the degree of
Doctor of Engineering

The University of Tokushima
Graduate School of Advanced Technology and Science
Department of Ecosystem Engineering

Azwan Bin Sapit

September 2013

Table of Contents

Nomenclature

Acronyms

ASAE : American Society of Agricultural Engineers

aSOI : after start of injection

ATDC : after top dead center

BTDC : before top dead center

CA : crank angle

CARB : California Air Resources Board

CO : carbon monoxide

CO_2 : carbon dioxide

DI : Direct Injection

FAME : Fatty-acid methyl ester

GO: Gas Oil (Diesel Fuel)

HC : hydrocarbon

HSDI : High Speed Diesel Engine

IDI : Indirect Injection

N_2: nitrogen

NOx : nitrogen oxides

O_2: oxygen

OPEC : Organization of the Petroleum Exporting Countries

PAHs : Polycyclic aromatic hydrocarbons

pdf : probility density fuction

PM : particulate matter

RO : Rapeseed Oil

SOF : soluble organic fraction

SVO : Straight Vegetable Oil

Chapter 1 Research Background

1.1 Introduction

After the 1973 oil embargo, the non-renewable nature and limited resources of petroleum fuels become a matter of great concern. The present source of fuels used in internal combustion engines is expected to be depleted in the near future, especially if the consumption rate increases yearly. It has become very important to study the alternative sources of fuel because of the concern over the availability and the price of petroleum based fuels.

Furthermore, 1997 Kyoto World Climatic Changes Conference directives have been issued with the aim of reducing by 5% by 2010 of the emission in the atmosphere of "greenhouse" gases from 1990 levels. This is important because, in considering the actual tendencies of growth, the real reduction corresponds to more than 25%. Thus, to make sure that the target is achieved, further reduction of CO_2 emission from automobile is required. Diesel engines are advantages for CO_2 emission and fuel diversity. All these aspects have drawn the attention to conserve and stretch the oil reserve, and at the same time to reduce the emission level from current engine; by the way of alternative fuel research.

Biomass fuel are mainly derived from biomass or bio waste such as a vegetable oil or animal fat-based diesel fuel. Besides being renewable and biodegradable, they have characteristics quite similar to those of a common diesel fuel. They contain no sulphur elements and are regarded as no contribution to the accumulation of CO_2 in the atmosphere. However, actual practice in the biomass as fuel for diesel engines is subjected to transesterification process. This is because carbon deposit, for instance, are produced by direct use of biomass fuel in DI (direct injection) diesel engines. The carbon deposit causes harmful damage to engines and unfavorable effects on engine durability. Blending biomass with practical fuel can partly solve the problem. On the other hand, it is still desirable to use neat biomass fuel to DI diesel engine without transesterification or blending.

As for fuel characteristics, it is widely known that biomass fuel has high level of kinematic viscosity and high distillation temperature, and it is oxygenated fuel. Numerous works proved that biomass fuel increases NOx emissions in many diesel engines. When using biomass fuel, particulate emissions decreases at heavy load due to oxygenated nature; in contrast, SOF (soluble organic fraction) emissions increases at light load operation. High viscosity of biomass fuel results in resistance of fuel flow during fuel injection, affecting the spray development and, in the end, affects the atomization process. SOF emissions is caused

partly by poor atomization and SOF emissions is supposed to be one of source of carbon deposit. Other problems concerning biomass fuel include oxidation and storage stability, a tendency to form deposits, corrosion issues, cold flow problems and questionable stability from diverse feed stocks.

One of the important strategies for low emission diesel engine is to control the combustion process. Precise control of the fuel injection, spray atomization and fuel-air mixing are among the fundamental factors that control the combustion and emission formation. It is reported that application of high-pressure injection and high ambient temperature could promote better spray atomization and fuel-air mixing. These strategies should be also applied to direct use of biomass fuel.

In this study, the spray characteristics of diesel and rape-seed oil (as a biomass fuel) including microscopic spray structure and spray development, fuel evaporation, and droplets atomization is studied by optical technique. Other parameters such as liquid and vapor phase distribution and droplet dynamic behavior were also studied. The optical technique used reveals macro-scale and micro-scale spray structures and proven to be successfully implemented in this study.

1.2 History of Diesel Engine and Internal Combustion Engine

Diesel engine (also known as compression ignition engine) is considered an internal combustion engine by the way it operates. It often compared to the more widely known gasoline fueled spark ignition engine which seem similar in design but operates differently. This section will try to convey a short history on important internal combustion engine advancement and diesel engine place on the timeline. In addition, steam engine will also be noted as its application and wide spread was significant, before the era of internal combustion engine.

Although not technically considered an internal combustion engine, steam-powered engine was very popular and has a long history. Since the early 18th century, steam power has been applied to a variety of practical uses. At first it was applied to reciprocating pumps, but from the 1780s rotative engines began to appear, driving factory machinery such as spinning mules and power looms. At the turn of the 19th century, steam-powered transport on both sea and land began to make its appearance becoming ever more dominant as the century progressed. During the late 1890s and early 1900s, it also becomes widely used in automobile.

In contrast to steam engine, the first person to experiment with an internal-

combustion engine was the Dutch physicist Christiaan Huygens, about 1680. But only in 1860, Jean Joseph Étienne Lenoir develop the first single-cylinder two-stroke engine which burnt a mixture of coal gas and air. Although it ran reasonably well, the engine was fuel inefficient, extremely noisy, tend to overheat and, if sufficient cooling water was not applied, seize up. During the next decade, several hundred of similar internal combustion engine were built with the power up to 4.5 kW and mechanical efficiency up to 5%. In 1876, using previous experience of making 2 stroke engine by improving on Étienne Lenoir engine, Nikolaus A. Otto with the help of Eugen Langen built a successful four-stroke engine inspired by the Alphonse Beau de Rochas which had patented the design in 1862 without actually building the engine. This four-stroke engine with an electrical spark ignition became known as the Otto cycle; although many other people are working on four stroke design, Otto was given the credit due to his prototype engine. This was the first commercially successful engine to use in-cylinder compression. Otto`s engine was practicable and fairly reliable compared to other earlier attempts, and become a financial success.

However, at that time, Otto's engine was design to run on gas (coal gas) rather than liquid fuel. Around the same time, George Bryan manages to build an engine using liquid fuel (kerosene and petroleum) and heated surface carburetor thus eliminating the need for a gas supply system. Since the successful effort of Otto's engine and the known possibility that such engine can use liquid fuel, other people make their own version and contribute to the advancement of internal combustion engine. Notable people are, Dugald Clark for his two-stroke engine and Karl Benz for developing gasoline powered automobile. Also, Herbert Akroyd-Stuart, which use kerosene with a pressurize fuel injection system, similar to the modern diesel but with low compression ratio and needing a heat plug (also known as hot bulb engine). The discovery of crude oil in 1859 which later evolved to be the fuel of 20th century also significantly influence the advancement in which it provide the availability of reliable fuel for the internal combustion engine.

Rudolph Diesel, a mechanical engineer himself with experience in engine design; out of a desire to improve upon inefficient, cumbersome and sometimes dangerous steam engines of the late 1800s, developed the idea of the diesel engine and thought up the principle of its operation[1]. The diesel engine works on the principal of compression ignition, in which fuel is injected into the engine’s cylinder after air has been compressed to a high pressure and temperature. As the fuel enters the cylinder it self-ignites and burns rapidly, forcing the piston back down and converting the chemical energy in the fuel into

mechanical energy. This is fundamentally different to the gasoline engine where the intake mixture of fuel and air need to be ignite by an ignition source, although it use the same four-stroke cycle. Also, it has a significant advantage of being more efficient when compared to steam engine and gasoline engine.

In 1892, Rudolph Diesel filed a patent in the patent office in Germany for his method and design for the combustion engine. And in the year 1893, that he was successful in putting out the first model that was able to run with its own power, with double the efficiency of the steam engines of that time. An upgraded version with better efficiency was later made in 1986. Starting from 1898, diesel engines were made commercial and used to power pipelines, electric and water plants, automobiles and trucks, and marine craft. They were also used in mines, oil fields, factories, and transoceanic shipping.

1.3 Diesel Engine Applications and Emission Standard

There are two classes of diesel engines: two-stroke and four-stroke. Most diesel engines generally use the four-stroke cycle, with some larger engines operating on the two-stroke cycle. Normally, banks of cylinders are used in multiples of two, though any number of cylinders can be used as long as the load on the crankshaft is counterbalanced to prevent excessive vibration.

High-speed diesel engines are used to power tractors, trucks, yachts, buses, cars, compressors, generators and pumps .The vast majority of modern heavy road vehicles like trucks and buses, ships, long-distance trains, and most farm and mining vehicles have diesel engines. Modern diesel engines have come a long way equipped with up-to-date technology and one would be hard-pressed to notice a difference between diesel and gasoline engines. Diesel engines also used to power ship. These diesel engines are very big, usually have low to medium speed, with some of them have power outputs up to 90,000 kW, turn at about 60 to 100 rpm, and are 15 meters tall.

A few airplanes have been using diesel engines since the late 1930s. The newer automotive diesel engines have power-weight ratios comparable to the ancient spark-ignition designs and have far superior fuel efficiency. Their use of electronic ignition, fuel injection, and sophisticated engine management systems also makes them far easier to operate than mass-produced spark-ignition aircraft engines. The cost of diesel fuel compared to petrol has led to considerable interest in diesel-powered small general aviation planes.

The mining and mineral extraction sector worldwide relies heavily on diesel power

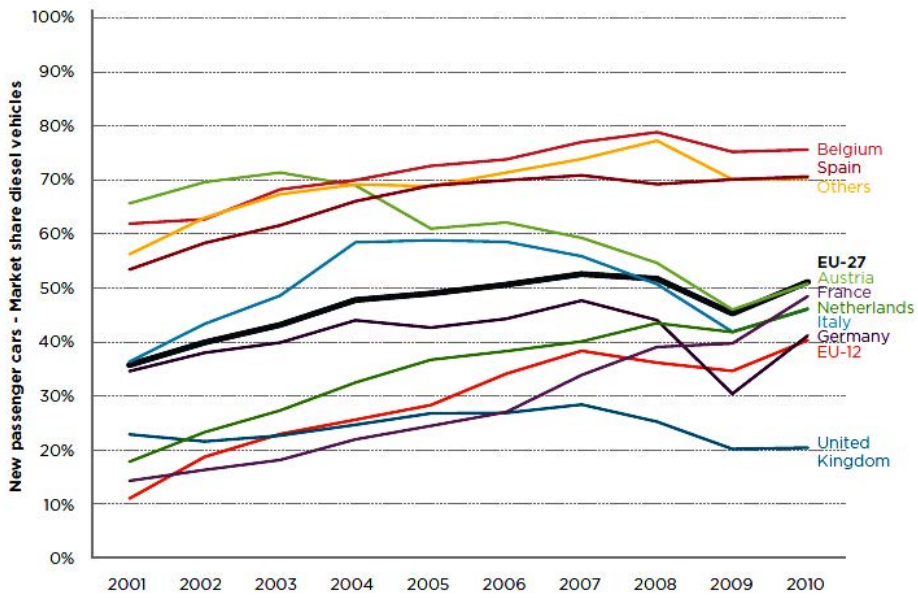

Fig.1-1 Market share of diesel vehicle in Europe by members state[2]

to harness natural resources such as aggregates, precious metals, iron ore, oil, gas, and coal. Diesel-powered shovels and drills excavate these products and load them into enormous mining trucks or onto conveyer belts that also operate on the same fuel. Overall, diesel accounts for 72 percent of the energy used by the mining sector. Both surface and underground mining operations rely on diesel-powered equipment to extract materials and load trucks. The largest rubber-tired, diesel-powered equipment used in mining are enormous off-road trucks with engines of over 2,500 horsepower, capable of hauling over 300 tons per load. These giant trucks are a sight to behold.

Diesel engine also used as electric power generator in required sectors and industries. For example, emergency backup generators are a must have for any major medical healthcare facilities. Due to the critical nature of the work these facilities do and the position their patients are in, power failures are simply not an option. Data center also a good example where these diesel electric power generators are being used. Computers are at the heart of today's industry. When servers and systems go down, communications can be lost, business stops, data is lost, workers sit idle, and just about everything comes to a halt. It is for that reason that almost all communications and telecommunications companies of all shapes turn to diesel generators as their primary backup power option.

Fig.1-1 shows market share of car powered by diesel engine in European state[2]. It can be seen that diesel car has on average 50% of the European market. This is very high when compared to other countries. For comparison, in United State of America, diesel car has about 1% market share. There are many reasons for difference in market share between

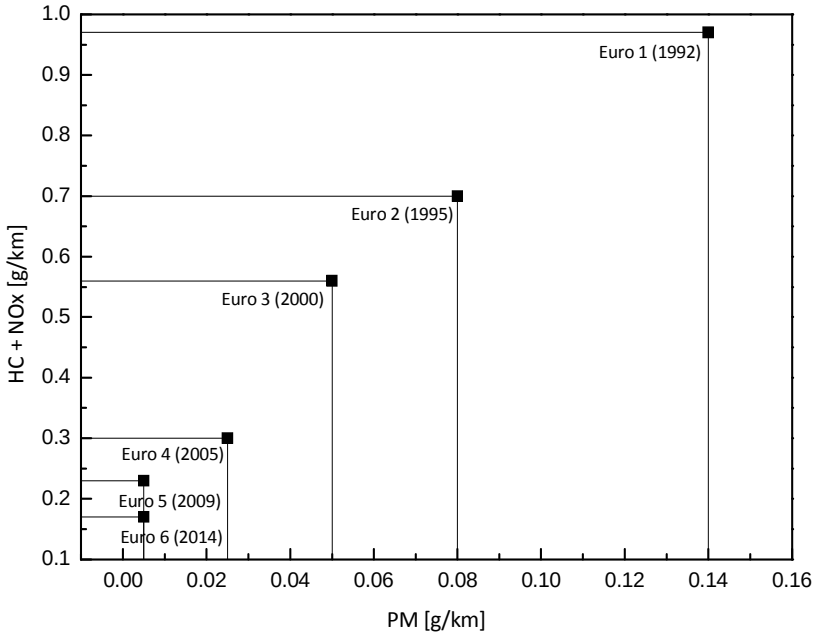

Fig.1-2 Progression of European air emission standard for diesel car[3]

countries. Fuel price and taxes, refueling installation (fuel station), subsidies from government are some factors that influence the adaption rate and market share. Even without government encouragement, trend show steady increase of market share for diesel car. This maybe related to the demand of low fuel consumption car. In addition, current diesel car is on par with petrol car when compared to the noise and exhaust emission level, and the negative image of the old engine diesel had subside.

Due to the wide-spread and diverse usage of diesel engine, emission standard was established to control the pollution due to diesel engine emission. In practice, some of the more influential emission standards are set by California Air Resources Board, known locally by its acronym "CARB" and another one set by the European Union directive known as European emission standard. Other countries tend to use these emission standards as reference and then develop and enforce their own.

Fig.1-2 shows the progression of European air emission standard requirement[3]. It can be seen clearly from the figure that with each iteration, the requirement becomes stricter. NOx combined with HC emission was reduced to 0.17g/km for Euro 6 from 0.97g/km for Euro 1 standard. The same significant reduction for PM requirement also can be observed; from 0.14g/km to 0.005g/km. This indicates that current diesel engine emission has to improve even more to meet the future air standard requirement. This made research on improvement of diesel engine in every aspect is essential; not only limited in area that directly contribute to emission reduction, but the overall efficiency of diesel engine as it will

eventually has a positive effect to emission.

1.4 Pollution Formation in Diesel Engine

As world population grew, pollution from internal combustion engine becomes a significant problem. Generally, location with large population density that retains many factories and large number of automobile has a significantly higher pollution level. It was recognized that the automobile was one of the major contributors to the problem. By 1960s, emission standards were beginning to be enforced starting in California. During the next decades, emission standard were adopted in the rest of the United States, also in Europe and in Japan. This shows that more fuel-efficient and close to zero pollution engine is needed. This chapter will try to shortly encompass the pollution formation in diesel engine.

The exhaust from diesel engine contains particulate matter (PM), oxides of nitrogen (NO and NO_2, collectively known as NOx), unburned hydrocarbon (UHC), and carbon monoxide (CO). Diesel engine is known as an important source of particulate emission. NOx emission is comparable to gasoline engine and the hydrocarbon emission is relatively lower as they operate with an overall fuel-lean equivalence ratio, around one-fifth to that of gasoline engine. However, diesel engine is not a significant source of CO[4].

NOx and PM are the two primary pollutants of the diesel engine. NO_2 has strong capacity to absorb infrared rays and is about 250 times more threatening to global warming than CO2. NOx destroys the ozone layer in the stratosphere, forms nitric acid and help forms acid rains. It irritates the eyes, throat and respiratory system. NOx react with ammonia, moisture, and other compounds to form small particles. These small particles penetrate deeply into sensitive parts of the lungs and can cause or worsen respiratory disease, such as emphysema and bronchitis, and can aggravate existing heart disease, leading to increased hospital admissions and premature death.

Increased ambient PM has been linked to observed increases in adverse cardiovascular and respiratory health events. In addition to the adverse respiratory effects, the cardiovascular effects of air pollution are particularly alarming because of the associated high mortality[5]. Particulate air pollution specifically has been shown to triple chronic cough and nocturnal cough in Swiss children living in communities with the highest PM_{10} levels compared with those children living in the least exposed areas[6]. Similarly, a large study of 6 US studies demonstrated a 3-fold increase in chronic cough with increased exposure to particulate pollution[7]. There is also study that link PM to allergy reactions[8].

1.4.1 Nitrogen Oxides

NOx is created mostly from the nitrogen in the air. Nitrogen can also be found in fuel blends, which may contain trace amount of NH3, NC and HCN. Thermal, fuel and prompt are the three basically recognized mechanisms for NOx formation. NOx produced due to the reaction of atmospheric oxygen and nitrogen at elevated temperatures is termed as thermal NOx[9].

For thermal NO formation, it is generally accepted that in combustion of near-stoichiometric fuel-air mixtures the principal reactions governing the formation of NO from molecular nitrogen are:

$$O + N2 \rightarrow NO + N$$

$$N + O2 \rightarrow NO + O$$

$$N + OH \rightarrow NO + H$$

This is often called the Zeldovich mechanism. NO formation rate has strong dependence on temperature in the exponential terms. High temperature and high oxygen concentration results in high NO formation rates.

Prompt NO that is generates in fuel-rich mixture, and has weak dependence on temperature. Fuel NO which is generated by oxidizing the nitrogen-containing compounds in fuel also source of NO, though the current levels of nitrogen in diesel fuel are not significant.

In contrast, NO_2 can be 10-30% of the total exhaust oxides of nitrogen emissions. NO formed in the flame zone can be rapidly converted to NO_2 via reaction such as

$$NO + HO_2 \rightarrow NO_2 + OH$$

Subsequently, conversion of this NO2 to NO occurs via

$$NO_2 + O \rightarrow NO + O_2$$

This is true unless the NO_2 formed in the flame is quenched by the mixing with cooler fluid. This explanation is consistence with the highest NO_2/NO ratio occurring at the light load in diesel engine, when cooler regions which quench the conversion back to NO is widespread.

1.4.2 Diesel Particulates

Soot particles are cluster of solid carbon spheres. These spheres have diameters from 10 nm to 80 nm, with most are within the range of 15-30 nm. The spheres are solid carbon with HC and traces of other components absorbed on the surface. [4].

Soot forms in the fuel-rich regions of the diffusion flames and the fuel-rich premixed flames. Highest soot concentrations are found in the core region of each fuel spray where

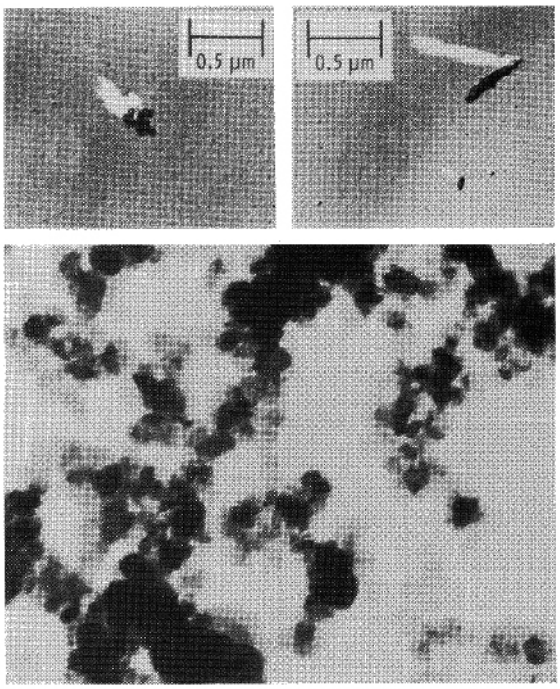

Fig.1-3 Photomicrograph of diesel particulate; cluster (upper left), chain (upper right), collection from filter (lower)[10]

local equivalence ratios are very rich. Generally, maximum density of particulate emissions occurs when the engine is under load at wide open throttle. Fig.1-3 shows samples of diesel particulates matter[10].

The formation of particulates matter in diesel engine is not fully understood but extensive research of many researcher suggested that the mechanism can be summarized as per shown in Fig.1-4[10] .

a) Thermal decomposition of fuel

In the pyrolysis zone (where fuel can not be oxidized completely due to the lack of air), an amount of decomposed species of various kinds may be formed. Analysis of these species includes various hydrocarbons such as C2H4, C2H2 and CH4.

b) Nucleation

Nucleation has been recognized as being a crucial step in the soot formation. Among the decomposed products, acetylene and its higher analogues, and polycyclic aromatic hydrocarbons (PAHs) are considered the most likely precursors of soot. In flames PAHs are most likely substance of nucleus. They play a significant role as the nuclei, either in liquid drops or in the solid form after dehydrogenated in he hotter zones.

c) Growth and Coagulation

Particle growth includes surface growth, coagulation, and aggregation. Surface growth, by which the bulk of the solid-phase material is generated, involves the attachment

of gas-phase species to the surface of the particles and their incorporation into the particulate phase. Other than PAHs and polyacetylene themselves, saturate and unsaturated carbonaceous gases might be substances for growth. Once surface growth stops, continued aggregation of particles into chains and clusters can occurs.

d) Oxidation

At each stage of soot formation, oxidation can occur and soot or soot precursors are burned in the presence of oxidizing species. The eventual emission of the soot from the engine depends on the balance between these process formation and burnout. Since the rate of the soot oxidation decreases with decrease in temperature, quenching of a soot-containing gas will hinder soot oxidation. Unoxidized soot particles are then expelled outside in frozen state.

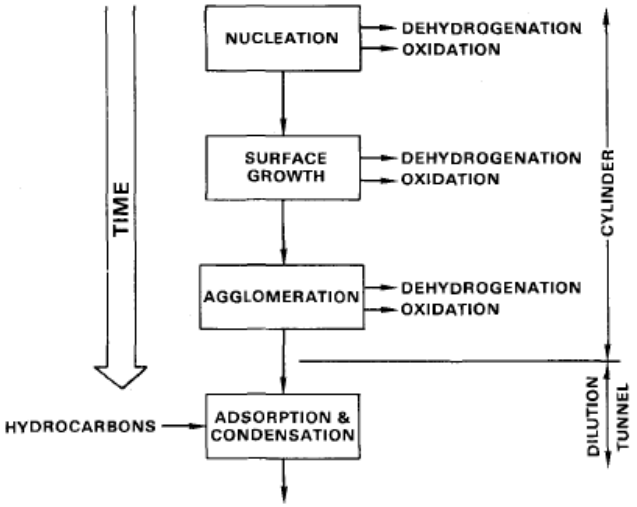

Fig.1-4 Processes to leading of net production of diesel particulates[10]

Over 90% of carbon particles originally generated within the engine are consumed and never get exhausted as engine diesel operates in overall lean condition. Because of the high compression ratios of diesel engine, a large expansion occurs during the power stroke, and the gases within the cylinder are cool by the expansion cooling to relatively low temperature. This causes the remaining high-boiling-point components found in the fuel and lubricating oil to condense on the surface of the carbon soot particles. This absorbed portion of the soot is called soluble organic fraction (SOF).

SOF amount is highly dependent on the cylinder temperature. At light load, cylinder temperatures are reduced and can drop to as low as 200°C during final expansion and exhaust blow-down. Under these conditions, SOF can be as high as 50% of the total mass of soot. The percentage of SOF in total particulates varies widely under other operating

conditions, and can be as low as 3%. SOF consists mostly of hydrocarbons components with some hydrogen, SO_2, NO, NO_2, and trace amount of sulfur, zinc, phosphorus, calcium, iron, silicon, and chromium from diesel fuel and lubricating oil.

1.4.3 Hydrocarbon

As diesel engine operates with an overall fuel-lean equivalence ratio, it has one fifth the (gaseous) hydrocarbon emissions of a gasoline engine. Additionally, the components of diesel fuel has higher molecular weights on average than those of the gasoline and results higher boiling and condensing temperature. This make some hydrocarbon particles to condense onto the surface of the carbon soot contributing to the soot mass, while at the same time reducing exhausted hydrocarbon emission[11].

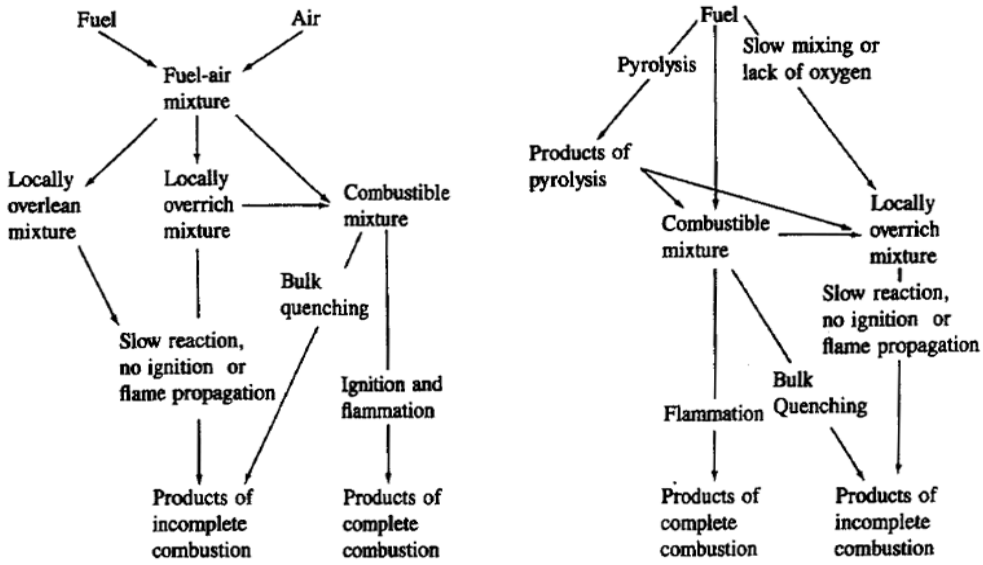

Fig.1-5 Schematic representation of diesel hydrocarbon formation mechanisms[12]

The composition of the unburned and partially oxidized hydrocarbons in the diesel exhaust is very complex and extends over a large molecular size range. Fig.1-5 show how the incomplete combustion products are produced[12]. In general, diesel engine has about 98% combustion efficiency with only 2% of the hydrocarbon fuel being emissions. Some local spots in the combustion chamber will be to lean to combust properly and other spots will be too rich with not enough oxygen to consume all fuel. With undermixing, some fuel particles in fuel-rch zones never find oxygen to react with. In fuel-lean zones, combustion is limited and some fuel does not get burned. With overmixing, some fuel particles will be mixed with the already burned gas and will therefore not combust totally.

1.5 Diesel Engine and Alternative Fuel (SVO & Biodiesel)

There is substantial evidence pointing to Rudolf Diesel's desire to use vegetable oils as a fuel in order to help support agrarian society and to enable independent craftsmen and artisans to compete with large industry. It was also noted that a version of diesel engine demonstrated at 1900 World's Fair in Paris, the Exposition Universalle; that runs smoothly using raw ground peanut oil[13]. This proven that diesel engine from the beginning can be run with biomass fuel in the form of vegetable oil. This chapter will try to summarize the current state of alternative fuel usage, advantage and disadvantage and its future; especially for the usage of straight vegetable oil and its methyl-ester biodiesel.

Even before the shortage issue of fossil fuel becomes a concern, there were reports that show studied done in countries such India, China and Belgium concluded that the use of vegetable oil as oil in diesel engine shows promise. The real interest in vegetable oil fuels began in the late 1970s during the OPEC oil embargo. A significant conference which documented the studies of the late 1970s was held in August 1982, under the auspices of the American Society of Agricultural Engineers (ASAE; now the American Society of Agricultural and Biological Engineers, ASABE). In the 1980s vegetable oils were considerably more expensive than diesel and it was mentioned that the additional processing would only drive the cost higher. The overall theme and outcome of the 1982 ASAE conference was that raw vegetable oils, while showing promise, had a tendency to cause injector coking, polymerization in the piston ring belt area causing stuck or broken piston rings, and a tendency to thicken lubricating oil causing sudden and catastrophic failure of the rod and/or crankshaft bearings[14]. By 1983 the process to produce fuel quality engine-tested biodiesel was completed and published internationally [15].

All vegetable oils consist primarily of triglycerides (also known as triacylglycerols). Triglycerides have a three-carbon backbone with a long hydrocarbon chain attached to each of the carbons. These chains are attached through an oxygen atom and a carbonyl carbon, which is a carbon atom that is double-bonded to second oxygen. Such, when used as fuel, SVO has the possibility to polymerized and gel at higher temperature. Additional, cold flow properties of SVO are inferior to diesel due to high viscosity[14]. The properties of various SVO are shown in Table 1-1.

SVO are renewable and biodegradable and they have characteristics quite similar to those of a common diesel fuel. Biodiesel (methyl-ester from vegetable oil) derived from SVO can be use directly to diesel engine without the engine needing any alteration[16][17][18]

Table 1-1 Properties of vegetable oil[15]

Vegetable oil	Kinematic viscosity at 38 °C (mm^2/S)	Cetane no.	Heating value (MJ/kg)	Cloud point (°C)	Pour point (°C)	Flash point (°C)	Density (kg/l)
Corn	34.9	37.6	39.5	1.1	40	277	0.9095
Cottonseed	33.5	41.8	39.5	1.7	15	234	0.9148
Crambe	53.6	44.6	40.5	10	12.2	274	0.9048
Linseed	27.2	34.6	39.3	1.7	15	241	0.9236
Peanut	39.6	41.8	39.8	12.8	6.7	271	0.9026
Rapeseed	37	37.6	39.7	-3.9	-31.7	246	0.9115
Safflower	31.3	41.3	39.5	18.3	6.7	260	0.9144
Sesame	35.5	40.2	39.3	3.9	9.4	260	0.9133
Soya bean	32.6	37.9	39.6	3.9	12.2	254	0.9138
Sunflower	33.9	37.1	39.6	7.2	15	274	0.9161
Palm	39.6	42		31	-	267	0.918
Babassu	30.3	38	-	20	-	150	0.946
Diesel	3.06	50	43.8	-	16	76	0.855

meanwhile pure SVO is suggested to undergo mixing or heating to reduce its viscosity before usage[19][20]. They contain no sulphur elements and are regarded as no contribution to the accumulation of CO_2 in the atmosphere, thus has minimum impact as a greenhouse gas contributor[21]. In addition, SVO does not contain poly-aromatic hydrocarbons and nitrous poly aromatic hydrocarbons, which mean it is less detrimental to human health[22]. SVO oxygen contents may promote more complete combustions and effectively reduce the production of unburned hydrocarbons[23]. Experiment on SVOs and its derived biodiesel shows similar or better emission than diesel[24][25]. In comparison of engine performance, there also no significant different; only to be noted that the SVO calorific value is about 10% lower that of diesel. But the BSFC is almost unchanged[21].

Although SVO can be use directly into diesel engine, it is widely known that the high viscosity pose a great problem especially to modern direct injection engine that operates at a very specific range of condition. High viscosity can damage fuel injection system on the long run. Furthermore, due to polymerization and gelling of SVO in high temperature, coking can be a serious problem and can effect engine performance[26][27]. Although alteration of the engine, usually by adding heating elements to adopt the direct usage of SVO[28][29][30], this does not completely eliminates problems that related to SVO usage in the first place; as this was done to mainly counter the effect of very high viscosity. There is also the method of mixing SVO with diesel before usage. This is actually more practical as blending with diesel will mitigate the negative effect of SVO usage and actually reduce its viscosity. Many studies has been done[31][14] and actual usage of SVO blended with diesel on a bus was also recorded[32]. Even though many researches conclude that using 100% SVO without blending could have a negative impact to engine life, in some situation and condition; example the usage of SVO in rural area where there is the availability of diesel and technology to process the SVO to produce its methyl-ester biodiesel is limited; is favorable in exchange to a more frequent engine maintenance. This is especially true to rural area that can produce SVO and

in which diesel engine is used as a generator for heating, producing electric and mechanical power. Other situation such in condition where diesel and biodiesel is priced much higher than SVO, can also be a valid reasons for SVO usage[33][13][34].

In contrast, many problems related to SVO usage can be solve by using its methyl-ester. This is done by undergoing SVO to transesterification process. Transesterification remove fatty acids from SVO, producing its methyl-ester (widely known as biodiesel) that does not have problem of polymerization and coking[35]. Transesterification also reduce the viscosity as the molecular weight of a typical ester molecule is roughly one third that of typical oil molecule[36]. Many researches have been done to study the usage of biodiesel, and concluded that it can be use without any significant problem in diesel engine[18][16][37]. In actual practice, the usage of SVOs derived biodiesel is currently wide-spread and many commercial party and authority has taken steps to implement the usage of this biodiesel to their existing fleet of vehicles[38].

1.6 Diesel Engine Spray and Combustion

Despite years of improvement attempts, diesel engines are still emitting a significant amount of NOx and particulate matter into the atmosphere. Improvement of emissions exhausted from diesel engines is urgently required to meet the future stringent emission regulations. Though there are many methods to achieve the desired level of emission, such as mixture formation, pilot injection and injection rate shaping, intake charge air cooling, injection timing retard, water emulsion, and exhaust after treatment and exhaust gas recirculation, most of them are directly or indirectly related with controlling the combustion process.

Though diesel engine provides many advantages, they tend to produce black soot or more specifically diesel particulate matter from their exhaust, which consists of unburned carbon compounds. They also produce NOx. As these are the result of combustion process, fundamental study and understanding on mixture formation mechanisms in diesel engine can significantly help in improving current emission level. The combustion characteristics of direct-injection diesel engines are determined by many factors such as the atomization of a spray, the fuel evaporation and the air-fuel mixing rate. Therefore, deep knowledge regarding the diesel fuel evaporation process is required.

1.6.1 Structure of Diesel Engine Spray

Diesel engine use high pressure injector with suitable nozzle to atomize the diesel fuel for combustion. It rely on the conversion of pressure that into kinetic energy to achieve a high relative velocity between the liquid and the surrounding gas. Design wise, diesel engine injector and nozzle can take any form, but in practice the most used is plain orifice (hole) spray nozzle that produces a full cone spray shape; mainly used in direct injection diesel engine. In comparison, indirect injection diesel engine usually uses a pintle-type nozzle; which produce a hollow spray shape. This section will try to summarize the main characteristic of diesel engine full cone spray shape produce by plain orifice spray nozzle.

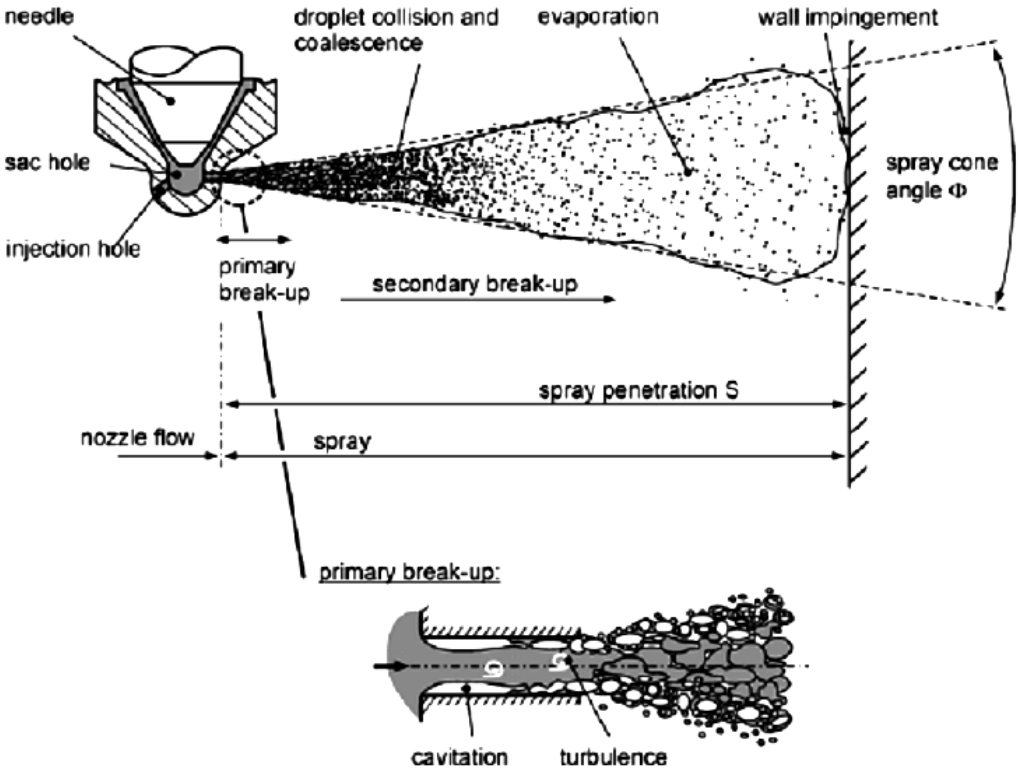

Fig.1-6 Schematic of full cone spray[39]

A schematic description of a full-cone high-pressure spray is given in Fig.1-6[39]. The graphic shows the lower part of an injection nozzle with needle, sac hole, and injection hole. Modern injectors for passenger cars have hole diameters of about 180μm and less, while the length of the injection holes is about 1 mm.

The first break-up of the liquid is called primary break-up and results in large ligaments and droplets that form the dense spray near the nozzle. In case of high-pressure injection, cavitation and turbulence, which are generated inside the injection holes, are the main break-up mechanisms.

The subsequent break-up processes of already existing droplets into smaller ones

are called secondary break-up and are due to aerodynamic forces caused by the relative velocity between droplets and surrounding gas. The aerodynamic forces decelerate the droplets. The drops at the spray tip experience the strongest drag force and are much more decelerated than droplets that follow in their wake. For this reason the droplets at the spray tip are continuously replaced by new ones, and the spray penetration S increases. The droplets with low kinetic energy are pushed aside and form the outer spray region.

Altogether, a conical full-cone spray is formed that is more and more diluted downstream the nozzle by the entrainment of air. Most of the liquid mass is concentrated near the spray axis, while the outer spray regions contain less liquid mass and more fuel vapor, Droplet velocities are maximal at the spray axis and decrease in the radial direction due to interaction with the entrained gas. In the dense spray, the probability of droplet collisions is high. These collisions can result in a change of droplet velocity and size. Droplets can break up into smaller ones, but they can also combine to form a larger drop, which is called droplet coalescence.

1.6.2 Mechanism of Atomization in Diesel Engine Spray

The process of atomization is one in which liquid is disintegrated into drops and ligaments by the action of internal and external forces; and finally leads to the spray formation. Atomization plays a major role in the combustion process, to promote better vaporization, mixing and combustion. Rapid atomization is required especially for high speed engine where the fuel and air mixing duration is very limited. The quality of atomization (droplet size) also plays an important role as combustion and exhaust emission is closely related to fuel-air mixing condition. The atomization processes, can be divided into incomplete (laminar flow regime in the injection hole) and complete sprays (cavitating flow regime).

The atomization process depends mainly on the injection velocity in the nozzle hole. The spray cannot be formed correctly (incomplete spray) for low injection velocities, causing an insufficient atomization, with a long transformation process from liquid column to droplets. However, by increasing the injection velocity, dramatic changes occur in the spray structure; a rapid disintegration process from jet to fine spray appears.

Generally, there are three possible break-up models that influence the primary break-up process and eventually affect the atomization process. These mechanism usually occurs simultaneously with different level of degree mainly depend on the spray velocity.

1. Aerodynamically induced atomization :

The very high relative velocities between jet and gas phase induce aerodynamic shear forces at the gas-liquid interface. Small surface waves are amplified by the aerodynamic shear forces, becomes instable, separated from the jet and eventually form primary droplets. However, the instable growth of waves due to aerodynamic forces is a time dependent process and cannot explain the immediate breakup of the jet at the nozzle exit, as aerodynamic forces can only effect the edge of the jet; but not its inner structure.

2. Turbulence induced atomization :

If the radial turbulence velocity fluctuation inside the jet, which are generated inside the nozzle are strong enough, turbulence eddies can overcome the surface tension and leave the jet to form primary droplet. (Wu et al)

3. Cavitation induced atomization :

Cavitation structure develops inside the nozzle holes because of the decrease of static pressure due to the strong acceleration of the liquid (axial pressure gradient) combined with the strong curvature of the streamlines at the inlet edge. Hence a two phase flow exists inside the nozzle holes. The cavitation bubbles implode when leaving the nozzle because of the high ambient pressure inside the cylinder. In addition, experimental investigations have shown that the transition from pure turbulent to a cavitating nozzle hole flow results in increase of the spray cone angle and in a decrease of penetration length. (Arai et al)

1.6.3 Atomization Role in Diesel Engine Combustion

Combustion in diesel engine is an unsteady process occurring simultaneously at many spot in a very non-homogeneous at a rate controlled by fuel injection. Air intake into the engine is unthrottled, with engine torque and power by the amount of fuel injected per cycle. Only air is contained in the cylinder during the compression with compression ratio ranging from 12 to 24. Fuel is injected into the cylinder late in the compression stroke by fuel injector; usually with a high injection velocity to spread the fuel throughout the cylinder and cause it to mix with air. After injection the fuel must go through a series of events as shown in Fig.1-7, to assure proper combustion process. This chapter will try to summarize the events leading to combustion after fuel injection and the importance and role of spray atomization.

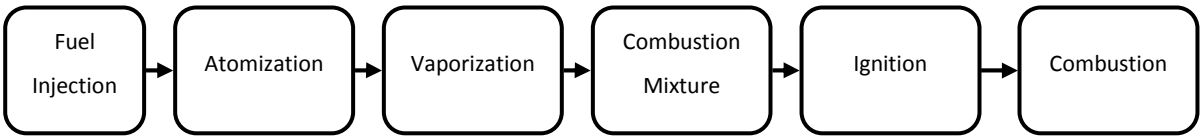

Fig.1-7 Events after fuel injection leading to combustion in diesel engine

a) Atomization

Fuel drops break into very small droplets. The smaller the original drop size emitted by the injector nozzle, the quicker and more efficient the atomization process. The atomization process depends on many variables and significantly affected by the injection pressure, ambient pressure and density. Nozzle geometry also play and important role on atomization process.

b) Vaporization

The fuel liquid droplets evaporate to vapor. This occurs very quickly due to the hot air temperatures created by the high compression. In some case, about 90% of the fuel injected into the cylinder has been vaporized within 0.001 second after injection. Near the core of the fuel jet, the combination of high fuel concentration and evaporative cooling will cause adiabatic saturation of fuel to occur. Evaporation will stop in this region and only after additional mixing and heating will this fuel evaporate.

c) Mixing

After vaporization, the fuel vapor must mix with air to form a mixture within the air-fuel ratio range which is combustible. This mixing is produce due to the high fuel injection velocity. In addition, some diesel engine is design to add swirl and turbulence in the cylinder air. Fig.1-8 shows the non-homogeneous distribution of fuel-air ratio that develops around the injected fuel jet. Combustion can occur within the equivalence ratio limits of Ø=1.8 (rich) and Ø=0.8 (lean).

d) Self-Ignition (Auto-ignition)

There is a slight delay after fuel is injected into the chamber and the self-ignition. Before the piston reach bTDC, the air fuel mixture starts to self-ignite. In most engines, this is around 8° bTDC and 6°-8° aSOI. Actual combustion is preceded by secondary reaction including breakdown of large hydrocarbon molecules into smaller species and some oxidation. These reaction caused by the high temperature air are exothermic and further raise the air temperature in the immediate local vicinity. This finally leads to actual sustained

combustion process.

e) Combustion

Combustion starts from self-ignition simultaneously at many locations in the slightly rich zone of the fuel jet. The equivalence ration of these regions is around Ø = 1 to 1.5. At this time, the fuel inside the combustion chamber is between 70% to 95% in vapor state. With multiple flame-fronts spreading, all the gas mixture is consume quickly. This gives a very quick rise in temperature and pressure in the cylinder. Liquid fuel is still being injected into the cylinder after the first fuel is already burning. After the initial start of combustion, the rest of the combustion process is controlled by the rate at which fuel can be injected, atomized, vaporized and mixed into the proper air-fuel ratio. Combustion lasts for about 40° to 50° of engine rotation, much longer than the 20° of fuel injection. This is because some particles take a long time to mix into a combustible mixture with the air, which leads combustions to lasts well into the power stroke.

As summarized in this section, diesel engine combustion is strongly affected and significantly depends on the atomization of fuel inside the cylinder, and in a larger sense, the spray characteristic of the diesel engine. As shorter ignition delay, relatively fast and complete burning of the fuel mixture is a favorable characteristic of engine diesel engine; in which faster atomization help to promote these qualities.

In real practice, engine design takes significant consideration to improve the mixture formation inside the cylinder. In general, direct injection (DI) diesel engine with large open chamber has a very high injection pressure to produce high velocity jet; that assure the penetration of the spray jet reaches across the chamber for greater assists in mixing of the fuel in air. In contrast, small diesel engine which also usually a high-speed

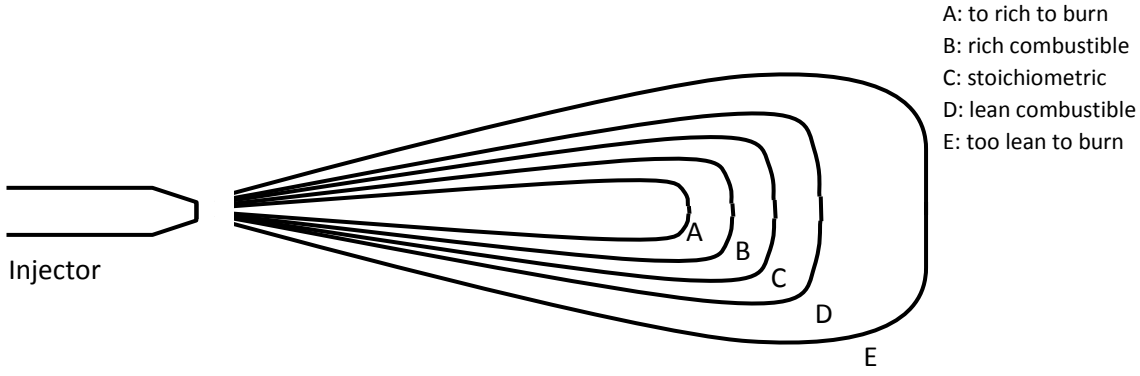

Fig.1-8 Schematic of fuel jet of diesel spray, showing air-fuel vapor zones around the inner liquid core.

engine diesel, use high swirl to enhance and speed the vaporization and mixing of the fuel. Special intake and cylinder geometries are needed to generate this necessary high swirl. This can be seen in indirect (IDI) diesel engine with small secondary chamber, which the fuel in first injected in this chamber and the swirl generated will assist the atomization before combustion occurring throughout the secondary and primary chambers. This design also facilitates the use of much lower injection pressure which is adequate to penetrate across the small secondary chamber. However, the final design of the engine and atomization strategy is up to the engine manufacturer as there are other aspects and consideration that has to put into account to achieve the final intended operating purpose of the fabricated engine.

1.7 Literature Review & Current Diesel Spray Research State

Precise control of the fuel injection, spray atomization and fuel-air mixing are among the fundamental factors focused by many researches in making improvements of the combustion process. Thus, there has been many works done related to diesel engine spray, covering the fundamental aspects for deeper understanding of the working operation; and also the direct application and improvement to current technology. This section will try to summarize the work done by previous researcher in this field, that influence the work after them, and also the works that follows, contributing new finding and fresh new views on the subject. Also included are studies on SVO and its methyl-ester biodiesel used in diesel engine spray, which cover the significant part of this thesis.

Some of the earliest works related to diesel engine spray are very fundamental and deals with the macroscopic characteristics. Spray penetration, droplet distribution and diesel spray breakup length were studied[40]–[43]. There are also works that studies the effect of spray to the engine emissions[12][44][45], and proven that diesel spray play a significantly role in diesel engine combustion. As most of the works studies deals with the macroscopic characteristics of diesel spray, the actual atomization process of diesel spray still remain a puzzle for researcher, though there are many models that have been proposed on this subject[4][46] these are not specifically limited to diesel spray. Further works were done especially in condition similar to diesel engine. A very comprehensive paper summarizing diesel engine spray structure and its characteristic was published in 1990[47] that become a major reference to work done by other researcher after that time. This paper try to explain the process of diesel spray formation by taking into account ideas and founding of previous works done by researcher in the same field (spray and diesel engine) and complemented it

with extensive experimental work. Results from this paper have been used to assist and its result acts as a comparison for works that came after it.

Recent works on diesel engine spray mainly deals with fundamental aspects or the applications of the spray itself. The method of study also varies differently, either experimental by the used of rapid compression machine[48]–[51], constant volume chamber[52]–[54], and even optic engine[55][56] to simulate diesel engine conditions; fixed with data accusation apparatus that can be in many form, described in details in Chapter 3. The use of commercial engine for diesel engine spray study also widely adapted but the focus of the study usually more on engine emission and usability. The use of numerical calculation modeling[57]–[60] also implemented as the current technology is now capable of fast computing and understanding of the spray atomization phenomenon is at a moderate level; which should be improve for a better result.

As engine diesel spray affect diesel combustion in significant and complicated ways, the objective of each individual study can be very different. Some works focus on the initial duration of the spray[61]–[63][64]; to carefully study the spray breakup phenomenon. Studies on the internal fluid flow inside the spray nozzle; which is commonly linked to the primary and secondary breakup are also done by many researchers[65]–[71]. Most of this studies act as reference to build the basic foundation and understanding to diesel spray atomization. Others try to study the mixture formation[72]–[77] of diesel engine spray on various nozzle design and geometry; such as single hole nozzle, multi-hole nozzle, small diameter nozzle. Mixture formation studies, especially around the ignition delay period[48][78][79] ; the period before auto-ignition occurs, are also very important as the diesel spray structure and characteristic during this period effect the combustion in a greater degree. There are also studies to improve mixture formation by the use of spray wall impingement[80]–[86]. This mixture formation strategy is favorable especially when the chamber wall temperature is high and when spray atomization cannot fully develops for efficient combustion under initial conditions. Also, the effect of nozzle geometry and design on the emission was studied by numerous researches[87]–[90]; which could be use as reference when linking spray characteristics to actual engine emission. Studies using high injection pressure[50][91][92] with micro-hole nozzle are also being done, as high injection pressure known to promote atomization and micro-hole nozzle is a viable option to HSDI, that usually has smaller combustion chamber and does not need long spray penetration. With the use of powerful x-ray equipment, a group of researcher successfully measure the

mass distribution of diesel spray[93]–[95]; a significant accomplishment as it has been very difficult to actually measure the mass distribution using other technique.

The general characteristic of diesel spray that has been observed throughout many studies can be summarized as, but not limited to:

- Injection pressure and ambient temperature does not affect much the total spray penetration length, but does affect the spray breakup length. The lengthening effect of velocity and the shortening effect of atomization and vaporization cancel each other out, which explains this lack of dependence.
- Distributions of the vapor concentration for the tested higher injection pressure showed faster fuel vaporization rates and slightly larger spray head volumes.
- Increased ambient temperature tends to shortened the liquid phase and enlarge the vapor phase area.
- Nozzle hole diameter is the most influential parameter in determine spray penetration. Decreasing this diameter causes a slower penetration and a faster mixing and atomization, which leads to a shorter maximum liquid phase.

Most of the issues of using SVO and its biodiesel are the high viscosity and polymerization at high temperature. Comparison studies have been made between these fuels to diesel[75][96][97]. Significant difference between these alternative fuels to diesel is that the former exhibits poor atomization and droplet SMD is higher, with smaller spray angle; but with longer penetration length. Results also suggested that the poor atomization is due to low level of cavitations and turbulence inside the nozzle. In addition, more details studies on these fuels spray characteristic were done by numerous researcher[98][99]–[101]. Some studies also try to improve the mixture formation by studying the effect of nozzle geometry and wall impingement on these fuels[102][103]. It is suggested that the use of certain nozzle geometry and suitable chamber design that provide the shape for wall impingement for the fuel can promote atomization and at the same time, limit the fuel that will reach the upper section of the chamber where the cylinder head is located; thus decreasing the chance of deposit buildup. Other researchers try to mitigate the negative impact of the high viscosity nature of these fuels by blending[104][105] or heating[106].

1.8 Thesis Composition

The objective of this study is to make clear characteristics of diesel engine spray fueled with rapeseed oil (as a biomass fuel) and find potential method to improve its atomization. First, the characteristics of rapeseed oil spray are compared to diesel spray. This is important as rapeseed oil has very high kinematic viscosity that negatively impacts spray development, and detail understanding on this topic is necessary. Next, this study explores the effect of nozzle geometry in multi-hole nozzle on rapeseed oil spray. It has be observed from many studies that smaller nozzle hole diameter improve atomization, while nozzle scaling and nozzle sac-volume affect spray development. The use of wall impingement technique as a possible method to improve atomization also has been considered in this study especially as rapeseed oil has very high distillation temperature. Impingement to piston wall forces the fuel liquid to disintegrate and this help to atomize the spray more quickly. Furthermore, piston geometry (piston wall shape) could also affects diesel engine emission, in rapeseed oil case by providing the wall spray an optimum penetration condition for larger spray boundary region that could help atomization. These strategies are used to promote diesel spray atomization and also should apply to direct use of rapeseed oil. Lastly, air movement affect on the rapeseed oil spray was also investigated. Although high speed swirl (air movement) strategy is usually used in IDI engine, it would be interesting to study this effect to rapeseed oil spray for both IDI and DI nozzle. The result would be very beneficial for future study.

This study uses model equipment to observe spray development optically using constant volume spray chamber. A rapid compression machine was utilized to simulate the high pressure and high ambient temperature in actual diesel engine. In this study, the spray characteristics of diesel (also referred as gas oil or GO) as a reference fuel and rapeseed oil (also referred as RO or SVO) including macroscopic and microscopic spray structure, spray development, fuel evaporation, and droplets atomization were studied. Shadowgraphy that utilize nano-spark light source (to freeze movement) was used for still picture capture[18]. The same apparatus can also be configured for taking dual exposure of the same spray (referred as dual nano-spark) to measure other parameters such as liquid and vapor phase progression, and also droplet dynamic behavior. Study on the effect of nozzle geometry and wall configuration on the wall impingement spray also utilized high-speed camera direct photography. Analysis of still picture is done by using image analysis software coupled with custom made algorithm that has been initially calibrated. This is especially important for

precise measurement of the fuel droplet.

This summary is arranged in eight major chapters. The first section; Chapter 1 to 3 describes the research background. This section also explained the experimental apparatus and image analysis method for in depth analysis of spray characteristics. Next, the characteristics of rapeseed oil spray and diesel spray were made clear in Chapter 4. Detail observations were made and finding shows poor atomization for rapeseed oil compared to diesel. Chapter 5 explains the effect of nozzle geometry in multi-hole nozzle spray to improve initial condition of rapeseed oil spray atomization. This is then continued to Chapter 6, which focus on the effect of wall shape configuration on impinging rapeseed oil spray to promote atomization. Chapter 7 study the effect of high speed air movement (swirl) to spray atomization process. The research finding regarding the characteristics of rapeseed oil spray and improvement of its atomization are concluded in Chapter 8.

REFERENCES

[1] Morton Grosser, Diesel, the man & the engine, 1st ed. New York: Atheneum, 1978, p. 166.

[2] "The International Council for Clean Transportation | ICCT." [Online]. Available: http://www.theicct.org/. [Accessed: 24-Apr-2013].

[3] "Emission Standards: Europe: Cars and Light Trucks." [Online]. Available: http://www.dieselnet.com/standards/eu/ld.php. [Accessed: 22-Apr-2013].

[4] John B. Heywood, Internal Combustion Engine Fundamentals. New York: McGraw-Hill, 1998, p. 930.

[5] Marc Riedl and David Diaz-Sanchez, "Biology of diesel exhaust effects on respiratory function.," The Journal of allergy and clinical immunology, vol. 115, no. 2, pp. 221–8; quiz 229, Feb. 2005.

[6] C. Braun-Fahrländer, J. C. Vuille, F. H. Sennhauser, U. Neu, T. Künzle, L. Grize, M. Gassner, C. Minder, C. Schindler, H. S. Varonier, and B. Wüthrich, "Respiratory health and long-term exposure to air pollutants in Swiss schoolchildren. SCARPOL Team. Swiss Study on Childhood Allergy and Respiratory Symptoms with Respect to Air Pollution," American journal of respiratory and critical care medicine, vol. 155, no. 3, pp. 1042–1049, Mar. 1997.

[7] D. W. Dockery, F. E. Speizer, D. O. Stram, J. H. Ware, J. D. Spengler, and B. G. Jr Ferris, "Effects of inhalable particles on respiratory health of children," The American review of respiratory disease, vol. 139, no. 3, pp. 587–594, Mar. 1989.

[8] O. Fahy, a Tsicopoulos, H. Hammad, J. Pestel, a B. Tonnel, and B. Wallaert, "Effects of diesel organic extracts on chemokine production by peripheral blood mononuclear cells.," The Journal of allergy and clinical immunology, vol. 103, no. 6, pp. 1115–24, Jun. 1999.

[9] S. Saravanan, G. Nagarajan, S. Anand, and S. Sampath, "Correlation for thermal NOx formation in compression ignition (CI) engine fuelled with diesel and biodiesel," Energy, vol. 42, no. 1, pp. 401–410, Jun. 2012.

[10] Charles A. Amann and Donald C. Siegla, "Diesel Particulates—What They Are and Why," Aerosol Science and Technology, vol. 1, no. 1, pp. 73–101, 1981.

[11] G. Greeves, I. M. Khan, C. H. T. Wang, and I. Fenne, "Origins of Hydrocarbon Emissions from Diesel Engines," SAE Paper, 770259, Feb. 1977.

[12] Robert C. Yu and Syed M. Shahed, "Effects of Injection Timing and Exhaust Gas Recirculation on Emissions from a D.I Diesel Engine," SAE Paper, 811234, 1981.

[13] Gerhard Knothe, "Historical Perspectives on Vegetable Oil-Based Diesel Fuels," Inform, vol. 12, pp. 103–1107, 2001.

[14] R. D. Misra and M. S. Murthy, “Straight vegetable oils usage in a compression ignition engine—A review,” Renewable and Sustainable Energy Reviews, vol. 14, pp. 3005–3013, 2010.

[15] C. S. Hawkins, J. Fuls, and F. J. C. Hugo, “Sunflower Oil Esters: An Alternative Fuel for Direct Injection Diesel Engines,” SAE Paper, 831356, Sep. 1983.

[16] B. Kegl, “Effects of biodiesel on emissions of a bus diesel engine,” Bioresource Technology, vol. 99, no. 4, pp. 863–873, 2008.

[17] Kaushik Acharya, Mufaddel Dahodwala, Walter Bryzik, and Naeim Henein, “Effect of Different Biodiesel Blends on Autoignition, Combustion, Performance and Engine-Out Emissions in a Single Cylinder HSDI Diesel Engine,” SAE Paper, 2009-01-0489, 2009.

[18] Daisuke Kawano, Hajime Ishii, Yuichi Goto, Akira Noda, and Yuzo Aoyagi, “Application of Biodiesel Fuel to Modern Diesel Engine,” SAE Paper, 2006-01-0233, 2006.

[19] Nadir Yilmaz and Byron Morton, “Effects of preheating vegetable oils on performance and emission characteristics of two diesel engines,” Biomass and Bioenergy, vol. 35, no. 5, pp. 2028–2033, 2011.

[20] S. Bari, T. H. Lim, and C. W. Yu, “Effects of preheating of crude palm oil (CPO) on injection system, performance and emission of a diesel engine,” Renewable Energy, vol. 27, pp. 339–351, 2002.

[21] A. K. Hossain and P. A. Davies, “Plant oils as fuels for compression ignition engines: A technical review and life-cycle analysis,” Renewable Energy, vol. 35, pp. 1–13, 2010.

[22] Graboski M.S., McCormick R.L., Michael S. Graboski, and Robert L. Mccormick, “COMBUSTION OF FAT AND VEGETABLE OIL DERIVED FUELS IN DIESEL ENGINES,” Progress in Energy and Combustion Science, vol. 24, no. 97, pp. 125–164, 1998.

[23] David Y. Chang and Jon H. Van Gerpen, “Determination of Particulate and Unburned Hydrocarbon Emissions from Diesel Engines Fueled with Biodiesel,” SAE Paper, 982527, 1998.

[24] Yu Zhang and Jon H. Van Gerpen, “Combustion Analysis of Esters of Soybean Oil in a Diesel Engine,” SAE Paper, 960765, Feb. 1996.

[25] Salvatore Alfuso, Maddalena Auriemma, Giuseppe Police, and Maria Vittoria Prati, “The Effect of Methyl-Ester of Rapeseed Oil on Combustion and Emissions of DI Diesel Engines,” SAE Paper, 932801, 1993.

[26] Gvidonas Labeckas and Stasys Slavinskas, “Performance of direct-injection off-road diesel engine on rapeseed oil,” Renewable Energy, vol. 31, pp. 846–863, 2006.

[27] Norbert Hemmerlein, Volker Korte, Herwig Richter, and Günter Schröder, “Performance, Exhaust Emissions and Durability of Modern Diesel Engines Running on Rapeseed Oil,” SAE Paper, 910848, 1991.

[28] M. Basinger, T. Reding, F. S. Rodriguez-Sanchez, K. S. Lackner, and V. Modi, “Durability testing modified compression ignition engines fueled with straight plant oil,” Energy, vol. 35, no. 8, pp. 3204–3220, 2010.

[29] Amanda Lea-Langton, Hu Li, Gordon E. Andrews, and Patrick Biller, “The Influence of Fuel Pre-Heating on Combustion and Emissions with 100% Rapeseed Oil for a DI Diesel Engine,” SAE Paper, 2009-01-0486, 2009.

[30] M. Basinger, T. Reding, C. Williams, K. S. Lackner, and V. Modi, “Compression ignition engine modifications for straight plant oil fueling in remote contexts: Modification design and short-run testing,” Fuel, vol. 89, no. 10, pp. 2925–2938, 2010.

[31] J. Czerwinski, “Performance of HD-DI-Diesel Engine with Addition of Ethanol and Rapeseed Oil,” SAE Paper, 940545, 1994.

[32] D. C. Rakopoulos, C. D. Rakopoulos, E. G. Giakoumis, a. M. Dimaratos, and M. a. Founti, “Comparative environmental behavior of bus engine operating on blends of diesel fuel with four straight vegetable oils of Greek origin: Sunflower, cottonseed, corn and olive,” Fuel, vol. 90, no. 11, pp. 3439–3446, Nov. 2011.

[33] Christina Schott, Socio-economic dynamics of biofuel development in Asia Pacific. Jakarta: Friedrich Ebert Stiftung (FES) Indonesia Office, 2009.

[34] S. S. Sidibe, J. Blin, G. Vaitilingom, Y. Azoumah, and S. S. Sidibé, “Use of crude filtered vegetable oil as a fuel in diesel engines state of the art: Literature review,” Renewable and Sustainable Energy Reviews, vol. 14, no. 9, pp. 2748–2759, 2010.

[35] Avinash Kumar Agarwal, “Biofuels (alcohols and biodiesel) applications as fuels for internal combustion engines,” Progress in Energy and Combustion Science, vol. 33, no. 3, pp. 233–271, Jun. 2007.

[36] Sukumar Puhana, N. Vedaramana, Boppana V.B. Rama, G. Sankarnarayananb, and K. Jeychandranb, “Mahua oil (Madhuca Indica seed oil) methyl ester as biodiesel-preparation and emission characterstics,” Biomass and Bioenergy, vol. 28, pp. 87–93, 2005.

[37] A. Senatore, M. Cardone, L. Allocca, S. Vitolo, and V. Rocco, “Experimental Characterization of a Common Rail Engine Fuelled with Different Biodiesel,” SAE Paper, 2005-01-2207, 2005.

[38] T. J. Wallington, C. K. Lambert, and W. C. Ruona, “Diesel vehicles and sustainable mobility in the U.S.,” Energy Policy, pp. 1–7, Dec. 2011.

[39] Carsten Baumgarten, Mixture Formation in Internal Combustion Engines, 2006 XVII. Berlin: Springer, 2006, p. 294.

[40] Yutaro Wakuri, Masaru Fuji, Tatsuo Amitani, and Reijiro Tsuneya, “Studies on the Penetration of Fuel Spray in a Diesel Engine,” Bulletin of JSME, vol. 3, no. 9, pp. 123–130, 1960.

[41] Hiroyuki Hiroyasu and Toshikazu Kadota, “Fuel Droplet Size Distribution in Diesel Combustion Chamber,” Bulletin of JSME, vol. 19, no. 135, pp. 1064–1072, 1976.

[42] Makoto Ikegami, Kei Miwa, and Mitsuru Inada, “A Study on Ignition and Combustion of Diesel Spray by Means of Rapid Compression Machine,” Bulletin of JSME, vol. 24, no. 195, pp. 1608–1615, 1981.

[43] Masanori Shimizu, Masataka Arai, and Hiroyuki Hiroyasu, “Measurement of Breakup Length in High Speed Jet ,” Bulletin of JSME, vol. 27, no. 230, pp. 1709–1715, 1984.

[44] T. W. Kuo R. C. Yu, S. M. Shahed, and T. W. Chang, “The Effect of Mixing Rate, End of Injection, and Sac Volume on Hydrocarbon Emissions from a D.I Diesel Engine,” SAE Paper, 831294, 1983.

[45] Yukio Matsui and Kunihiko Sugihara, “Sources of Hydrocarbon Emissions from a Small Direct Injection Diesel Engine,” SAE Paper, 871613, Sep. 1987.

[46] Arthur H. Lefebvre, Atomization and sprays. New York: Hemisphere Pub. Corp, 1989, p. 421.

[47] Hiro Hiroyasu and Masataka Arai, “Structures of Fuel Sprays in Diesel Engines,” SAE Paper, 900475, 1990.

[48] Kei Miwa, Tsunehiro Ohmija, and Tosio Nishitani, “A Study of the Ignition Delay of Diesel Fuel Spray Using a Rapid Compression Machine,” The Japan Society of Mechanical Engineer, vol. 31, no. 1, pp. 166–173, 1998.

[49] Marie Bysveen, Terje Almås, Kjell Arne Ulvund, Atle Jørgensen, and Frode Kvinge, “Development of a Shadowgraph Image Technique Describing the Fuel Spray Behavior in a Rapid Compression Machine,” SAE Paper, 2004-01-2934, 2004.

[50] Jinha Lee and Norimasa Iida, “Study on Iginition Delay and Combustion of Diesel Spray with High Pressure Fuel Injection and Micro Hole Nozzle Suing Rapid Compresion Machine,” JSME, vol. 67, no. 658, pp. 259–266, 2001.

[51] Hideo Takahashi, Katsuya Tomaru, Selichi Shiga, Takao Karasawa, and Toshio Kurabayashi, “Characteristics of Diesel Spray with Unsteady and Higher Injection Pressure Using a Rapid Compression Machine,” SAE Paper, 910226, 1991.

[52] Hyun Kyu Suh and Chang Sik Lee, “Experimental and analytical study on the spray characteristics of dimethyl ether (DME) and diesel fuels within a common-rail injection system in a diesel engine,” Fuel, vol. 87, pp. 925–932, 2008.

[53] Avinash Kumar Agarwal and Vipul H. Chaudhury, “Spray characteristics of biodiesel/blends in a high pressure constant volume spray chamber,” Experimental Thermal and Fluid Science, vol. 42, pp. 212–218, Oct. 2012.

[54] Seang-wock Lee, Jin Kusaka, and Yasuhiro Daisho, “Spray characteristics of alternative fuels in constant volume chamber (comparison of the spray characteristics of LPG, DME and n-dodecane),” JSAE Review, vol. 22, no. 3, pp. 271–276, Jul. 2001.

[55] T. G. Fang, R. E. Coverdill, C. F. F. Lee, and R. A. White, “Effect of the injection angle on liquid spray development in a high-speed direct-injection optical diesel engine,” Journal of Automobile Engineering, vol. 223, pp. 1077–1092, 2009.

[56] Tiegang Fang, Yuan-Chung Lin, Tien Mun Foong, and Chia-fon Lee, “Biodiesel combustion in an optical HSDI diesel engine under low load premixed combustion conditions,” Fuel, vol. 88, no. 11, pp. 2154–2162, Nov. 2009.

[57] Mao Gongping, Wang Zhong, Yang Dianyong, and Yuan Yinnan, “Numerical Simulation and Experimental Research on the Free Spray Characteristics of Bio-diesel Fuel,” SAE Paper, 2008-01-1598, 2008.

[58] Su Han Park, Hyung Jun Kim, Hyun Kyu Suh, and Chang Sik Lee, “Experimental and numerical analysis of spray-atomization characteristics of biodiesel fuel in various fuel and ambient temperatures conditions,” International Journal of Heat and Fluid Flow, vol. 30, no. 5, pp. 960–970, 2009.

[59] Hyung Jun Kim, Hyun Kyu Suh, Su Han Park, and Chang Sik Lee, “An Experimental and Numerical Investigation of Atomization Characteristics of Biodiesel, Dimethyl Ether, and Biodiesel-Ethanol Blended Fuel,” Energy & Fuel, vol. 22, pp. 2091–2098, 2008.

[60] B. Kegl, “Numerical analysis of injection characteristics using biodiesel fuel,” Fuel, vol. 85, no. 17–18, pp. 2377–2387, 2006.

[61] Hiroshi Hattori, Kikuo Narumiya, Mitsuhiro Tsue, and Toshikazu Kadota, “Analysis of Initial Breakup Mechanism of Diesel Spray Injected into High-Pressure Ambience,” SAE Paper, 2004-01-0528, 2004.

[62] Sergei Sazhin, Cyril Crua, David Kennaird, and Morgan Heikal, “The initial stage of fuel spray penetration,” Fuel, vol. 82, no. 8, pp. 875–885, May 2003.

[63] J. Kang, C. Bae, and K. O. Lee, “Initial development of non-evaporating diesel sprays in common-rail injection systems,” International Journal of Engine Research, vol. 4, no. 4, pp. 283–298, Jan. 2003.

[64] S. Hossainpour and A. R. Binesh, “Investigation of fuel spray atomization in a DI heavy-duty diesel engine and comparison of various spray breakup models,” Fuel, vol. 88, pp. 799–805, 2009.

[65] C. Badock, R. Wirth, A. Fath, and A. Leipertz, “Investigation of cavitation in real size diesel injection nozzles,” International Journal of Heat and Fluid Flow, vol. 20, pp. 538–544, 1999.

[66] Akira Sou, Maulana Muhammad Ilham, Shigeo Hosokawa, and Akio Tomiyama, “EFFECTS OF CAVITATION IN A NOZZLE ON LIQUID JET ATOMIZATION,” ICLASS 2006, Kyoto, Japan, 2006.

[67] M. Blessing, G. König, C. Krüger, U. Michels, and V. Schwarz, “Analysis of Flow and Cavitation Phenomena in Diesel Injection Nozzles and Its Effects on Spray and Mixture Formation,” SAE Paper, 2003-01-1358, 2003.

[68] J. M. Desantes, R. Payri, F. J. Salvador, and J. De la Morena, “Influence of cavitation phenomenon on primary break-up and spray behavior at stationary conditions,” Fuel, vol. 89, no. 10, pp. 3033–3041, Oct. 2010.

[69] F. Payri, V. Bermúdez, R. Payri, and F. J. Salvador, “The influence of cavitation on the internal flow and the spray characteristics in diesel injection nozzles,” Fuel, vol. 83, no. 4–5, pp. 419–431, Mar. 2004.

[70] A. Andriotis, M. Gavaises, and C. Arcoumanis, “Vortex flow and cavitation in diesel injector nozzles,” Journal of Fluid Mechanics, vol. 610, pp. 195–215, Aug. 2008.

[71] H. Roth, M. Gavaises, and C. Arcoumanis, “Cavitation Initiation, Its Development and Link with Flow Turbulence in Diesel Injector Nozzles,” SAE Paper, 2002-01-0214, 2002.

[72] T. Vogel, M. Lutz, M. Wensing, and A. Leipertz, “Influence of fuel mixture on spray formation in diesel processes,” ILASS – Europe 2010, 23rd Annual Conference on Liquid Atomization and Spray Systems, Brno, Czech Republic, September 2010, 2010.

[73] Sung Wook Park and Rolf D. Reitz, “Optimization of fuel/air mixture formation for stoichiometric diesel combustion using a 2-spray-angle group-hole nozzle,” Fuel, vol. 88, no. 5, pp. 843–852, May 2009.

[74] Kazuhiro Umemoto, Toshihiro Nakashima, Yoshiyuki Kidoguchi, and Kei Miwa, “A Study of Mixture Formation, Ignition and Combustion of Multi-hole Diesel Spray,” JSME, vol. 3, pp. 285–286, 2006.

[75] C. Hüttl, U. Leidenberger, and D. Brüggemann, “Mixture Formation and Combustion of Biodiesel Blended Fuels in a DI Diesel Engine,” ILASS – Europe 2010, 23rd Annual Conference on Liquid Atomization and Spray Systems, Brno, Czech Republic, September 2010, 2010.

[76] T. Hoffmann, P. Hottenbach, H. Koss, C. Pauls, and G. Grünefeld, “Investigation of Mixture Formation in Diesel Sprays under Quiescent Conditions using Raman , Mie and LIF Diagnostics,” SAE Paper, 2008-01-0945, 2008.

[77] Jian Gao, Yuhei Matsumoto, Makoto Namba, and Keiya Nishida, “Group-Hole Nozzle Effects on Mixture Formation and In-cylinder Combustion Processes in Direct-Injection Diesel Engines,” SAE Paper, 2007-01-4050, 2007.

[78] Abdullah Adam, Naoki Inukai, Yoshiyuki Kidoguchi, and Kei Miwa, “A Study on Droplets Evaporation at Diesel Spray Boundary during Ignition Delay Period,” SAE Paper, 2007-01-1893, 2007.

[79] C. Crua, D. A. Kennaird, S. S. Sazhin, M. R. Heikal, and M. R. Gold, “Diesel autogignition at elevated in-cylinder pressueres,” International Journal of Engine Research, vol. 5, no. 4, pp. 365–374, Jan. 2004.

[80] Ali Mohammadi, Yoshiyuki Kidoguchi, and Kei Miwa, “Effect of Injection Parameters and Wall-Impingement on Atomization and Gas Entrainment Processes in Diesel Sprays,” SAE Paper, 2002-01-0497, 2002.

[81] Kyungnam Ko and Masataka Arai, “Diesel Spray and Adhering Fuel on an Impingement Wall,” SAE Paper, 2002-01-1628, 2002.

[82] Kenji Amagai, Yasuhiro Maruyama, Masahiro Saito, and Masataka Arai, “Spray-to-Spray Interactions after Wall Impingement,” SAE Paper, 2003-01-1835, 2003.

[83] Kazuhiko Kawajiri, Takashi Yonezawa, Hirofumi Ohuchi, Mamoru Sumida, and Hideaki Katashiba, “Study of Interaction Between Spray and Air Motion, and Spray Wall Impingement,” SAE Paper, 2002-01-0836, 2002.

[84] A. Magnusson, M. Begliatti, F. Borja Hervás, and M. Andersson, “Characterization of Wall Film Formation from Impinging Diesel Fuel Sprays using LIF,” ILASS – Europe 2010, 23rd Annual Conference on Liquid Atomization and Spray Systems, Brno, Czech Republic, September 2010, 2010.

[85] Takumi Ebara, Kenji Amagai, and Masataka Arai, “Movement and Structure of Diesel Spray Impinging on an Inclined Wall,” SAE Paper, 970046, 1997.

[86] M. Gavaises, A. Theodorakakos, and G. Bergeles, “Modeling wall impaction of diesel sprays,” International Journal of Heat and Fluid Flow, vol. 17, pp. 130–138, 1996.

[87] Sibendu Som, Anita I. Ramirez, Douglas E. Longman, and Suresh K. Aggarwal, “Effect of nozzle orifice geometry on spray, combustion, and emission characteristics under diesel engine conditions,” Fuel, vol. 90, no. 3, pp. 1267–1276, Mar. 2011.

[88] H. Tsunemoto, R. M. Montajir, H. Ishitani, and T. Hayashi, “The Influence of Pressure in the Nozzle Sac and Needle Lift on Fuel Spray Behavior and HC Emissions in DI Diesel Engines,” SAE Paper, 1999-01-3491, 1999.

[89] T. F. Su, C. T. Chang, R. D. Reitz, P. V Farrell, A. D. Pierpont, and T. C. Tow, “Effects of Injection Pressure and Nozzle Geometry on Spray SMD and D.I. Emissions,” SAE paper, 952360, 1995.

[90] Jaeman Lim and Kyoungdoug Min, “The Effects of Spray Angle and Piston Bowl Shape on Diesel Engine Soot Emissions Using 3-D CFD Simulation,” SAE Paper, 2005-01-2117, 2005.

[91] Keiya Nishida and Wu Zhang, “Effects of Micro-Hole and Ultra-High Injection Pressure on Mixture Properties of D . I . Diesel Spray,” SAE Paper, 2007-01-1890, pp. 1353–1361, 2007.

[92] Xiangang Wang, Zuohua Huang, Wu Zhang, Olawole Abiola Kuti, and Keiya Nishida, “Effects of ultra-high injection pressure and micro-hole nozzle on flame structure and soot formation of impinging diesel spray,” Applied Energy, vol. 88, no. 5, pp. 1620–1628, May 2011.

[93] P. Leick, T. Riedel, G. Bittlinger, C. F. Powell, A. L. Kastengren, and J. Wang, “X-Ray Measurements of the Mass Distribution in the Dense Primary Break-Up Region of the Spray from a Standard Multi-Hole Common-Rail Diesel Injection System,” Proceedings of the 21st ILASS - Europe Meeting 2007, 2007.

[94] A. I. Ramírez, S. Som, Suresh K. Aggarwal, A. L. Kastengren, E. M. El-Hannouny, D. E. Longman, and C. F. Powell, “Quantitative X-ray measurements of high-pressure fuel sprays from a production heavy duty diesel injector,” Experiments in Fluids, vol. 47, no. 1, pp. 119–134, Mar. 2009.

[95] Alan L. Kastengren and Christopher F. Powell, “X-Ray Radiography Measurements of Diesel Spray Structure at Engine-Like Ambient,” ILASS Americas, 21st Annual Conference on Liquid Atomization and Spray Systems, Orlando, FL, May 2008, 2008.

[96] S. Som, D. E. Longman, A. I. Ramírez, and S. K. Aggarwal, “A comparison of injector flow and spray characteristics of biodiesel with petrodiesel,” Fuel, vol. 89, no. 12, pp. 4014–4024, 2010.

[97] Chao He, Yunshan Ge, Jianwei Tan, and Xiukun Han, “Spray properties of alternative fuels: A comparative analysis of biodiesel and diesel,” International Journal of Energy Research, vol. 32, no. 14, pp. 1329–1338, 2008.

[98] Ezio Mancaruso, Luigi Sequino, and Bianca M. Vaglieco, “First and second generation biodiesels spray characterization in a diesel engine,” Fuel, vol. 90, no. 9, pp. 2870–2883, Sep. 2011.

[99] M. Alam, J. Song, V. Zello, and a Boehman, “Spray and combustion visualization of a direct-injection diesel engine operated with oxygenated fuel blends,” International Journal of Engine Research, vol. 7, no. 6, pp. 503–521, Jan. 2006.

[100] L. Allocca, E. Mancaruso, A. Montanaro, L. Sequino, and B. M. Vaglieco, “Bio- and Mineral-Fuel Spray Evolution in Non-Evaporating and Evaporating Conditions by Image Processing Techniques,” ILASS – Europe 2010, 23rd Annual Conference on Liquid Atomization and Spray Systems, Brno, Czech Republic, September 2010, 2010.

[101] Xiangang Wang, Zuohua Huang, Olawole Abiola Kuti, Wu Zhang, and Keiya Nishida, “Experimental and analytical study on biodiesel and diesel spray characteristics under ultra-high injection pressure,” International Journal of Heat and Fluid Flow, vol. 31, no. 4, pp. 659–666, Aug. 2010.

[102] Sho Nagayasu, Azwan Sapit, Takashi Yano, Yuzuru Nada, and Yoshiyuki Kidoguchi, “Diesel Spray Characteristics of Rape-seed Oil under Conditions of Wall-impingement and Deposit-sticking,” 22nd Internal Combustion Engine Symposium, 2011.

[103] Azwan Sapit, Sho Nagayasu, Yasunori Tsuboi, Yuzuru Nada, and Yoshiyuki Kidoguchi, “A Study on Improvement of Diesel Spray Characteristics Fueled by Rape-seed Oil,” SAE Paper, 2011-32-0561, 2011.

[104] Chang Sik Lee, Sung Wook Park, and Sang Il Kwon, “An Experimental Study on the Atomization and Combustion Characteristics of Biodiesel-Blended Fuels,” Energy & Fuel, vol. 19, pp. 2201–2208, 2005.

[105] Jose´ M. Desantes, Rau´l Payri, Antonio Garcı´a, and Julien Manin, “Experimental Study of Biodiesel Blends’ Effects on Diesel Injection,” Energy & Fuel, vol. 23, pp. 3227–3235, 2009.

[106] Yung-Sung Lin and Hai-Ping Lin, “Study on the spray characteristics of methyl esters from waste cooking oil at elevated temperature,” Renewable Energy, vol. 35, no. 9, pp. 1900–1907, 2010.

Chapter 2 Experimental Apparatus and Procedures

2.1 Introduction

Many different techniques and instruments have been employed in the research upon spray and atomization to investigate spray characteristics, such as the sizes and velocities of droplets, and the spray patterns produced by different atomization devices. Generally, these techniques may be classified into three broad categories: mechanical (droplet capture, cascade impaction, frozen drop and wax methods and sedimentation technique), electrical (charged wire probe and the hot wire anemometer) and, and optical (photography, holography, laser diffraction, laser anemometry and various other techniques based on light scattering)[1].

Though mechanical and electrical technique is applicable in measuring the spray droplet size and spray breakup length[2], it is intrusive in nature. Initial diesel spray study that measure droplet size[3] and breakup length[4] did use these two methods but proven to be very limited in measuring the temporal and spatial diesel spray evolution. Also the intrusive nature makes these techniques very difficult to apply for study under diesel engine like condition of high ambient pressure and high temperature.

As for optical technique, due to its non-intrusive nature, it is currently consider the most suitable technique for diesel spray study. Furthermore, it can be use to study the macroscopic and microscopic aspect of the spray, with good temporal and spatial resolution[5][6]. In particular, a variety of optical systems for spray analysis has been developed in recent years. Each system has its own advantages and limitations, but all benefit because of their non-intrusive natures. Some of these technique can be difficult to implement, need high level of operator skill to be successfully applied and also can be very expensive[1]. Examples of the mainly used optical techniques are direct visualization[7][8] (including high speed camera, shadowgraphy, schlieren, etc…), Particle Image Velocimetry (PIV)[9][10], Laser Beam Extinction (LBE)[11], Laser Induced Fluorescence (LIF)[12][13], Phase Doppler Particle Anemometer (PDPA)[14][15]. Also in very current research, the use of x-ray (x-ray absorption)[14–16] and ballistic imaging[19][20] were explored for the use of diesel spray study with great success especially for study on the spray core region.

2.2 Optical Technique Overview

This section will briefly describe the most commonly used optical technique for diesel spray study. As the author work is using a collection of visualization technique, mainly single nanospark shadowgraphy, dual nanospark shadowgraphy and high speed camera

direct imaging; this section will function as a comparison of author work to other optical technique.

2.2.1 Visualization Technique

The most frequently used optical measurement technique for fuel spray measurement is the direct visualization method. The visualization of digital imaging either in solid state (still camera, digital camera) or continuous recording (high speed video camera) can be employed to expose the conditions of the spray, capturing the macroscopic and microscopic structure. Usually, macroscopic characteristic such spray geometry, penetration depth and wall impingement can be studied well using this technique. With the use of high quality high magnification optical lens, microscopic parameter such as droplet size and droplet distribution also can be studied. By capturing high definition sequential image, the droplet trajectory and velocity also can be calculated, though this required an elaborate imaging technique an analysis method[21]. Similar technique was used in this study and will be describe later.

2.2.2 PIV (Particle Image Velocimetry)

PIV is a full field non-intrusive technique, derived from Laser Speckle Velocimetry (LSV), which was first introduced in the mid-1980. The PIV will measure the distance traveled by particles (introduced to the flow or naturally occurring) in the flow within a known time interval. These particles are known as seeding particles. In order to resolve the speed of each particle, two consecutive shots are taken either on one single image or on two different images. To detect the seeding particle movement, an area of the flow is illuminated by a light sheet that is generated by a double pulses laser and optical system, and the recorded by a CCD camera located at right angles to the light sheet. The particle position will appear as light specks on a dark background on each camera frame. The different placements of the particles in each frame are then analyzed and the velocity and trajectory of the particles then can be calculated.

2.2.3 LIF (Laser Induced Fluorescence)

LIF uses light emission from an atom or molecule following excitation by a laser beam. It use the inelastic scattering methods lies in the exploitation of the ability of atoms and molecules to fluoresce. The principle mechanism in LIF is the excitation of a molecule from its initial lower electronic state to an upper electronic state due to laser source. The five main energy transfer processes that can occur after excitation are:

· Emission of a photon of the same wavelength as the excitation wavelength (elastic

scattering).

- Absorption of an additional photon, which can excite the molecule to even higher states.
- Inelastic collisions with other molecules, as well as electronic energy transfer (often called 'quenching').
- Collisions between the separate atoms of the molecule.
- Spontaneous fluorescence (LIF signal).

LIF can be used to visualize the liquid droplet and fuel vapor at the same time. The main problem that arises when applying LIF is the dependence of the fluorescence signal on electronic quenching. Quenching can be strongly influenced by local temperature, pressure and species concentration. In fuel spray, although the liquid and vapor may present at the same time, the signal from the liquid phase normally is much stronger than the signal from fuel vapor. The image can be obtained using an intensified CCD camera. To obtain the fluorescence image and to avoid elastically scattered light, an objective lens that is opaque to UV (ultra violet)-rays can be used with a color filter attached to the front of the lens.

2.2.4 PDPA (Phase Doppler Particle Anemometer)

PDPA technique can be used for droplet sizing investigation in the fuel spray. The PDPA system consists of an Ar-ion laser, a transmitter, a receiver and a data acquisition system. In this system, the Ar-ion laser is used as the light source and the signal analyzer is synchronized with the fuel injection signal to obtain the transient characteristics of the fuel

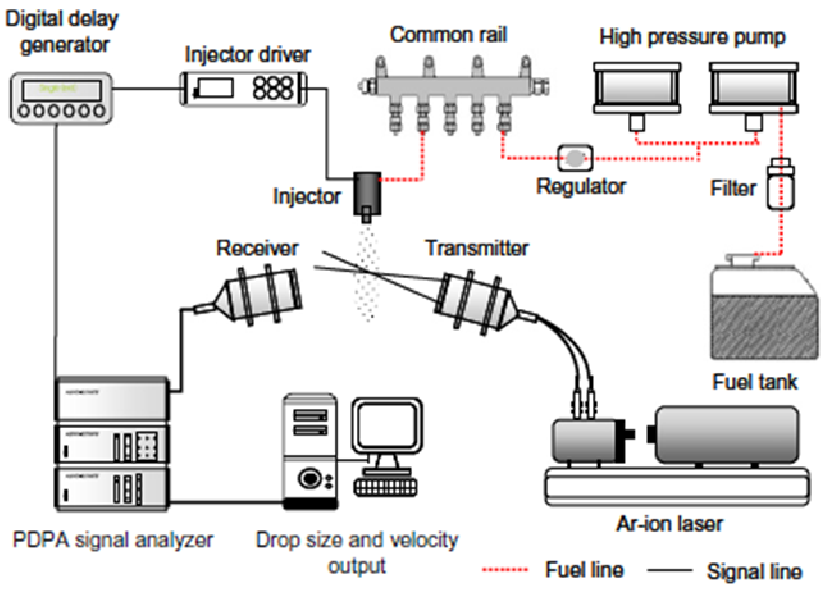

Fig.2-1 Droplet particle analyzer system using PDPA [15]

atomization. The laser output and PMT (photomultiplier tube) voltage are set based on the data acquisition rate and signal intensity. In order to utilize this technique, interference fringe pattern is needed to be created within a small volume in the spray by the laser beam. A scattered light signal is generated when a droplet moves through the small volume. When fuel droplets pass through the measurement volume, the dispersed beam is detected at the receiver. Example of the apparatus is shown in Fig.2-1[15]. The detected phase difference and Doppler signal frequency are then converted to the mean droplet size and velocity. The velocity of the droplet will be related to the temporal modulation, while the droplet size will be related to the spatial frequency.

However, this technique is not suitable for study of dense spray due to the measuring method that only needs one droplet to be inside the measuring volume. Moreover, this technique also cannot provide size distribution in a single transient injection. However, important information such as fuel droplet size and velocity, density, volume flux and time resolved can be obtained.

2.2.5 X-Ray Absorption

The x-ray radiography technique is based on a simple application of linear absorption. A monochromatic beam of x-rays passes through the spray, and the x-ray intensity passing through the spray is measured as a function of time. The x-ray intensity is first measured before the spray event. As the spray event occurs, fuel enters the path of the x-ray beam, absorbing part of the beam. This x-ray intensity can be converted into the fuel mass per unit area present in the beam as shown in Fig.2-2[16].

Limitation of the technique is due to that of the spatial resolution depend on the x-

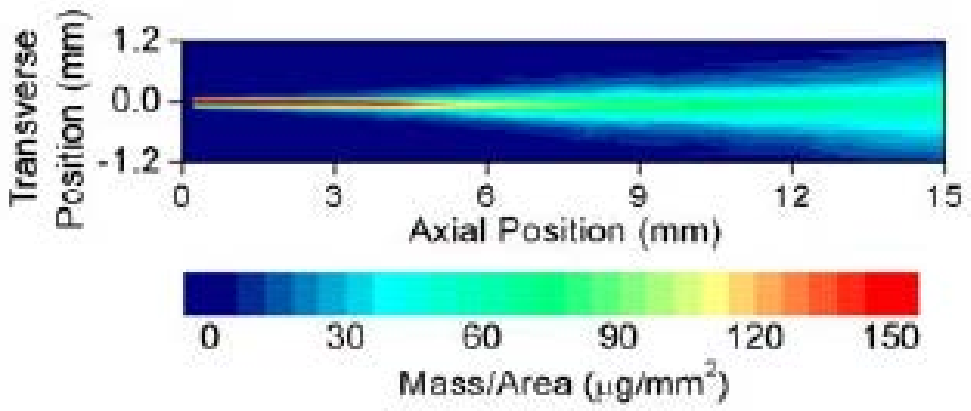

Fig.2-2 Example of spray mass/area distribution result by using x-ray measurement technique (750 μs aSOI, P_{inj}=1000 bar, P_{amb}=30 bar) [16]

ray beam which is quite narrow. Thus, to study the spray structure in detail, the spray chamber must be moved to various positions, allowing the data regarding spray density vs. time to be collected for many positions throughout the flowfield. However the technique ability to map the fuel mass fraction of diesel spray is very valuable to diesel spray study.

2.2.6 Ballistic Imaging

Ballistic imaging is a form of optical shadowgraphy that can acquire images through turbid materials that are opaque to simpler imaging techniques. When light passes through a highly turbid medium, some of the photons actually pass straight through without scattering, exiting the medium within the same solid angle that they entered. These relatively few photons are termed ‘‘ballistic’’. Because they travel the shortest path, they also exit first. A somewhat larger group of photons is called the ‘‘snake’’ photon group, because they are scattered just once or twice. They exit the medium in the same direction as the input light but with a somewhat larger solid angle than the ballistic photons. Because they travel a bit further, they exit just after the ballistic photons. Light exiting the medium that has scattered multiply (‘‘diffuse photons’’) has a larger photon number density, but it also is scattered into a very large solid angle and it exits last as illustrate in Fig.2-3[20]. Due to their undisturbed path, ballistic photons retain an undistorted shadowgram image of structures that may be embedded within the turbid material. The ballistic photons can thus provide diffraction-limited imaging of these structures shown in Fig.2-4[20].

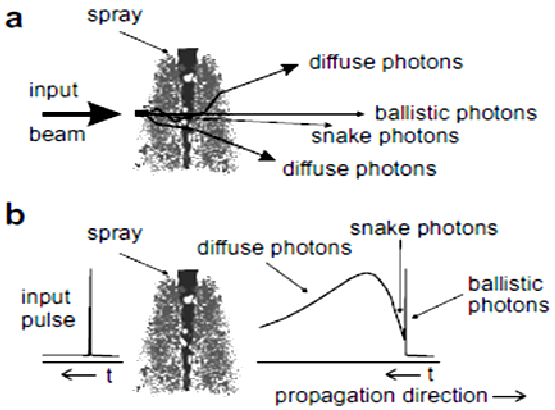

Fig.2-3 Schematic of ballistic, snake and diffuse photon.
(a) geometric dependence (b) time dependence[20]

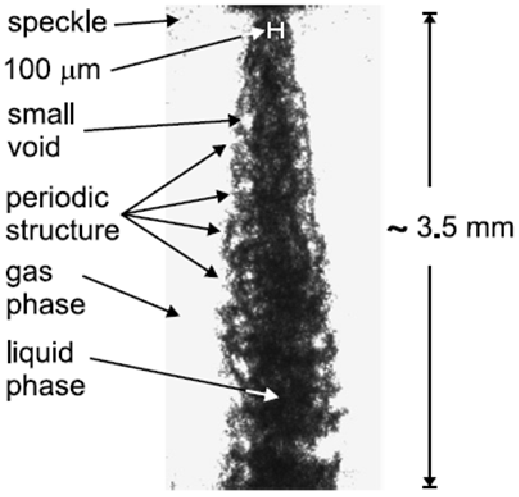

Fig.2-4 Typical ballistic image of a diesel fuel spray at ambient pressure of 1 atm. [20]

This technique was originally developed for medical applications. The use of this technique to study diesel spray is relatively new and improvement is required. However, the imaging technique ability to reconstruct the spray core which is obscure by the dense fog around the spray is beneficial to diesel spray study.

2.3 Experiment Apparatus

In this study, the atomization process of evaporating diesel sprays injected into a high pressure and high ambient temperature was investigated. Images were captured using a nano-spark shadowgraph photography technique and also high speed video imaging. Macrostructures of diesel sprays such as spray tip penetration length, spray shape, spray cone angle were obtained. Microstructures, such as droplet distribution and size were also studied. Furthermore, droplet dynamic behavior such as velocity and flying angle, also spray liquid phase and vapor phase were also analyzed.

The experimental apparatus shown in Fig.2-5 consists of a spray chamber, a rapid compression machine, a single-shot common rail fuel injection system and a nano-spark photography unit for nano-spark photography method to capture image from the side view. As for high-speed video direct imaging, a metal halide lamp was used as the light source with a high speed video camera (Nac MEMRECAM GX1) to capture image from the bottom view shown in Fig.2-6. A specialize chamber different from the nano spark spray chamber was also used.

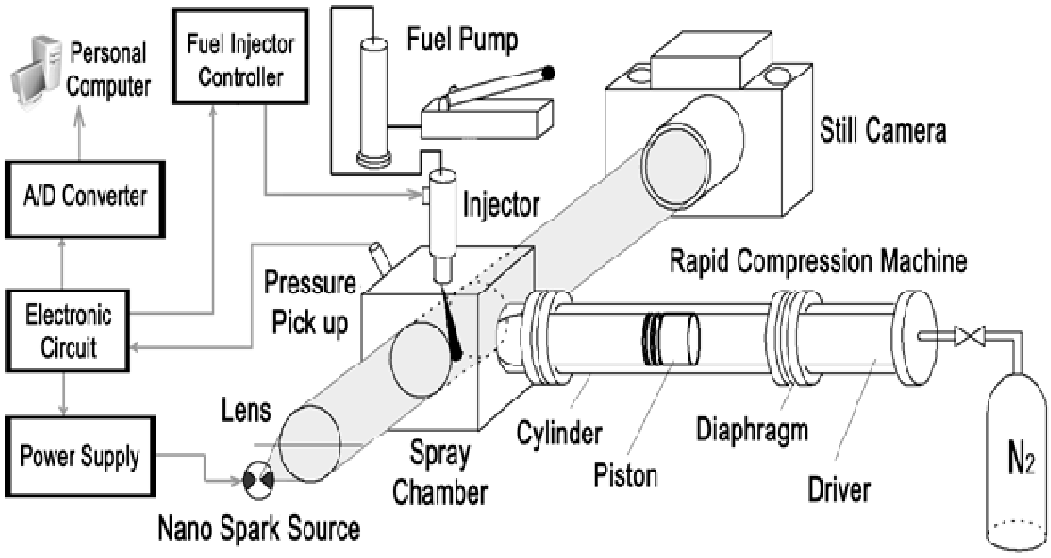

Fig.2-5 Schematic diagram of nano spark shadowgraphy method

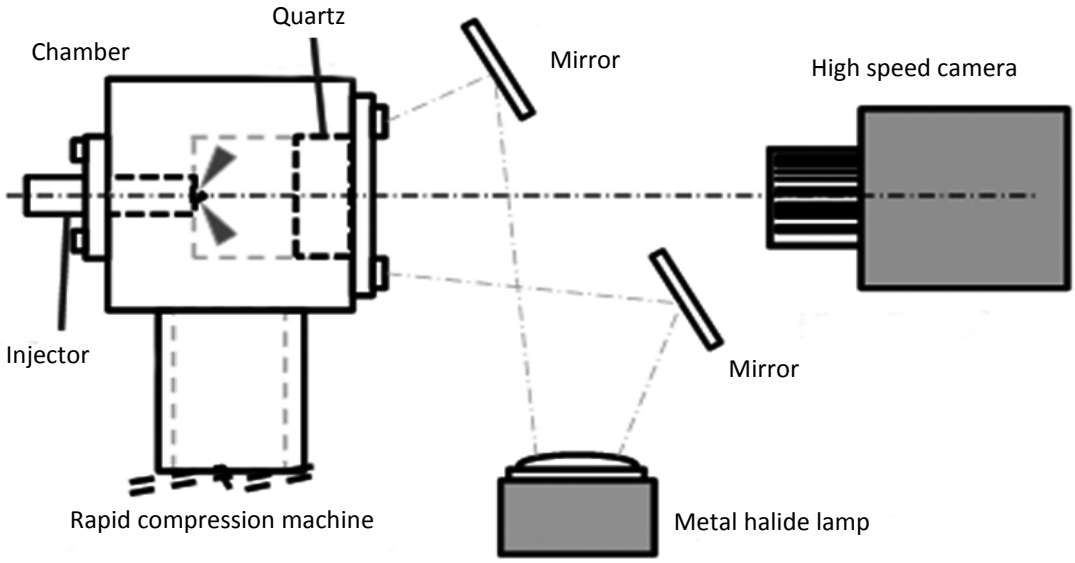

Fig.2-6 Schematic diagram of high-speed camera direct imaging method

2.3.1 Spray Chamber

Fig.2-7 shows a schematic cross-section diagram of the spray chamber. The spray chamber has a diameter of 60mm, a width of 20mm and a volume of 110cm^3. The spray chamber has an upper access for the fuel injector unit and two accesses sized 60mm in diameter located at both side of the chamber. Both accesses were sealed with optical windows which were made of quartz glass (diameter 60mm, thickness 25mm). One side of the window was used for the nano-spark access into the spray chamber and the other side of the window was used for the still camera photography access. This chamber is exclusively used for the nano spark photography method.

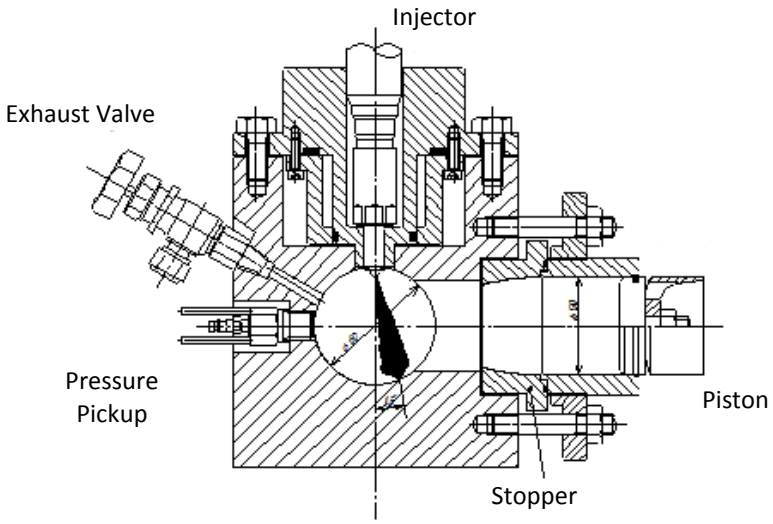

Fig.2-7 Cross section of spray chamber (nano spark)

As for the high-speed camera direct imaging method, another spray chamber was used. The internal dimension is similar to that used for the nano spark but with only one optical window. The same quartz glass was used to seal the chamber meanwhile the injector was fixed on the other side of the optical window for capturing image from the bottom view.

2.3.2 Fuel Injection System

Fig.2-8 shows a single shot common rail fuel injection system. This system consists of manual hand-screw pump, fuel tank, accumulator unit and fuel injector unit. Manual hand-screw pump (KP-5-AW, Kouatsu Machine) is used to pump the fuel into the accumulator unit to generate high pressure fuel for experiment. Accumulator unit can keep fuel up to 200cc and maximum pressure of 200MPa. By using this system, the fuel injection pressure can be varied in the range of P_{inj}=40 to 150MPa for experiment. This fuel injection system was used to inject the fuel into the spray chamber through required injector nozzle. The injection period was fixed constantly at 2.0ms for diesel and varied for rapeseed oil.

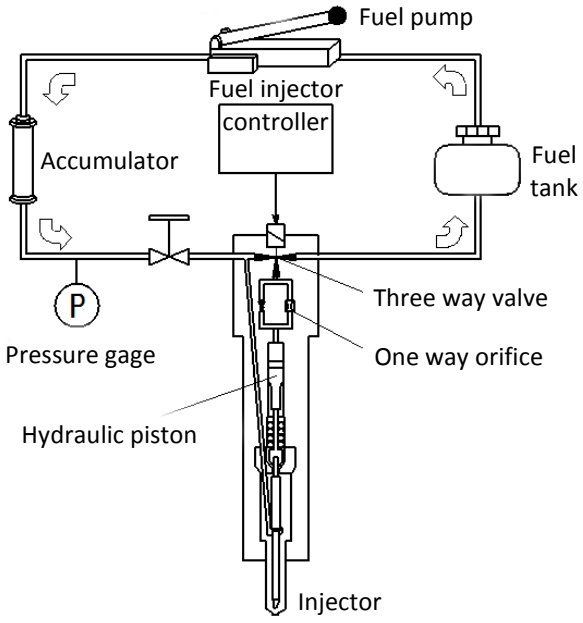

Fig.2-8 High pressure fuel injection system

2.3.3 Rapid Compression Machine

A rapid compression machine is used to simulate the diesel spray in a constant volume over a wide range of ambient temperatures and pressures conditions, close to actual diesel engines. This unit includes two separate units; a compression cylinder unit and a driving cylinder unit. Aluminum piston (17S T-4, diameter 50mm and weight 110g) is inserted first inside the compression cylinder. Meanwhile, high pressure of N_2 gas is charged inside

the driving cylinder unit at the pressure of P_g= 2MPa. A thin diaphragm is used to separate both units. High pressure N_2 gas in the driving cylinder drives the piston inside the cylinder section as soon as the diaphragm is broken. Then the piston stops at stopper section generating high pressure and high ambient temperature inside the spray chamber. The ambient temperature and the pressure in the spray chamber decrease due to the heat release to the wall. A time history of ambient temperature was plotted to determine the desired ambient condition inside the spray chamber. When the ambient condition reached the required value, a single-shot common rail fuel injection system will inject the fuel into the chamber.

2.3.4 Nano Spark Unit

The nano-spark photography unit was employed to capture the still image of the evaporating sprays and droplets. As shown in Fig.2-9, this unit includes a nano second spark light sources known as spark-head. A capacitor with a capacity of 1400pF was installed inside the spark head. This capacitor was pulse-charged in about 60ns from the high voltage pulse generator switched by a thyratron. Automatic preionization of gas in the vicinity of the electrodes helps to create a highly reproducible instant gas breakdown. The time jitter is shorter than 60ns relative to the input trigger pulse.

High-intensity light can be produced by electric discharge between electrodes located inside the spark head. Referring to Fig.2-10, the spark light can be intensified by increasing the power supply voltage and using a larger electrode gap. The electrodes gap was fixed at 3mm and the supplied voltage was kept constant at 12kV, providing a spark

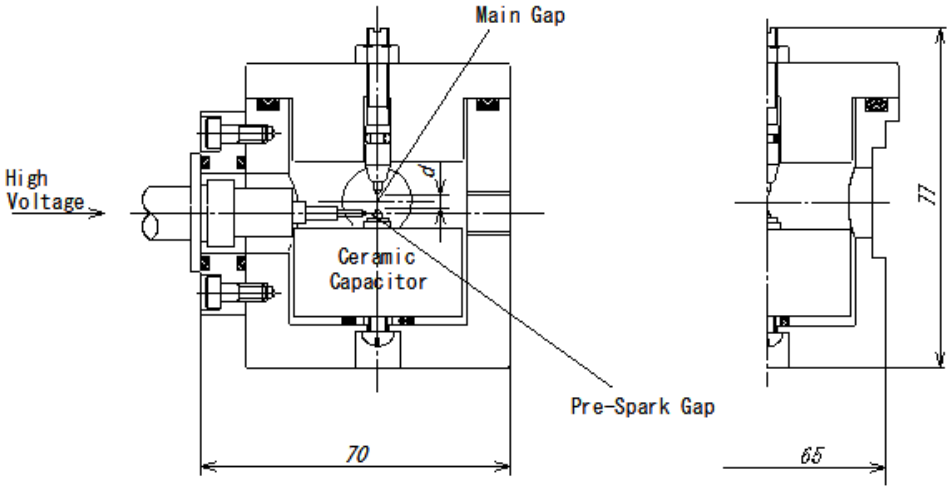

Fig.2-9 Cross section of spark head

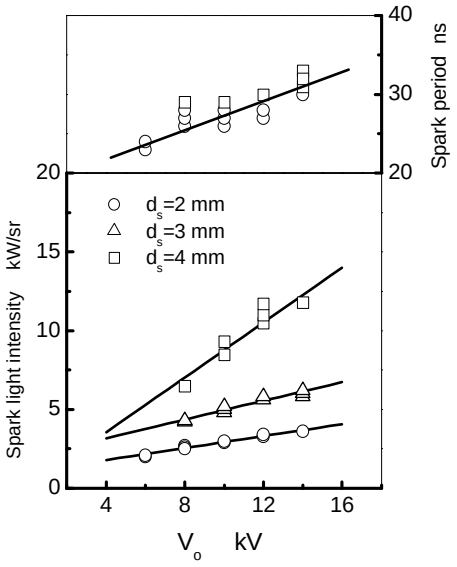

Fig.2-10 Characteristic of nano-spark light source

duration of 30ns. Spray penetration speed generally exceeds 200m/s. However, the maximum droplets speed at the spray periphery was about 25m/s. Therefore, spark duration of 30ns is sufficient to capture the still images of the droplets.

2.4 Experiment Procedures and Optical Arrangement

This section will explain the procedure of image capture, the control system, the fuel and nozzle specification and the optical arrangement used in details.

2.4.1 Photography Method

Shadowgraph photography by a still camera of telescopic lens is performed in the complete dark room. During the process, the camera shutter will be left opened to enable the access of nano spark at short duration of 30ns into the camera. Fuel will be injected inside the spray chamber at desired ambient temperature. The bright backlight from nano-head will then illuminates the spray inside the spray chamber. Therefore, images acquired are the result of the attenuation of light emitted from nano spark through the spray liquid, scattered droplets and vapor phase. By using this system, moment images of evaporating sprays including a liquid phase, droplets and a vapor phase can be obtained. The same principal is use for the dual-nano spark photography setup. Two nano-spark light sources and two still cameras were used. Optical

Meanwhile, high-speed camera direct imaging method was done under ambient room lighting. The light from metal halide lamp is directed to illuminate the spray chamber with the help of mirrors. Then, by using the camera setting and changing the light intensity, clear video of sprays can be obtained.

2.4.2 Control System

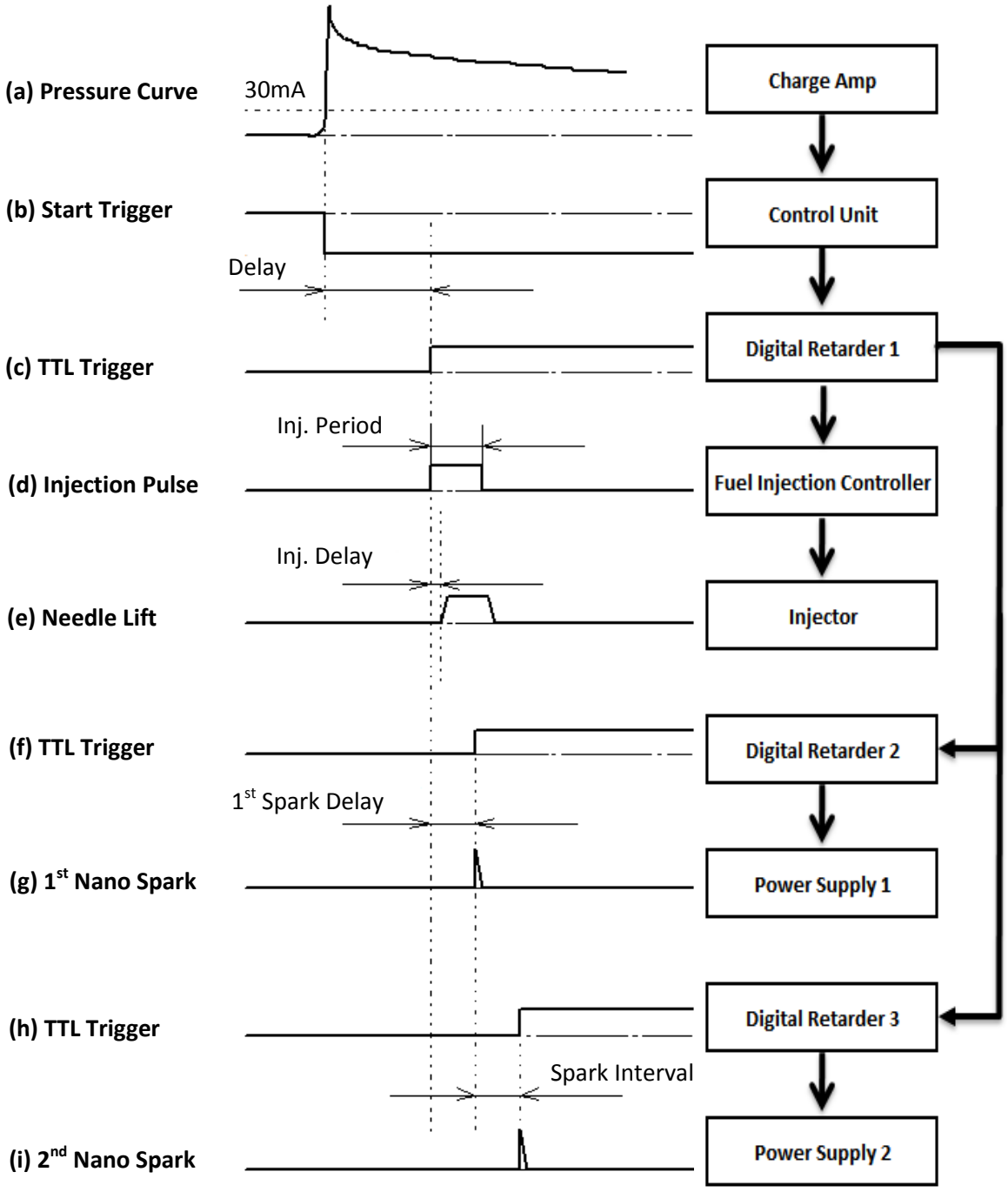

Fig.2-11 Electronic circuit pulse sequence during nano-spark photography

Fig.2-11 shows the pulse sequence of nano-spark shadowgraph photography. A rapid compression machine creates a high pressure and high ambient temperature inside the spray chamber. The pressure increment inside the spray chamber was detected by pressure pick-up sensor (Kistler, 6051A), amplified by charge amplifier (Kistler, 5011) and

then plotted by Data Capture (WR8500-4S) as shown in Fig. 10(a). An increment over 30mA will trigger the control unit to send a start trigger (b). Digital retarder 1 received the signal from control unit and after delay time, t_{delay} (duration for the chamber to be at the required temperature after piston reached the stopper) elapsed, the digital retarder will send TTL trigger (c) to fuel injection controller unit, digital retarder 2.

Fuel injection controller sends the signal (d) to injector unit and a time lag of $t_{injdelay}$ required for needle to lift (e). Meanwhile, the time delay of $t_{injdelay}+\Delta t_1$ ms for nano-spark will be set at digital retarder 2. As a result, after delay time elapsed, the digital retarder 2 send TTL trigger (f) to power supply to create a nano-spark (g). For dual nano-spark, another TTL trigger will also be sent to retarder 3 (h) with time delay of $t_{injdelay}+\Delta t_1+\Delta t_2$ and this will make the power supply (i) to activate the second nano-spark. So in summary, the first nano-spark will have a delay time of Δt_1 aSOI and the second nano spark will have a delay time of $\Delta t_1+\Delta t_2$ aSOI with the interval of each nano-spark is Δt_2.

2.4.3 Fuel Type and Nozzle Specification

Rape-seed oil (RO) was used representative as biomass fuel. JIS#2 diesel fuel also known as Gas Oil (GO) was also used as reference fuel. Table 2-1 shows the fuel properties. Referring to the table, kinematic viscosity for RO is almost 14.5 times higher that GO. Pre experiment was done to analyze the effect of fuel temperature on kinematic viscosity. The result is plotted in Fig.2-13. All the test fuel samples, RO and GO show that their kinematics viscosity value decreases with increase of temperature. In addition, RO shows more rapid decrease in its kinematics viscosity when compared to GO.

Table 2-1 Fuel properties

Fuel and Notation		Diesel (GO)	Rape-seed oil (RO)
Density	@15°C g/cm^3	0.827	0.911
Kinematic viscosity	mm^2/s@303K	3.30	47.78
Carbon	wt -%	0.86	0.78
Hydrogen	wt -%	0.14	0.11
Oxygen	wt -%	0	0.11
Lower heating value	kJ/Kg	42.70	38.14
Cetane index		58.2	unknown

Fig.2-13 shows the distillation characteristic of the test fuel reported by Yoshimoto et al.[22]. The measurement was strictly done following the JIS K2254 which is Japan Standard Measurement Method for fuel distillation test. RO has characteristics of high

viscosity and high distillation temperature. To summarize, density and kinematic viscosity at room temperature of RO is 911 kg/m^3 and 62cSt, respectively, and GO 836kg/m^3 and 3.2cSt. SVO starts distillation at over 700K while GO reaches 90% distillation mass at about 600K.

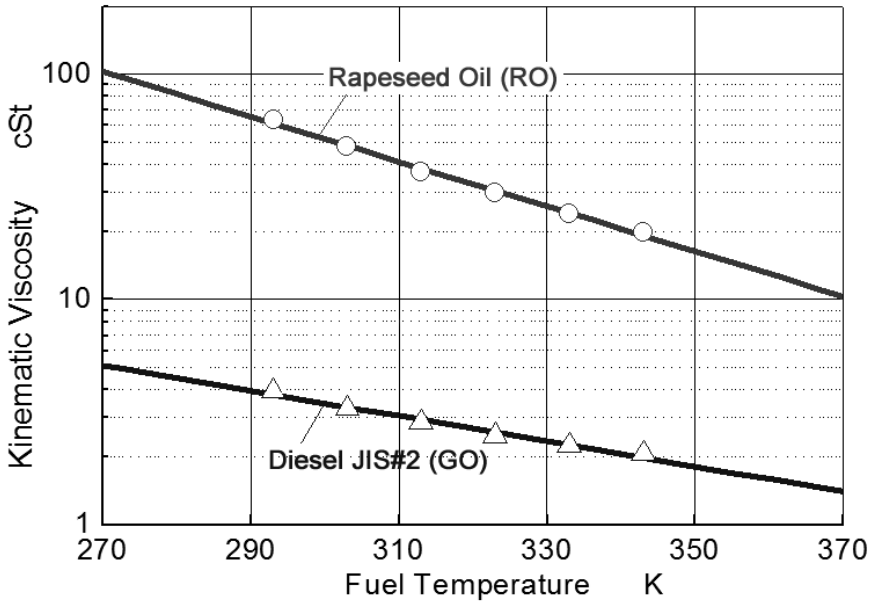

Fig.2-12 Effect of fuel temperature on fuel kinematic viscosity

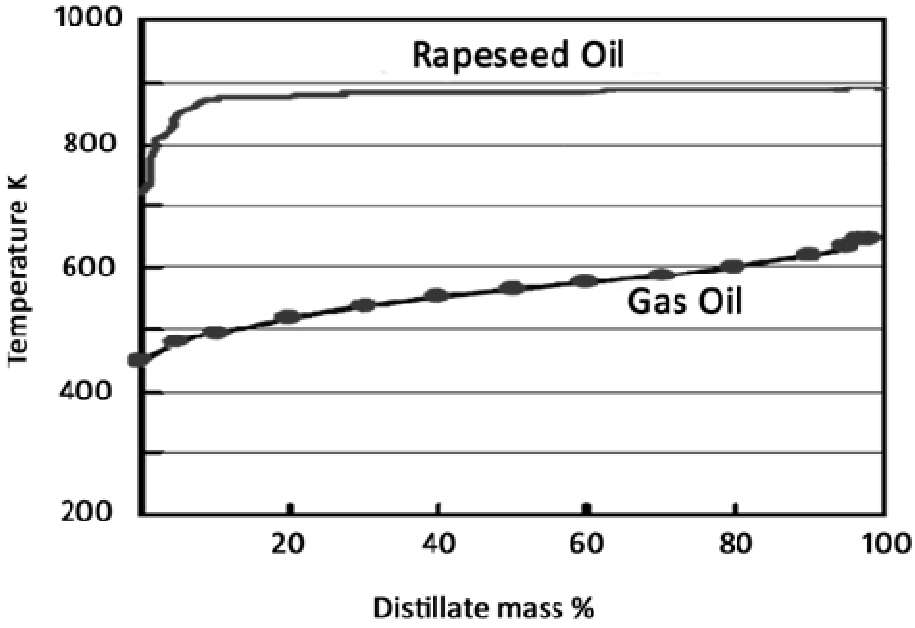

Fig.2-13 Distillation characteristics of test fuel

2.4.4 Single Nano Spark Photography – Lens Arrangement & Method

To obtain more detail information of fuel spray, magnification factor of 3.5 was applied throughout this experiment. Macro lens (PENTAX 135mm) was separately installed from camera body (Asahi Pentax 6x7) as shown in Fig.2-5. As a result, photography of spray was divided into three 15×20mm sections that were upstream, midstream and downstream of the spray as shown in Fig.2-14. A complete set of the three spray photos were combined to get a full figure of spray. Spray photos combination task was done precisely according to the scale of each part that was taken prior to the experiment.

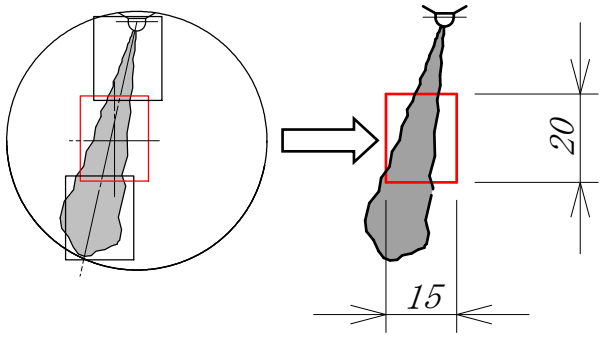

Fig.2-14 Photography setting for spray images

Fig.2-15 shows the optical arrangement of single spark shadowgraph method used in the study. A spark head providing spark duration of 30ns was employed in order to capture fast moving images of droplets and to eliminate the blurring of subject[3-5]. Rapid spark duration at 30ns was needed in order to capture high quality of spray images which include detail images of flying fine droplets and vapor development.

Photography was done inside a complete dark room and nano-spark at spark duration of 30ns performed as a backlight to the spray. Therefore, images acquired are the result of the attenuation of light emitted from nano spark source through the spray.

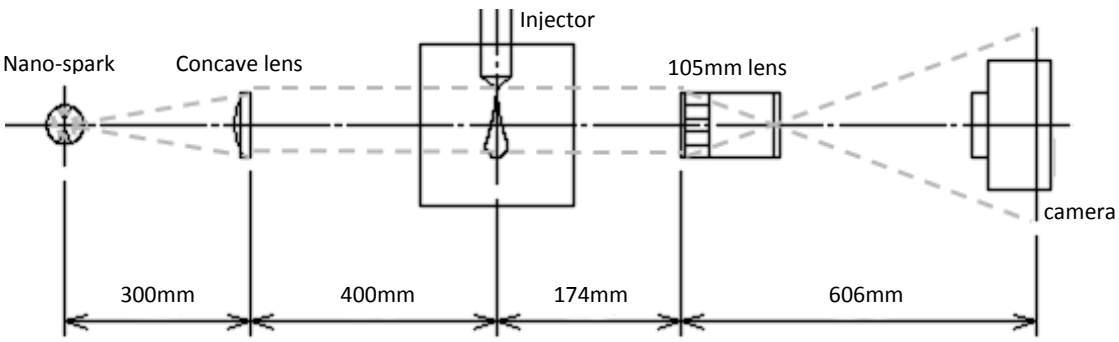

Fig.2-15 Optical setting for single spark shadowgraph method

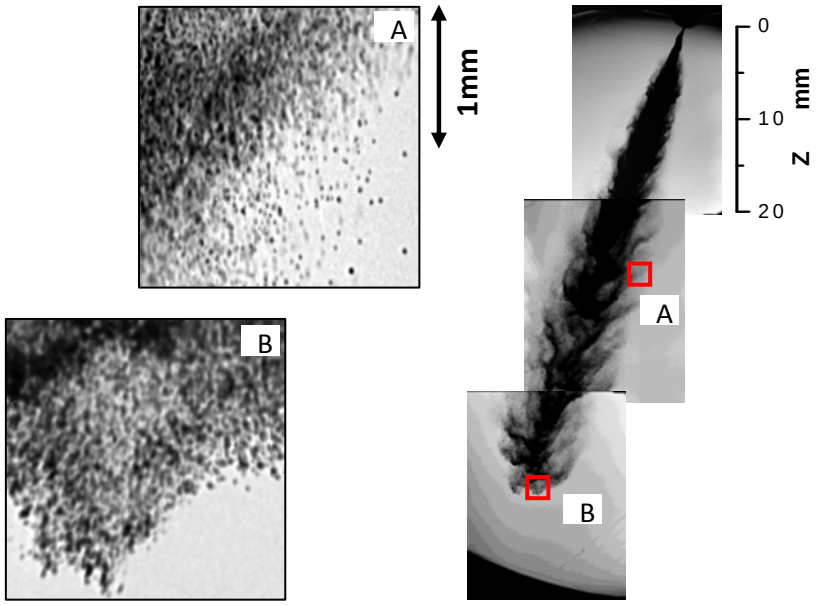

Fig.2-16 Single spark image spray

Fig.2-16 shows the non-evaporating spray image obtained by single nano-spark photography method. The dark area in the images corresponds to the location of the spray liquid phase, the droplets and the vapor phase. Experimental conditions were ambient temperature of T_i=298K and injection pressure of P_{inj}=40MPa. The significant feature of this photograph is high resolution. Macroscopically, the high-density region can be observed along the spray axis from nozzle tip to the spray tip area. Simultaneously, many branch-like structures can be observed along the spray boundary from the midstream area to spray tip.

Left side figures show magnified images at spray boundary region (areas A and B). The images show droplets behavior at midstream and downstream of the spray. Inside every image, highly clear droplets images can be seen. Owing to these images, single spark method offers simultaneous measurement of macroscopic and microscopic parameters such as spray cone angle, spray penetration length, droplets diameter and droplets number at spray boundary region.

However, several important parameters to imagine droplets behavior such as droplets velocity, droplets flying direction, droplets size reduction rate or droplets evaporation rate cannot be obtained by single nano-spark photography method. To obtain these parameters, time depending variations of parameters should be measured. Thus, dual-nanospark photograph method is implemented to obtain the above mentioned parameters.

2.4.5 Dual Nano Spark Photography – Lens Arrangement & Method

To obtain the dynamic behavior of spray droplet, and also study the progression of diesel spray, a new photography method was developed. This method is named dual nano-spark shadowgraph method, whereby two sets of spark head were used in this experiment. Dual nano-spark shadowgraph method enables to capture two images at different timing into separate films without any interference from other optics.

Referring to Fig.2-17, this method employs two identical sets of optics including spark head, camera body, polarized filters and half mirrors. To perform the dual nano-spark photography method, two cameras with completely same specifications were used. In this experiment, two still cameras (Pentax 6x7) were steady fixed on a special bracket which was made to hold both cameras during the photography process.

Referring to the figure, optics 1 was installed along the single straight line. Meanwhile, optics 2 was installed along the C shape line at the center of experimental setup. As shown in the figure, spark light emerged from nano spark 1 illuminates spray at desired time after start of injection. As a result, first spray image will be captured on camera 1. Later, at a very short delay time interval, spark light from nano spark 2 illuminates spray and delayed spray image will be captured on camera 2.

During this process, both camera shutters were open simultaneously. To restrain images illuminated by nano spark 1 to be captured on camera 2 or vice versa, four polarized filters (PL) were used in this experiment. Each filter was set in front of spark head 1, spark head 2, camera 1 and camera 2 respectively. Polarization angle of PL filter installed in optics

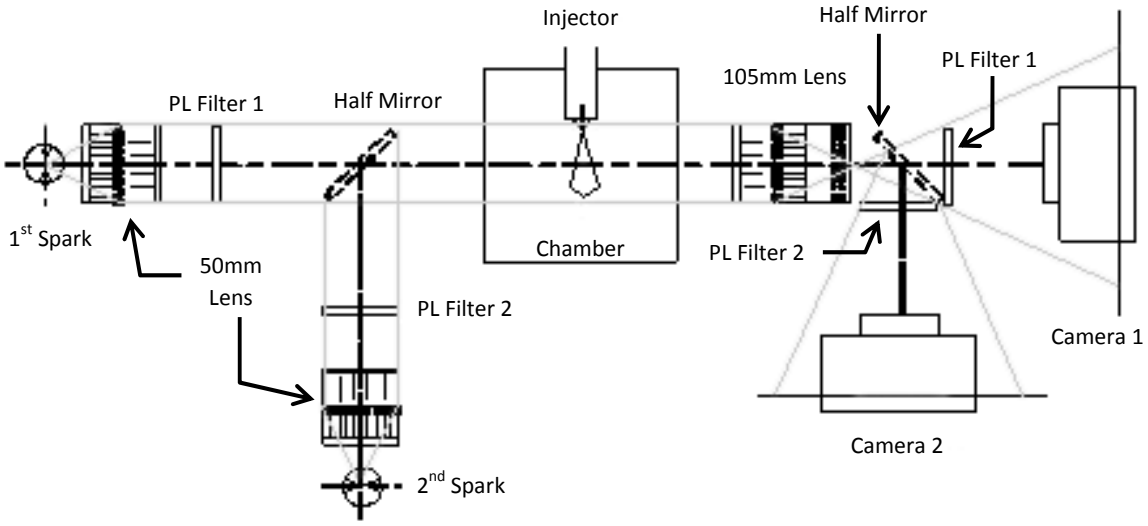

Fig.2-17 Optical setting for dual nano-spark shadowgraph photography method

1 and optics 2 has difference of 90 degree from each other. Therefore, the PL filter in front of camera 2 could cut light beam emerged from spark head 1 and could allow light beam from spark head 2 to pass, or vice versa. As a result, only nano-spark 1 will be allowed to enter camera 1 and only nano-spark 2 will be allowed to enter camera 2. Polarization angle of optics 2 was adjusted to s-polarization angle to maximize the light intensity in optics 2. In addition to this, two half mirrors were set at 45 degree facing to spark head 2 and camera 2.

These half mirrors were used to put the part of optical passes in optics 1 and optics 2 on common axis in spray chamber and to divide them into camera 1 and camera 2. Although it is inevitable to have small angle difference of light beam axis between optics 1 and optics 2 passing through spray chamber, the two images of objects at focal point inside spray chamber were identical due to single lens(Nikkor) was used to process both images.

Images shown in Fig.2-18 and Fig.2-19 shows set of spray images taken with dual nano-spark method. Fig.2-18 shows spray condition of low temperature T_i=298K, P_{inj}=40MPa, t=0.5ms, and Fig.2-19 is high temperature condition of T_i=700K, P_{inj}=70MPa, t=0.5ms. Spark interval between nano-spark 1 and nano-spark 2 was set at Δt=15μs. As seen in the figure, two consecutive images from one single shot of spray at specific short time interval can be obtained.

Referring to Fig.2-18, magnified images of A1 and A2 show a lot of clear droplets.

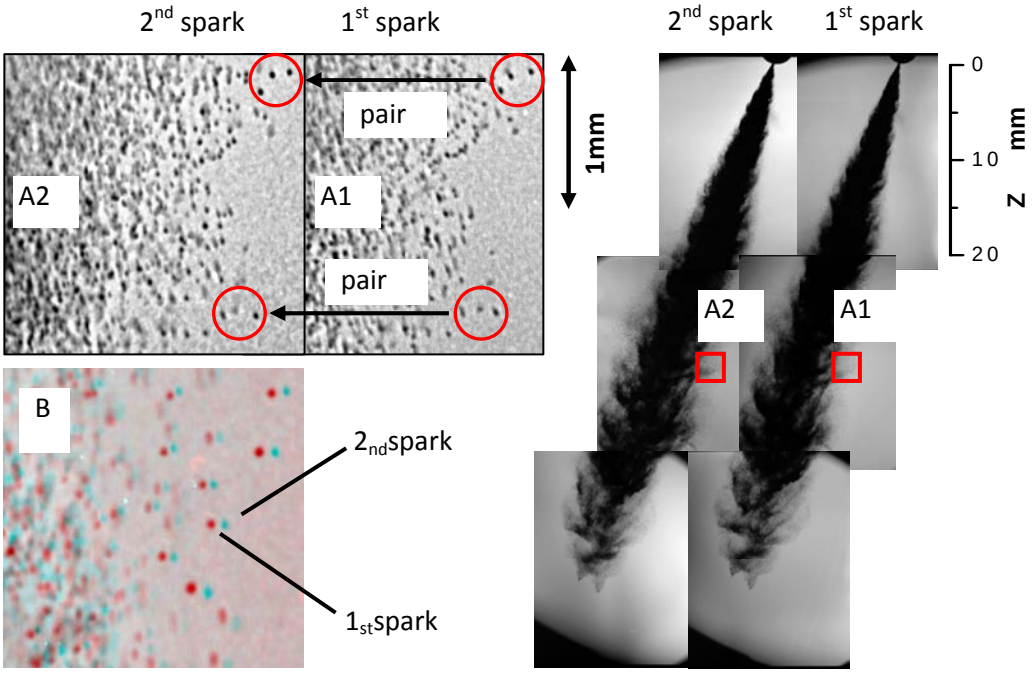

Fig.2-18 Dual nano spark images of non-evaporating spray
(T_i=298K, P_{inj}=40MPa, t=0.5ms, Δt=15μs)

Cross visual reference between detailed images from the A1 (1st spark) and A2 (2nd spark) enabled many pairs of droplets to be detected. Using this method, droplets pairing process could be done not only at low droplets number-density region but also at high droplets number-density region where droplets pairing was impossible with double exposure method.

Meanwhile, image B show overlapped spray images of A1 (1st spark) and A2 (2nd spark). In this image, droplets exposed by 1st spark at inner side while its pair of 2nd spark at outer part of the spray. Clearly, at adequate time interval, many pair of droplets can be seen. These pair of droplets can be detected not only at spray boundary area but also inside high droplets density region. Using this method, flying droplets can still be seen clearly even at spray tip region. By applying dual nano-spark method, difficulties in single spark method and double exposure method were overcome. This method can offer information on droplets behavior such as droplets velocity, flying direction and droplets size reduction rate inside spray boundary region and spray tip region.

In contrast, Fig.2-19 shows evaporating spray from dual nano-spark method at spray condition of high temperature T_i=700K, P_{inj}=70MPa, t=0.5ms. Clearly, two consecutive vapor images can be seen from the A1 (1st spark) and the A2 (2nd spark), respectively. Parameters such as vapor development rate and liquid phase reduction rate can be

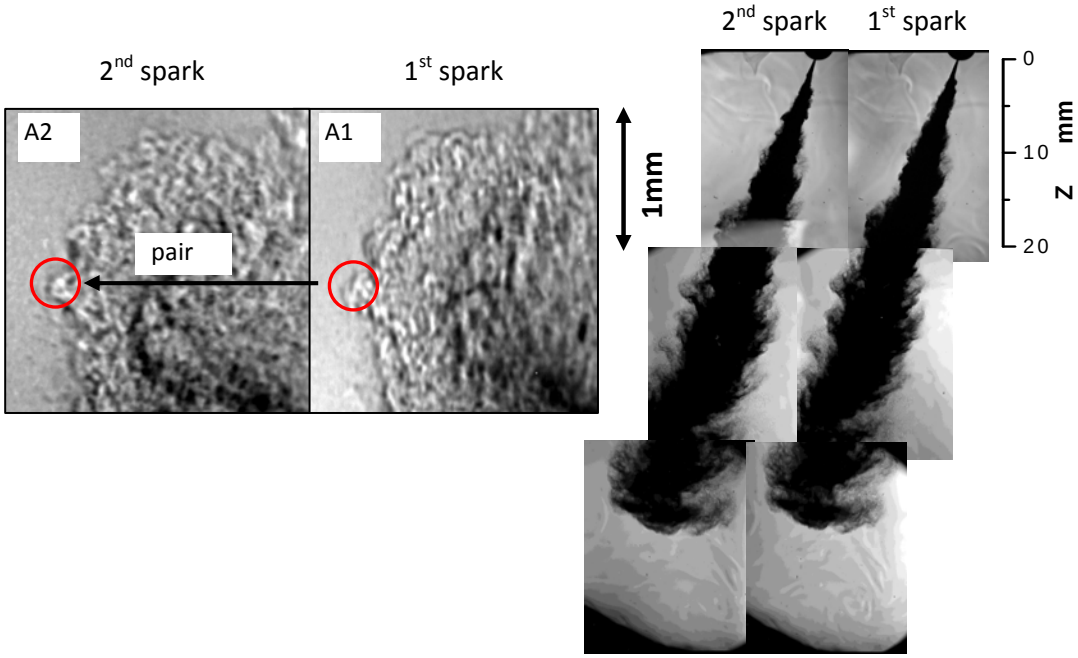

Fig.2-19 Dual nano spark images of evaporating spray
(T_i=700K, P_{inj}=70MPa, t=0.5ms, Δt=15μs)

measured. This information will help better understanding of the behavior of evaporating spray. Furthermore, another advantage of dual nano-spark photography method is high density region inside spray can be isolate vapor from background images, thus the changing rate of the area of the region could be measured.

As mentioned above, applying dual nano-spark shadowgraph photography method covers the weak point in the single spark method. Therefore, droplets behavior such as droplets velocity, flying angle and droplets size reduce rate inside spray boundary region and spray tip region can be measured.

REFERENCES

[1] S. N. Soid and Z. a. Zainal, “Spray and combustion characterization for internal combustion engines using optical measuring techniques – A review,” Energy, vol. 36, no. 2, pp. 724–741, Feb. 2011.

[2] Hiro Hiroyasu and Masataka Arai, “Structures of Fuel Sprays in Diesel Engines,” SAE Paper, 900475, 1990.

[3] Hiroyuki Hiroyasu and Toshikazu Kadota, “Fuel Droplet Size Distribution in Diesel Combustion Chamber,” Bulletin of JSME, vol. 19, no. 135, pp. 1064–1072, 1976.

[4] Masanori Shimizu, Masataka Arai, and Hiroyuki Hiroyasu, “Measurement of Breakup Length in High Speed Jet ,” Bulletin of JSME, vol. 27, no. 230, pp. 1709–1715, 1984.

[5] Koch, Schmid, and Leipertz, “INFLUENCE OF INJECTION NOZZLE PARAMETERS ON THE SPRAY PROPAGATION AND COMBUSTION IN A DI-DIESEL-ENGINE,” ICLASS 2006, Kyoto, Japan, 2006.

[6] H. Gen Fujimoto, H. Adachi, T. Yano, N. Marubayashi, T. Hori, and J. Senda, “Spatial Droplets Size Distribution in a Diesel Spray Taken by Photography with Super High Resolution,” ILASS – Europe 2010, 23rd Annual Conference on Liquid Atomization and Spray Systems, Brno, Czech Republic, September 2010, 2010.

[7] Marie Bysveen, Terje Almås, Kjell Arne Ulvund, Atle Jørgensen, and Frode Kvinge, “Development of a Shadowgraph Image Technique Describing the Fuel Spray Behavior in a Rapid Compression Machine,” SAE Paper, 2004-01-2934, 2004.

[8] Choongsik Bae and Jinsuk Kang, “The structure of a break-up zone in the transient diesel spray of a valve-covered orifice nozzle,” International Journal of Engine Research, vol. 7, no. 4, p. 319, Jan. 2006.

[9] Harri Hillamo, Ossi Kaario, and Martti Larmi, “Particle Image Velocimetry Measurements of a Diesel Spray,” SAE Paper, 2008-01-0942, 2008.

[10] Wook Choi, Byung-Chul Choi, Hyung-Koo Park, Kyung-Jei Joo, and Je-Hyung Lee, “In-Cylinder Flow Field Anaysis of a Single Cylinder DI Diesel Engine Using PIV and CFD,” SAE Paper, 203-01-1846, 2003.

[11] Jeong-Kuk Yeom, Tomoyuki Tanaka, Jiro Senda, and Hajime Fujimoto, “The Structure Analysis of Evaporative Diesel Spray,” SAE Paper, 2002-01-0498, 2002.

[12] Julian T. Kashdan and Jean-françois Papagni, “LIF Imaging of Auto-ignition and Combustion in a Direct Injection Diesel-fuelled HCCI Engine,” SAE Paper, 2005-01-3739, 2005.

[13] T. Hoffmann, P. Hottenbach, H. Koss, C. Pauls, and G. Grünefeld, “Investigation of Mixture Formation in Diesel Sprays under Quiescent Conditions using Raman , Mie and LIF Diagnostics,” SAE Paper, 2008-01-0945, 2008.

[14] Pekka Rantanen, Antti Valkonen, and Andreas Cronhjort, “Measurements of a diesel spray with a normal size nozzle and a large-scale model,” International Journal of Heat and Fluid Flow, vol. 20, no. 5, pp. 545–551, Oct. 1999.

[15] Hyun Kyu Suh, Sung Wook Park, and Chang Sik Lee, “Effect of piezo-driven injection system on the macroscopic and microscopic atomization characteristics of diesel fuel spray,” Fuel, vol. 86, pp. 2833–2845, 2007.

[16] Alan L. Kastengren and Christopher F. Powell, “X-Ray Radiography Measurements of Diesel Spray Structure at Engine-Like Ambient,” ILASS Americas, 21st Annual Conference on Liquid Atomization and Spray Systems, Orlando, FL, May 2008, 2008.

[17] A. I. Ramírez, S. Som, Suresh K. Aggarwal, A. L. Kastengren, E. M. El-Hannouny, D. E. Longman, and C. F. Powell, “Quantitative X-ray measurements of high-pressure fuel sprays from a production heavy duty diesel injector,” Experiments in Fluids, vol. 47, no. 1, pp. 119–134, Mar. 2009.

[18] P. Leick, T. Riedel, G. Bittlinger, C. F. Powell, A. L. Kastengren, and J. Wang, “X-Ray Measurements of the Mass Distribution in the Dense Primary Break-Up Region of the Spray from a Standard Multi-Hole Common-Rail Diesel Injection System,” Proceedings of the 21st ILASS - Europe Meeting 2007, 2007.

[19] Mark Linne, Megan Paciaroni, Tyler Hall, and Terry Parker, “Ballistic imaging of the near field in a diesel spray,” Experiments in Fluids, vol. 40, no. 6, pp. 836–846, Feb. 2006.

[20] Mark A. Linne, Megan Paciaroni, Edouard Berrocal, and David Sedarsky, “Ballistic imaging of liquid breakup processes in dense sprays,” Proceedings of the Combustion Institute, vol. 32, no. 2, pp. 2147–2161, 2009.

[21] Abdullah Adam, Tomoaki Yatsufusa, Tomonori Gomi, Nobuyuki Irie, and Yoshiyuki Kidoguchi, “Analysis of Droplets Evaporation Process of Diesel Spray at Ignition Delay Period using Dual Nano-spark Shadowgraphy Photography Method,” SAE Paper, 2009-32-0017, 2009.

[22] Yasufumi Yoshimoto and Masayuki Onodera, “Performance of a Diesel Engine Fueled by Rapeseed oil Blended with Oxygenated Organic Compounds,” SAE Paper, 2002-01-2854, Oct. 2002.

Chapter 3 Image Analysis System

3.1 Introduction

Study on diesel engine spray has made researcher employed many different techniques and instruments. Each has its own advantages and disadvantages. Due to its non-intrusive nature, optical technique is currently considered the most used technique for diesel spray study. Furthermore, it can be use to study the macroscopic and microscopic aspect of the spray, with good temporal and spatial resolution[1][2].

In particular, a variety of optical systems for spray analysis has been developed in recent years; with its own advantages and limitations. Some of these technique can be difficult to implement, and also can be very expensive[3]. In addition, high level of operator skill is also needed to be successfully applied.

Most of the data obtained from optical technique are generally in image form. This required the raw image to undergo some kind of image analysis procedure before useful data can be obtained. Study that used optical imaging technique shows that a reliable image analysis system is required for a high reproducibility[4]–[8].

3.2 Image Analysis Technique

Although it has been proven in Chapter 2 that optical technique can be used to obtain macroscopic and microscopic spray structure and characteristic, the quality and the accuracy of the results are however very dependent on the analysis method. This section will explain the image analysis technique used in this study.

An optical imaging technique was employed in this experiment. This include nano-spark unit (as a light source, similar function as photography flash unit) allowing the spray droplet to be captured at the point and time where knowledge of their size and distribution is required. In this research analysis of the captured image has been done to quantify the macroscopic and microscopic characteristic including tip penetration, droplet size, droplet distribution and dynamic behavior, and also diesel spray liquid and vapor phase distribution.

To do so, strict procedure with the help of dedicated image processing software has been developed. The end result obtained from this image analysis technique under various spray condition demonstrate that it is capable of producing accurate, consistent and efficient results. Next, the detail procedures and consideration made on the image analysis technique used throughout the experiment will be explained.

3.3 Spray Image Digitization

First, spray images were recorded on normal black and white photographic film (Fuji Neopan ASA400) by a magnification factor of 3.5 using a still camera (Pentax, 6x7) which translates to area coverage of about 16x20cm. The images were then scanned by CCD scanner (EPSON GT-X970) at high resolution of 3200dpi (equivalent to around 2.2 μm/pixel) and 16bit (65536 gradations) as a TIFF file format. Analysis of the images was then made by using dedicated image analysis software (WaveMetrics IGOR Pro 6) with custom made algorithm.

3.4 Droplet Images Features Extraction

The first stage of the processing algorithm is to extract droplets image from background images. The background of a spray photograph has a heterogeneous gray level due to noise, light fluctuation of the illumination source and the film developing process. In this work, spray photographs were developed with special care to obtain a homogeneous background, nevertheless background heterogeneity was still observed on the photography plate.

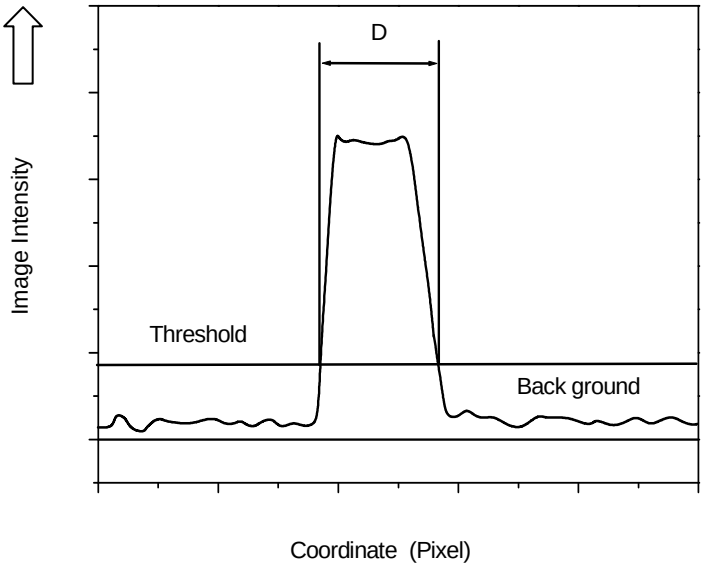

Fig.3-1 Thresholding level effect on a droplet size

In this case, the image of sprays must be thresholded during the image analysis. As can be seen in Fig.3-1, it can be said that if the thresholding level is extremely high, the measured diameter of droplet will be smaller than the real size and if it is extremely low, a halo around the droplet image will be added to the droplet image and the measured diameter of the droplet will be larger than the real diameter.

Threshold level for processing binary image was acquired following below mathematical equation:

$$Threshold = (Avg\_intensity - Min\_intensity) * \alpha + Min\_intensity \quad (1)$$

Referring to equation (1), *Avg_intensity* represents average intensity value throughout the image while *Min_intensity* represents minimum intensity value for the image. While α is the base threshold value (with a value of 0.8). Fig.3-2 shows original TIFF image and its extracted binary image of droplets, which show the ability of this algorithm to generate suitable binary image for further process. From the binary image, location of the possible droplets images can be detected and an algorithm will analyze the images to acquire the gravity center of each of the possible droplets image. Later, the different levels of gradient intensity of droplets image was utilize for droplets position and size detection.

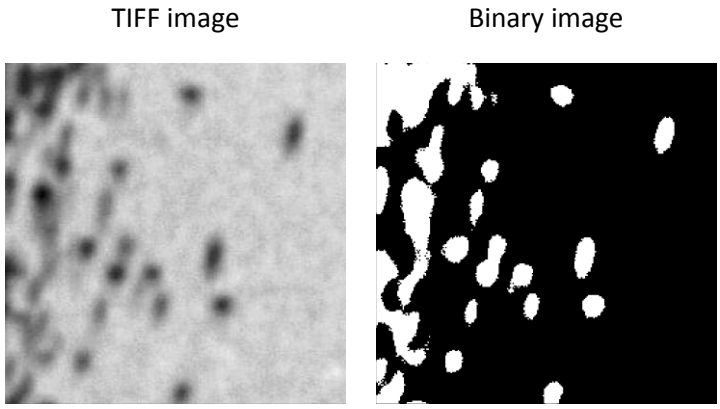

Fig.3-2 Original image and binary image

3.5 Droplets Characteristics and Labeling

Apart from the binary image made from the original TIFF image, a gradient image is also made. An image gradient is a directional change in the intensity or color in an image and could be used to extract information from images. This was made to assist the droplet sizing algorithm and will be explain in detail later.

From the processed binary image, possible spray droplets are extracted by IGOR standard *ImageAnalyzeParticle* function. Droplets gravity center was then acquired by the program. Next, each extracted possible spray droplet (where the droplet gravity center has been confirmed) undergo processing which calculate pixel intensity for 50 pixels from the center point toward outside of the center gravity. Fig.3-3 shows droplet image intensity

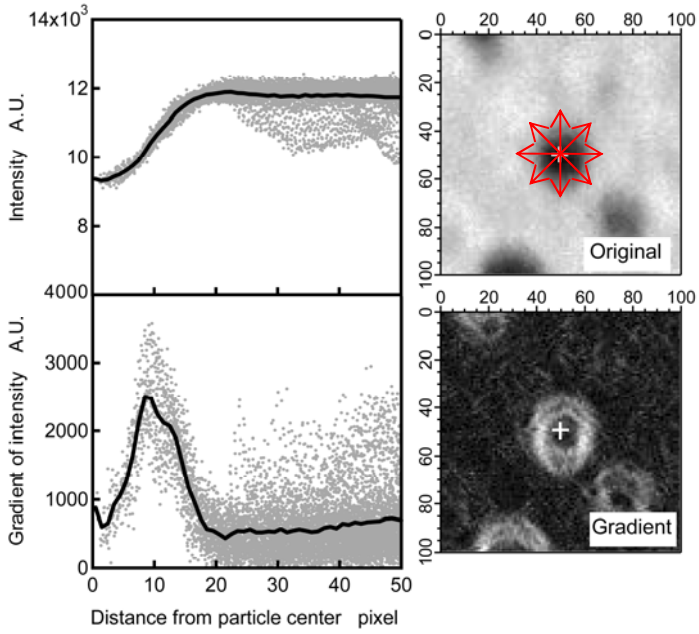

Fig.3-3 Intensity and gradient intensity profiles

profile for TIFF image (upper part) and gradient image (lower part).

The solid line is the averaged intensity value while the gray dot is the calculated intensity for every pixel. The averaged intensity value is at more importance as it omits noise and error from the image intensity profile. As shown in the figure, droplet averaged image intensity profile for the TIFF image shows increasing value with distance from particle center. After reaching the peak which suggested the droplet outer perimeter, the intensity value plateaued and remains the same. This kind of intensity profile is difficult to manipulate for droplet image characteristic and sizing.

When compared to TIFF droplet image averaged intensity profile, the averaged droplet image gradient intensity profile peaked at around the outer droplet perimeter and afterward decreases with distance, until reaching minimum intensity where the line plateaued. This is easier to manipulate as the droplet perimeter can be confidently measured due to the profile unique characteristic. However, further consideration and processing has to be made to make sure correct measurement.

Fig.3-4 shows gradient image intensity profiles of a single droplets image. From the graph, highest peak of gradient intensity shows maximum intensity (*Max*) value for the image while average intensity value can be acquired by calculating the total intensity value measured throughout the pixel image calculation (*Avg_OUT*). Other valuable information acquire from the gradient intensity profile are lowest minimum intensity at droplet center (*Min_ IN*) and lowest minimum intensity at droplet outer perimeter (*Min_OUT*). Perimeter of

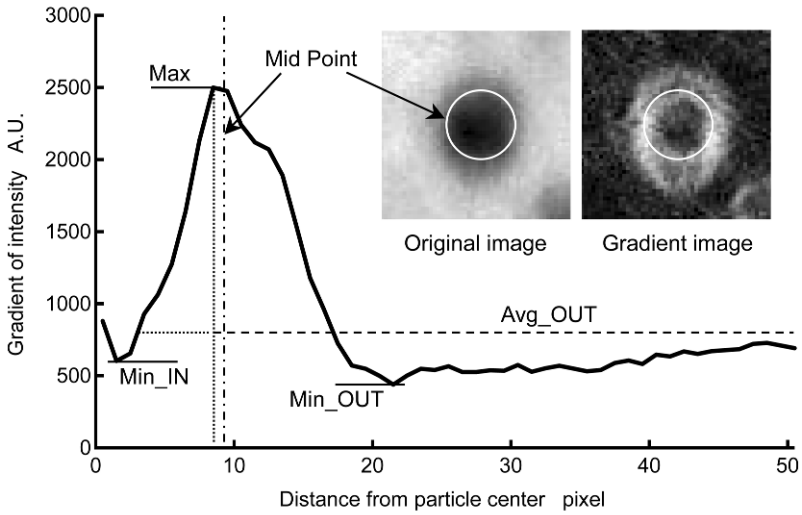

Fig.3-4 Details of intensity gradient profiles

the droplet then is approximated and labeled as Mid Point (*MP*), which is acquired by selecting the next peak (after *Max*) of the gradient intensity value which above the average intensity (*Avg_OUT*) .

3.6 Droplets Images Confirmation Method

During the droplets image analyzed process, not all the droplets images acquired are in fine round shape as shown in Fig.3-4. In some cases, irregular droplets images as shown in Fig.3-5 can frequently be found during the analysis process. Therefore, these droplets images must be further analyzed before it can be accepted as droplets image.

Comparing Fig.3-4 to Fig.3-5, different shape of gradient intensity can be utilized for droplets images confirmation method. Below shows mathematical equation applied in this algorithm to confirm the gradient intensity shape was within the acceptable value as a droplet or should be exclude from analysis.

$$Ratio\_IN = \frac{Max - Min\_IN}{Max - Min\_OUT} \quad (3)$$

$$Ratio\_OUT = \frac{Avg\_OUT - Min}{Max - Min} \quad (4)$$

Here, *Min* represents lowest intensity either *Min_IN* or *Min_OUT*. From above equation, shape of the gradient intensity peak can be determined. Large value of *Ratio_IN* or small value of *Ratio_OUT* shows that gradient intensity shape has high peak intensity value profiles and will be accepted as a droplet image by the algorithm. Meanwhile, small value of

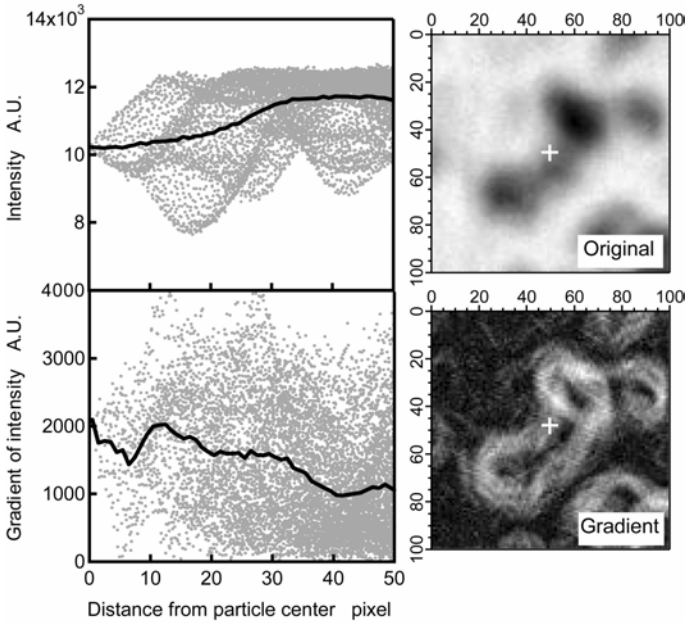

Fig.3-5 Gradient intensity profile on irregular shape of droplets

Ratio_IN or large value of *Ratio_OUT* shows the gradient intensity shape has no high peak and will not be selected by algorithm for further analysis.

Fig.3-6 shows schematic deviation of particle radius of droplet. Relative deviation was defined and used to recalculate the equivalent round image of droplet. Equation (5) is applied in this algorithm to finalize the irregular shape droplet image and calculate the equivalent round image. Referring to the equation (5), *r(ϑ)* shows distance from center gravity to droplet boundary, r_{ave} refers to average radius and n refers to numbers of analysis point taken at droplet boundary. Small value of *prdev* shows spherical shape of the droplet image.

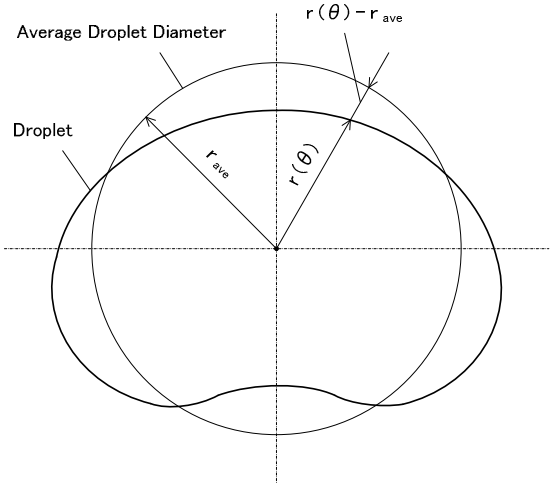

$$\boldsymbol{prdev} = \sqrt{\frac{\sum (\boldsymbol{r}(\theta) - \boldsymbol{r_{ave}})^2}{\boldsymbol{n}}}$$

Fig.3-6 Schematic deviation of particle radius

3.7 Droplets Size Measurement Calibration Method

Pre-experiment was done to collect comparison in order to build an algorithm which can measured spray droplets size inside spray images. Accordingly, similar size particle of sphere plastics was placed on the thin glass and was measured by using laboratory microscope. These plastic particle images were captured at magnification factor of 4 by

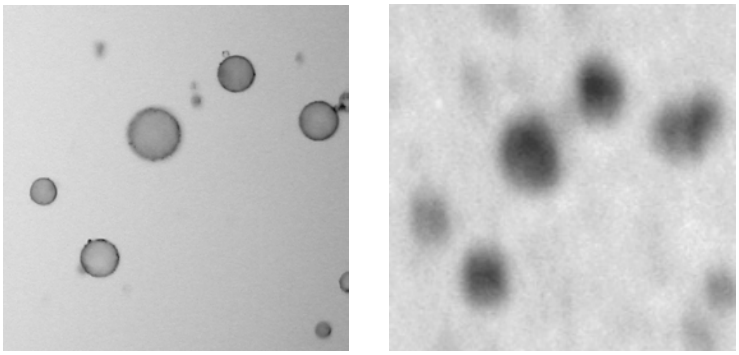

Microscope Pentax67 macro 135mm

Fig.3-7 Comparison of the particle images

microscope lens and by Pentax67 135mm macro lens at actual experiment setting.

Fig.3-7 shows sample of comparison images of plastic particle (left) and fuel spray images (right). As can be seen at Fig.3-7, plastic particle images taken by microscope show clear sphere image and sharp edge of each particle, meanwhile images taken by Pentax67 135mm lens shows blurred images with edges that were not as sharp as the microscope lens. Also the image from Pentax67 135mm lens seem to capture a noisier background image that make the observation and confirmation of area of interest, in this case the sphere shape

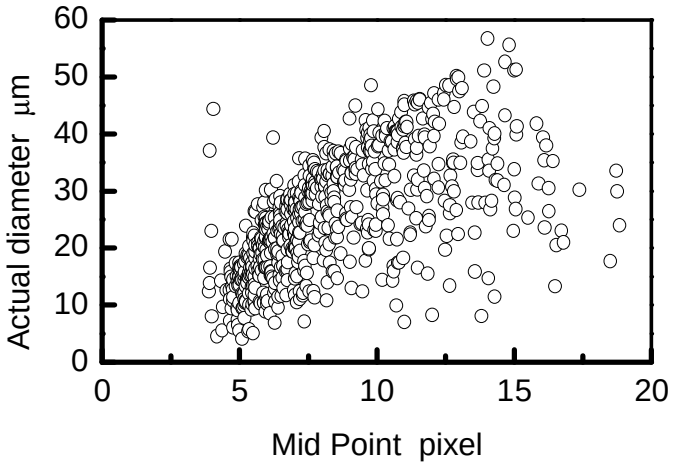

Fig.3-8 Correlation between Mid Point and actual diameter of particles

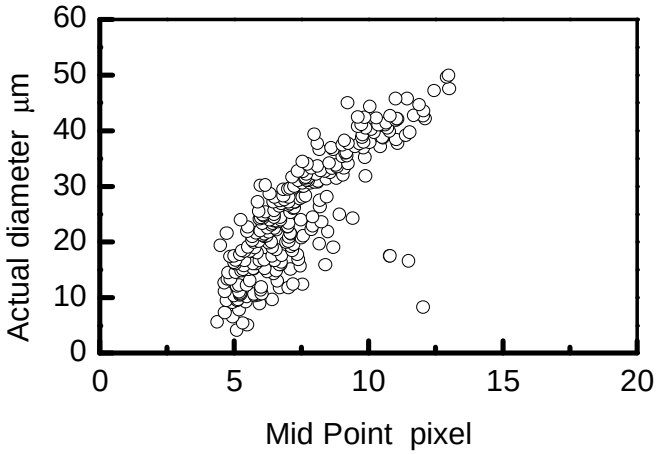

Fig.3-9 Correlation between Mid Point and actual diameter of particles filtered by *Ratio_IN*, *Ratio_OUT*, and *prdev*

more difficult. This is due to the limitation capability of Pentax67 135mm lens.

The particle images taken by microscope were measured by using the algorithm. At least 1000 particles samples were measured its size and position and the data was compared to same particles samples images taken by Pentax lens. Fig.3-8 shows correlation between Mid Point of each particle image and actual diameter of particle measured with microscope images and lens images. As can be seen in Fig.3-8, scattered data correlation can be seen forming a curve pattern inside graph. However, at the same time, many unwanted data was picked up and measured show the algorithm was no so reliable. Therefore, mid point calculation data must be stringent and the unwanted data must be removed in order to increase the accuracy of the program algorithm so the algorithm becomes reliable for fuel droplets measurement. As a result, any data which was not fulfill the acceptable value of 0.6

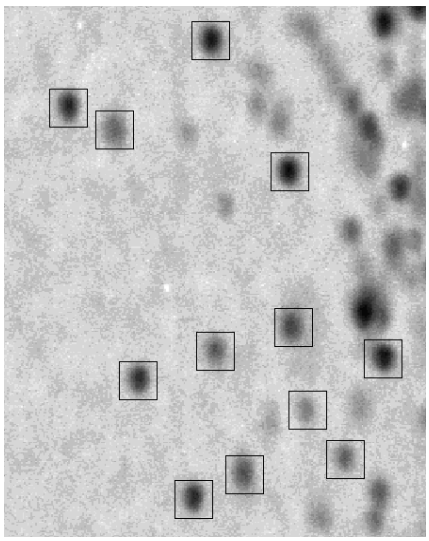

Fig.3-10 Example of the elimination of miss-detected particles

above for *Ratio_IN*, less than 0.3 for *Ratio_OUT* and less than 1.5pixel for *prdev* will be exclude from analysis and was not considered as droplets.

The re-calculation result was shown in Fig.3-9. Data correlation formed a detectable curve line thus and the unwanted data were excluded from the result. The examples of data pick up and elimination of miss detected particles was shown in Fig.3-10. As shown in Fig.3-10, only clear shape and stand alone particles were picked up inside box while unclear shape and daubs particle at right upper edge of images was exclude from analysis.

3.8 Calibration of Droplets Position within Focal Depth Region

Since the actual spray is in three dimension geometry, changes in term of the droplets/particle characteristics as it becomes out of focus, (when its position not inside focal depth region) are among an important factor to be considered in the algorithm. Accordingly, the in-focus particle images appears to be sharp and clear while out of focus particle images appears to be blur and hard to recognized. When particle are inside the focal depth region, its image has a high image intensity gradient around the image boundary thus it has a clear image. However, when it is not inside (either in front or backside) the focal depth region, its image intensity decreases and unclear image can be seen on the photograph. The effect of particle position with regards to the focal depth on particle images was examined using the algorithm and the result is shown in Fig.3-11.

As shown in Fig.3-11 particles were set at position of 0.5mm, 1.5mm and above 1.5mm offset from focal point (center of focal depth region). The correlation results shows that at 0.5mm offset from focal point, Mid Point measurement value are leaning toward actual particle diameter and shows that at 0.5mm offset from focal point, the algorithm

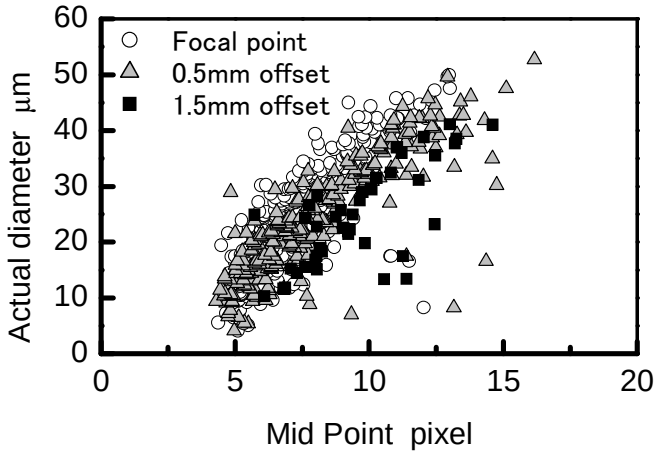

Fig.3-11 Effect of deviation from focal depth on correlation Mid Point and particles actual diameter

measurement still has high accuracy and reliable. Meanwhile, at 1.5mm offset from focal point, Mid Point measurement shows larger value compared to actual diameter size. As a result, the number of particles selected for analysis by the algorithm also reduced thus lowered the accuracy to the measurement. Meanwhile, particles position at above 1.5mm offset from focal point were considered not reliable for analysis and successfully not selected by the algorithm.

Referring to Fig.3-8, correlation between Mid Point particle measurement and actual particle diameter measured by the algorithm formed a stable curve line at large size particles (on top) while scattered and unsteady curve line was formed at smaller size particles area (bottom). Moreover, at large Mid Point value of 12-13pixel include small range of particles size from 45-50μm where at small Mid Point value of 5-6pixel include large range of particles size from 4-25μm. This reveals that small size particles measurement has tendency to increase the measurement error.

Fig.3-12 shows error ratio versus actual diameter graph plotted using specifically small Mid Point value of 4-5pixel and 5-6pixel which concentrate on small size particles. Referring to Fig.3-11, measurement on a particle which size at around 10μm shows a measurement error ratio at almost 40% shown by ○ symbol inside Fig.3-12. The error was too big and cannot be accepted in the algorithm. However, in order to reduce error, the number of particles selected for analysis must be increased. Left side of the graph in Fig.3-12 shows minimum particle number needed in order for the error ratio to be less than 5%. As a results, as shown by △ symbol inside Fig.3-12, more than 60 numbers of particles must be selected in case of small particle size around 10μm in order to lessen the error ratio at 5%.

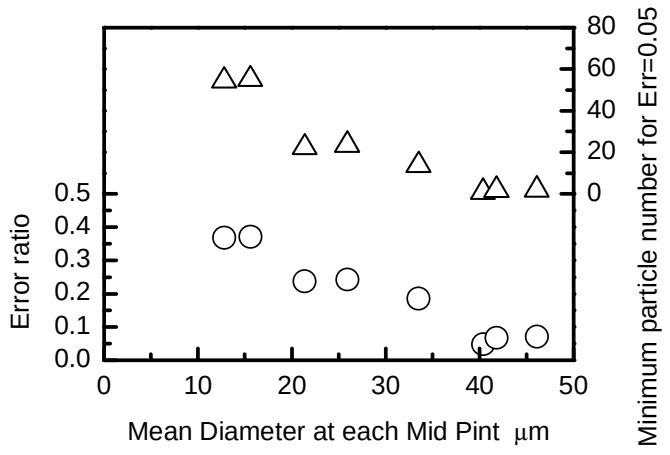

Fig.3-12 Relation between accuracy of particle diameter measurement and particle diameter

3.9 An Absolute Coordinate

As dual nano-spark shadowgraph photography captures 2 individual images in two different still cameras with a time interval, an absolute coordinate is one of the crucial points in this image analysis technique. This is due that coordinate of each droplets and spray figure need to be determined and then related in order to gain parameters such as velocity and flying angle. To obtain absolute coordinates, absolute point or reference is required. In this research, three set of needles (as reference point) are positioned at each observation area (upstream, midstream and downstream). Fig.3-13 show image example of scale with needles at left side and spray with needles at right side for midstream section.

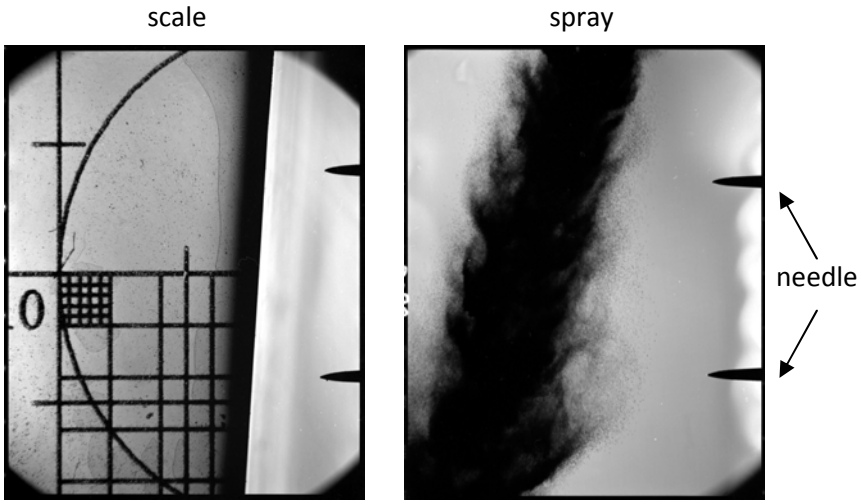

Fig.3-13 Example of spray and scale with reference needle

From the image, origin point (0,0) in pixel unit is located at upper left of the image. Coordinate increase from left to right (X-axis) and up to down (Y-axis). Coordinate of image from camera 1 and camera 2 to will be referred as $\mathbf{P}_{cm1}(x_{cm1}, y_{cm1})$ for camera 1 and $\mathbf{P}_{cm2}(x_{cm2}, y_{cm2})$ for camera 2, respectively. An absolute coordinate $\mathbf{P}_{abs}(x_{abs}, y_{abs})$, refers to the coordinate (0,0) in mm unit, is located at the middle of the spray chamber, increase to right (positive X-axis), up (positive Y-axis), left (negative X-axis) and down (negative Y-axis). Transformation including parallel movement, rotation, scaling (expansion and contraction) of one location $\mathbf{P}_0(x_0,y_0)$ to another location $\mathbf{P}_1(x_1,y_1)$ using linear transformation matrix of **A**, can be explain by these coefficient as shown below.

$$\begin{pmatrix} x_1 \\ y_1 \\ 1 \end{pmatrix} = \begin{pmatrix} a & b & c \\ d & e & f \\ 0 & 0 & 1 \end{pmatrix} \begin{pmatrix} x_0 \\ y_0 \\ 1 \end{pmatrix} \qquad (4\text{-}1)$$

Firstly, the algorithm will overlap image of camera 2 to image of camera 1 and calculate the matrix transformation of $\mathbf{P}_{cm2s}$ (camera2: scale and needles) to $\mathbf{P}_{cm1s}$ (camera 1: scale and needles), by referring to the scale vertical and horizontal lines, and also the needle contour. The algorithm will perform multiple (parallel, rotation, scaling) transformation process and calculate the smallest possible matrix $\mathbf{A}_{cm2s>cm1s}$.

$$\mathbf{P}_{cm1s} = \mathbf{A}_{cm2s>cm1s}\mathbf{P}_{cm2s} \quad (4\text{-}2)$$

Then, the algorithm will find the relative matrix transformation $\mathbf{A}_{cm1s>abs}$ between $\mathbf{P}_{cm1s}$ (camera 1: scale and needles) and absolute coordinate $\mathbf{P}_{abs}$.

$$\mathbf{P}_{abs1} = \mathbf{A}_{cm1s>abs}\mathbf{P}_{cm1s} \quad (4\text{-}3)$$

Next, the spray and needles images will be align to each other. The algorithm will overlap image of camera 2 to image of camera 1, and then perform matrix transformation $\mathbf{A}_{cm2>cm1}$ by referring to the needle location using parallel and rotation transformation, also with scaling transformation previously obtain by $\mathbf{A}_{cm2s>cm1s}$ as in (4-2).

$$\mathbf{P}_{cm1} = \mathbf{A}_{cm1>cm1}\mathbf{P}_{cm2} \quad (4\text{-}4)$$

Lastly, the algorithm will define the matrix transformation between $\mathbf{P}_{cm1}$ (spray and needles) and $\mathbf{P}_{cm1s}$ (scale and needles) and calculate the matrix transformation $\mathbf{A}_{cm1>cm1s}$ as below:

$$\mathbf{P}_{cm1s} = \mathbf{A}_{cm1>cm1s}\mathbf{P}_{cm1} \quad (4\text{-}5)$$

By performing transformation process from (4-1) to (4-5), the absolute coordinate for image from camera 1 and camera 2 can be derived by using the procedure below:

$$\mathbf{P}_{abs1} = \mathbf{A}_{cm1s>abs1}\,\mathbf{A}_{cm1>cm1s}\mathbf{P}_{cm1} \quad (4\text{-}6)$$

$$\mathbf{P}_{abs2} = \mathbf{A}_{cm1s>abs1}\,\mathbf{A}_{cm1>cm1s}\,\mathbf{A}_{cm2>cm1}\mathbf{P}_{cm2} \quad (4\text{-}7)$$

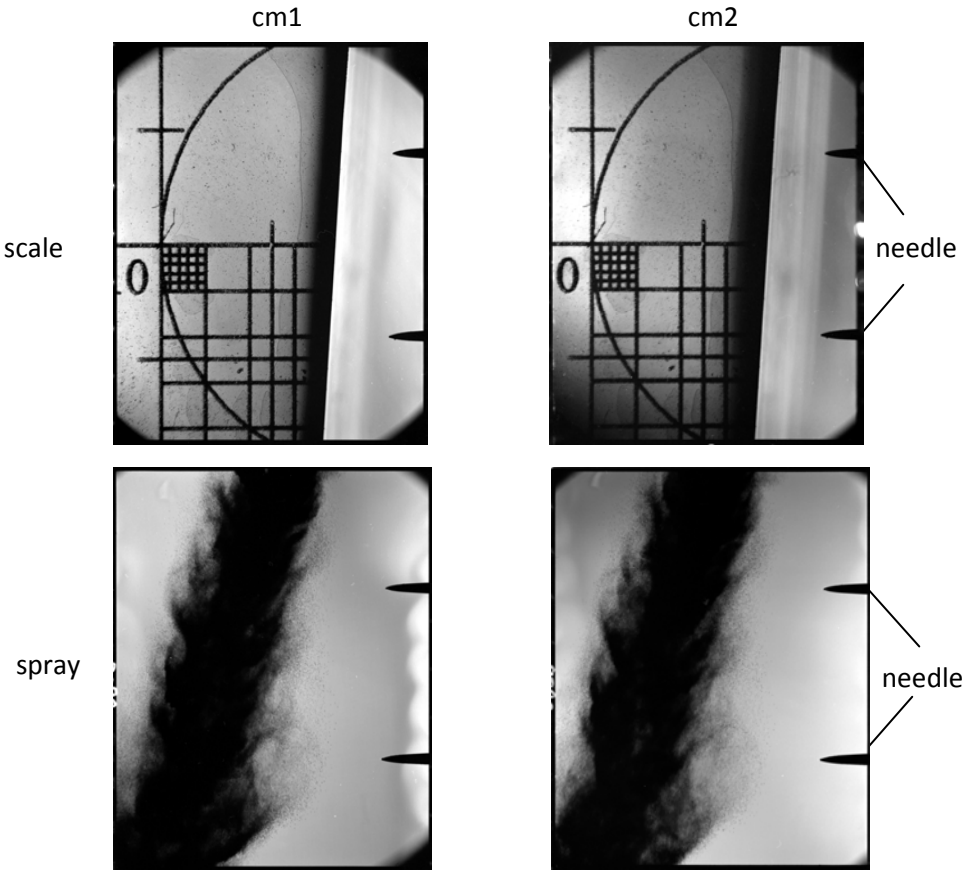

Fig.3-14 Reference needle in scale and spray image for camera 1 and camera 2

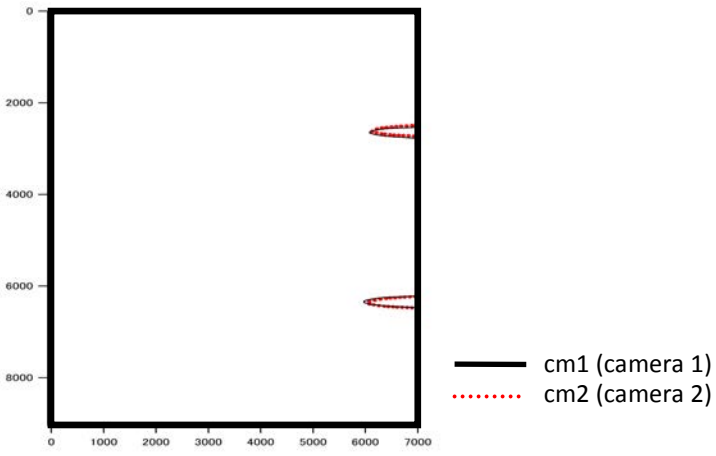

Fig.3-15 Extracted needle overview

Referring to matrix transformation above (4-6) and (4-7), both matrix include same value of Acm1s>abs1 thus the alignment error will only be cause by Acm2>cm1. This is minimal since camera 2 position is fixed throughout the experiment. Fig.3-15 shows the extracted needle location from Fig.3-14 that have been aligned and prove that this algorithm function as per required.

3.10 Droplets Velocity and Flying Angle Measurement

After using the algorithm to align images from camera 1 and camera 2 (to the absolute coordinate), pair droplets (droplet that considered being the same exact droplet in camera 1 image and camera 2 image) were searched. Then, by calculating the difference between the locations of the droplet in camera 1 to its new locations in camera 2, the droplet dynamic velocity and flying angle can be measure.

3.11 High Density Region Extraction Method

Another interesting characteristic of diesel engine spray is the vapor and liquid phase distribution, and its dynamic behavior (progression). Study on this characteristic is believed could help deeper understanding of spray atomization process which is currently not fully understood. However, this aspect of diesel engine spray has been very difficult to study due to numerous reasons such as the dense spray formation on the spray core and the identification and differentiation of liquid phase and vapor phase[9]. This section will explain the procedures on how the author uses custom made algorithm to extract each liquid phase (spray liquid core) and vapor phase.

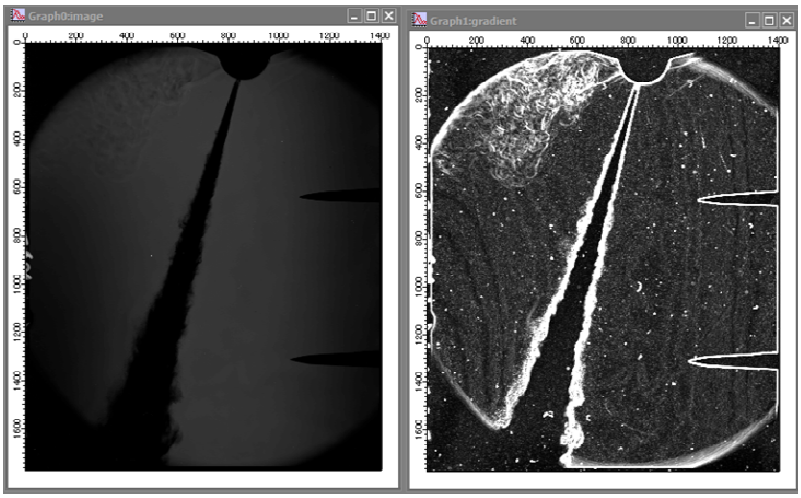

Fig.3-16 Gradient image produced from original TIFF image

First, the original digitalized image will be change to gradient image as shown in Fig.3-16. This will facilitate the next procedure where the gradient image will then change to binary image using an initial threshold value. This procedure is similar to that of the droplet detection.

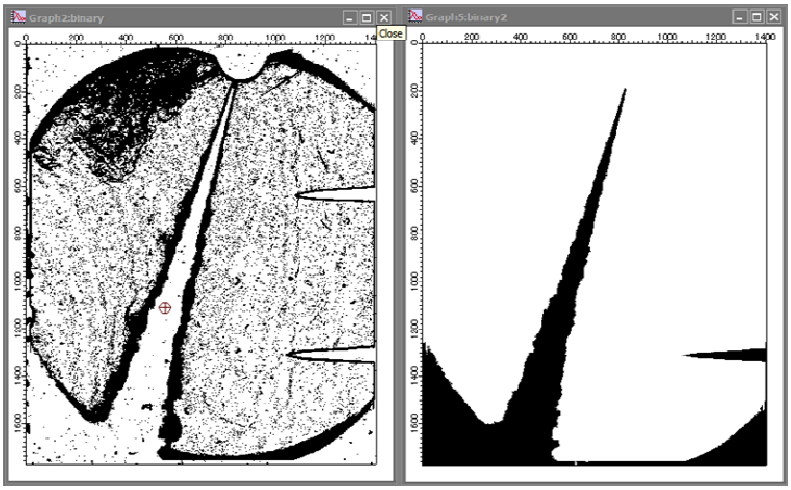

Fig.3-17 Liquid phase binary image extracted from the initial binary image

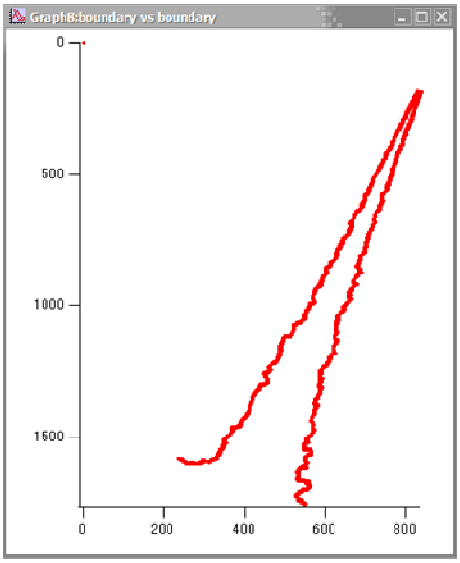

Fig.3-18 Liquid phase boundary extracted from binary image

After the binary image is generated, the author then will ask the algorithm to select the liquid phase of the spray. The algorithm will then try to separate the liquid core and the vapor core by analyzing each pixel by comparing it to the neighboring pixel and search for a separation boundary. The extracted binary image will then be generated with only the spray liquid phase and relatively free of noise (unwanted pixel) as shown in Fig.3-17. However, this step consumes much time and sometimes the algorithm fail to produce good separation boundary between the liquid phase and vapor phase. Should this be the case, the analysis will need to be done again with a new threshold value for the first binary image extraction from the gradient image.

Later, the final binary image of the liquid phase will then be translated to coordinate plot as shown in Fig.3-18 (unwanted plot can be deleted) and ready to be combine with other result for a full spray analysis. As for the vapor phase extraction, similar procedures were used. But as the vapor phase exist on each side of the liquid phase; the separation boundary detection must be made for each side and combined afterward.

REFERENCES

[1] Koch, Schmid, and Leipertz, “INFLUENCE OF INJECTION NOZZLE PARAMETERS ON THE SPRAY PROPAGATION AND COMBUSTION IN A DI-DIESEL-ENGINE,” ICLASS 2006, Kyoto, Japan, 2006.

[2] H. Gen Fujimoto, H. Adachi, T. Yano, N. Marubayashi, T. Hori, and J. Senda, “Spatial Droplets Size Distribution in a Diesel Spray Taken by Photography with Super High Resolution,” ILASS – Europe 2010, 23rd Annual Conference on Liquid Atomization and Spray Systems, Brno, Czech Republic, September 2010, 2010.

[3] S. N. Soid and Z. a. Zainal, “Spray and combustion characterization for internal combustion engines using optical measuring techniques – A review,” Energy, vol. 36, no. 2, pp. 724–741, Feb. 2011.

[4] Hiroshi Hattori, Kikuo Narumiya, Mitsuhiro Tsue, and Toshikazu Kadota, “Analysis of Initial Breakup Mechanism of Diesel Spray Injected into High-Pressure Ambience,” SAE Paper, 2004-01-0528, 2004.

[5] Pekka Rantanen, Antti Valkonen, and Andreas Cronhjort, “Measurements of a diesel spray with a normal size nozzle and a large-scale model,” International Journal of Heat and Fluid Flow, vol. 20, no. 5, pp. 545–551, Oct. 1999.

[6] Marie Bysveen, Terje Almås, Kjell Arne Ulvund, Atle Jørgensen, and Frode Kvinge, “Development of a Shadowgraph Image Technique Describing the Fuel Spray Behavior in a Rapid Compression Machine,” SAE Paper, 2004-01-2934, 2004.

[7] D. Deshmukh, A. Madan Mohan, and R. V Ravikrishna, “Spray Characterization of Pongamia Pure Plant Oil in a High Pressure Chamber,” ILASS – Europe 2011, 24th European Conference on Liquid Atomization and Spray Systems, Estoril, Portugal, September 2011, 2011.

[8] T. F. Su, C. T. Chang, R. D. Reitz, P. V Farrell, A. D. Pierpont, and T. C. Tow, “Effects of Injection Pressure and Nozzle Geometry on Spray SMD and D.I. Emissions,” SAE paper, 952360, 1995.

[9] K. Nishida, J. Gao, T. Manabe, and Y. Zhang, “Spray and mixture properties of evaporating fuel spray injected by hole-type direct injection diesel injector,” International Journal of Engine Research, vol. 9, pp. 347–360, 2008.

Chapter 4 Comparison of Free Jet Spray between Diesel and Rapeseed Oil

4.1 Introduction

The atomization of liquids is a process of great practical importance. It affects the process in many branches of industry: mechanical, chemical, aerospace, metallurgy, medicine, agriculture. For different application, the spray is manipulated by changing the operating conditions to satisfy the requirement of the process. In order to understand how changes in operating conditions change spray characteristics, studies on the spray characterization and the basic physical mechanisms involved in the formation of spray have to be carried out.

Currently, the mechanisms of the diesel engine spray formation are not completely understood. Although there are break-up models reported to be the mechanism of spray break-up and atomization, details understanding on the actual process is still limited. Thus, the best way to understand the influence of different operation condition to diesel engine spray needed to be first characterized to provide necessary information for their applications.

This section will study spray structure of RO (rapeseed oil) by comparing it to GO (diesel fuel) to make clear spray characteristics of rapeseed oil. Fuels were injected using a single-hole nozzle with hole-diameter of d_n=0.18mm at an orientation angle of 15° from the injector centerline. The still images of spray were taken by shadowgraph technique, utilizing nano-spark light source; in which the spray was captured by still camera with the spray chamber was divided to 3 sections; each around 20 x 15mm in size with around 3.5 magnification ratio. Experiment parameter will compare the effect of injection pressure and also ambient temperature. It is known that these parameter has significant impact on spray development on diesel engine, thus it is believed that these same parameters should be take into consideration during this study.

The images then will be analyzed using a image analysis technique that was developed specially for this study. Results will provide details on spray macroscopic and microscopic characteristics. Parameter such as penetration length, droplet size distribution, droplet flying velocity and trajectory, can be measured from the high resolution images taken. These images also provide high density liquid core (region) and vapor phase (region).

4.2 Characteristics of Spray Structure and Droplet Formation

Fig.4-1 compares spray images taken at time t=0.5ms after start of injection (aSOI) under condition of ambient temperature T_i=298K and injection pressure P_{inj}=40MPa. As seen from the macro-scale structure of the two sprays, RO spray forms a stick-like structure. The so-called branching structure that derives from mainstream can be little observed at spray boundary as compared with GO spray. This is because RO has high viscosity nature. Furthermore, the penetration of RO spray is shorter than GO spray at this case. This is because RO is hard to emit a jet at start of injection, which will be further discussed later. As seen from the enlarged images at spray boundary, the droplets size formed by RO spray is bigger than that of GO spray and the number of droplets with RO spray is less than GO spray. The droplets size and their distribution as well as the stick-like spray structure indicate that the atomization of RO spray is worse than that of GO spray.

Fig.4-2 show same comparison as Fig.4-1 at higher injection pressure of P_{inj}=70MPa. High injection pressure produces great spray momentum and large injection rate that cause aerodynamic force. As seen from the macro-scale structures, spray penetration of RO fuel gets longer as compared with GO spray when injection pressure increases. High viscosity characteristics of RO produce high density and great momentum spray, which lengthens penetration. Branching structure that cannot be observed at P_{inj}=40MPa can be detected along the RO spray boundary at P_{inj}=70MPa. However, spray cone of RO spray has still narrow-angle. Micro-scale images at spray boundary show that high injection pressure produces fine droplets even in RO spray, especially at downstream of the spray.

Fig.4-3 compares RO and GO sprays at ambient temperature of T_i=700K higher than T_i=298K in Fig.4-1. Injection pressure is P_{inj}=40MPa same as Fig.4-1. When RO is injected into high temperature atmosphere, although spray penetration length changes little, spray cone angle gets greater especially at downstream of the spray and branching structure is clearly visible at spray boundary. In addition, the droplets of RO spray seem to be smaller size and more consistence diameter as compared with Fig.4-1. This is due to decrease of kinematic viscosity caused by higher ambient temperature. High ambient temperature is required to support atomization of RO spray.

Fig.4-4 shows sprays under condition of high injection pressure P_{inj}=70MPa and high ambient temperature T_i=700K. RO spray expands further from the center line especially at downstream of the spray forming a spray tip. In comparison with GO spray, spray cone angle of RO spray is small at upper stream of the spray. Magnified images at spray boundary

indicate that vapor phase can be clearly observed in GO spray; in contrast with GO spray, RO spray seems to be difficult to form vapor phase. It is hard to improve droplets evaporation for RO spray. RO has difficulty in evaporation due to extremely high distillation temperature. When RO is used in DI diesel engine, atomization can be improved by high injection pressure with high ambient temperature; however, it is hard to improve droplets evaporation, in particular, at light load operation.

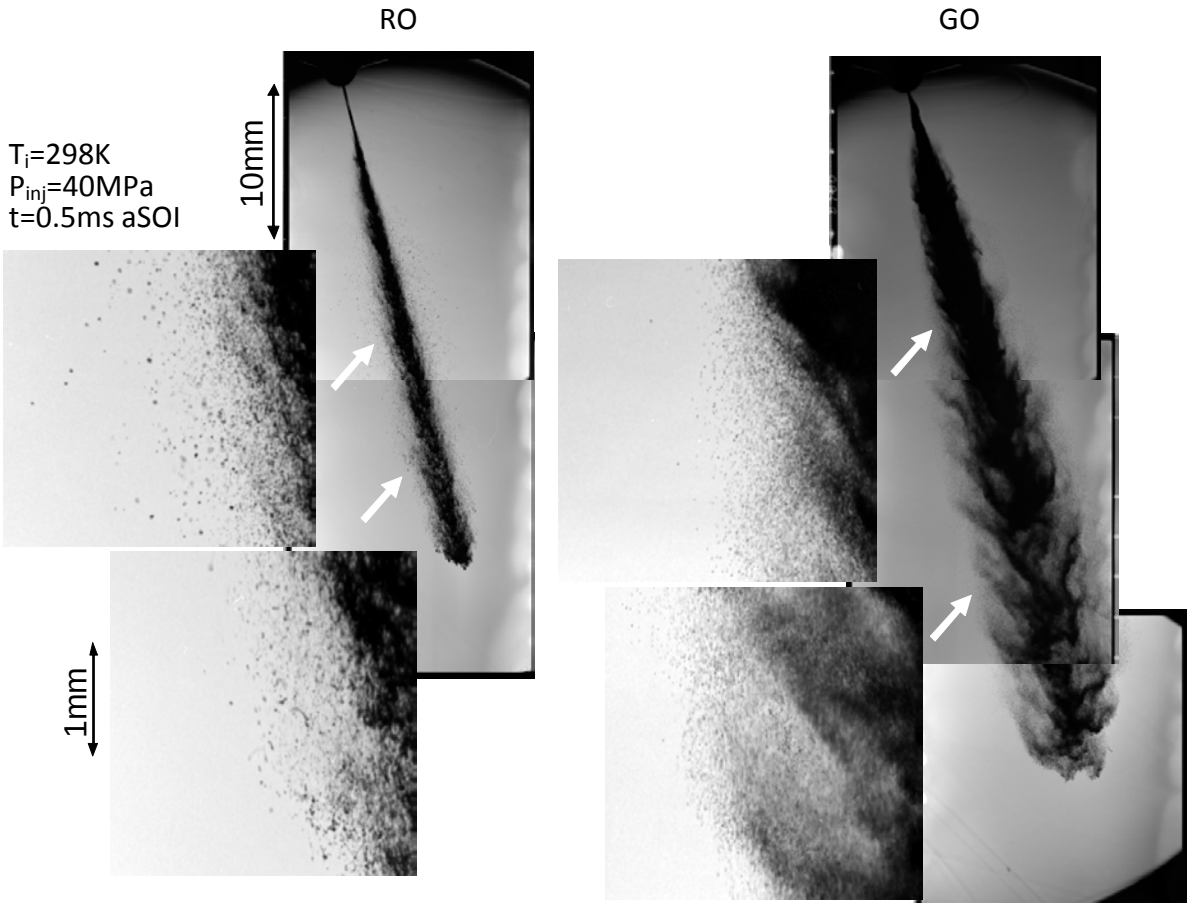

Fig.4-1 Comparison of spray structure and droplets between rape-seed oil and gas oil sprays (T_i=298K, P_{inj}=40MPa)

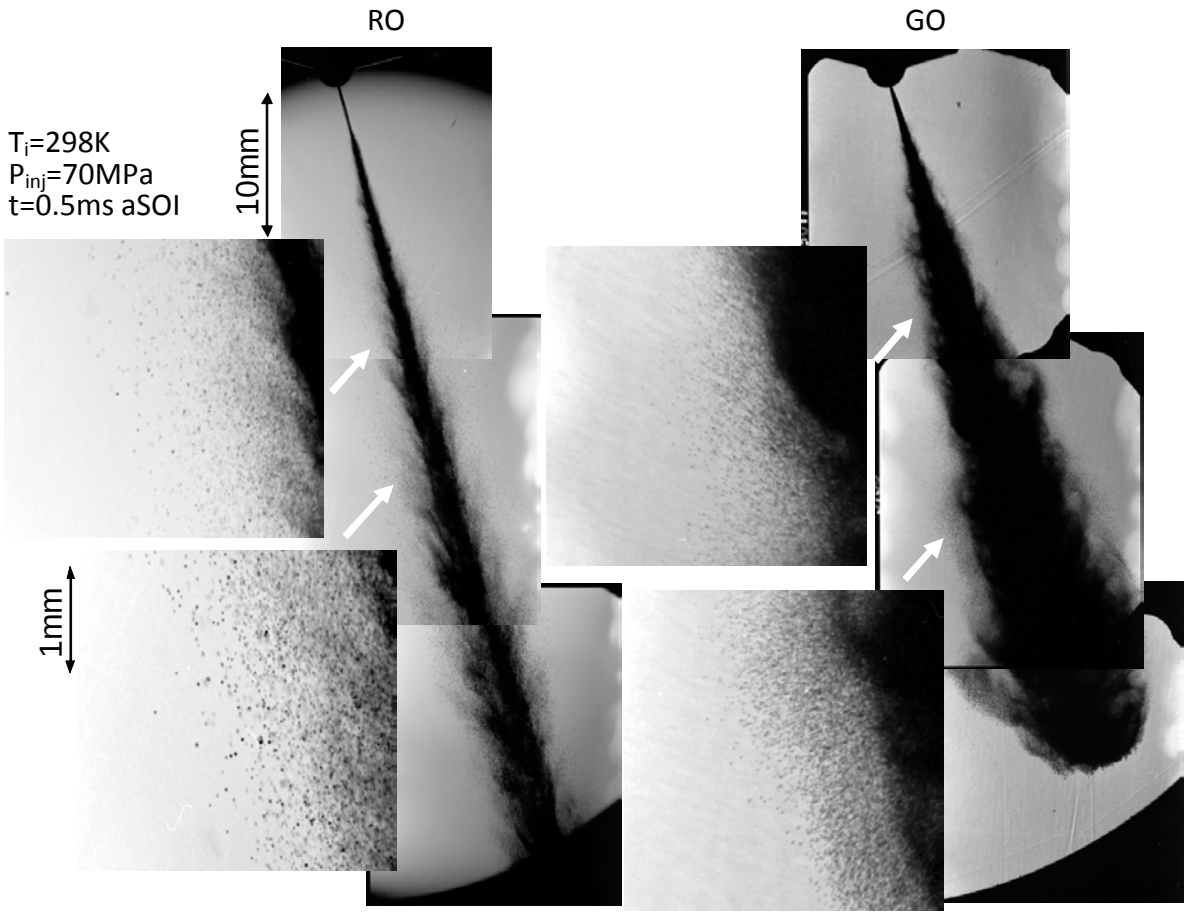

Fig.4-2 Comparison of spray structure and droplets between rape-seed oil and gas oil sprays (T_i=298K, P_{inj}=70MPa)

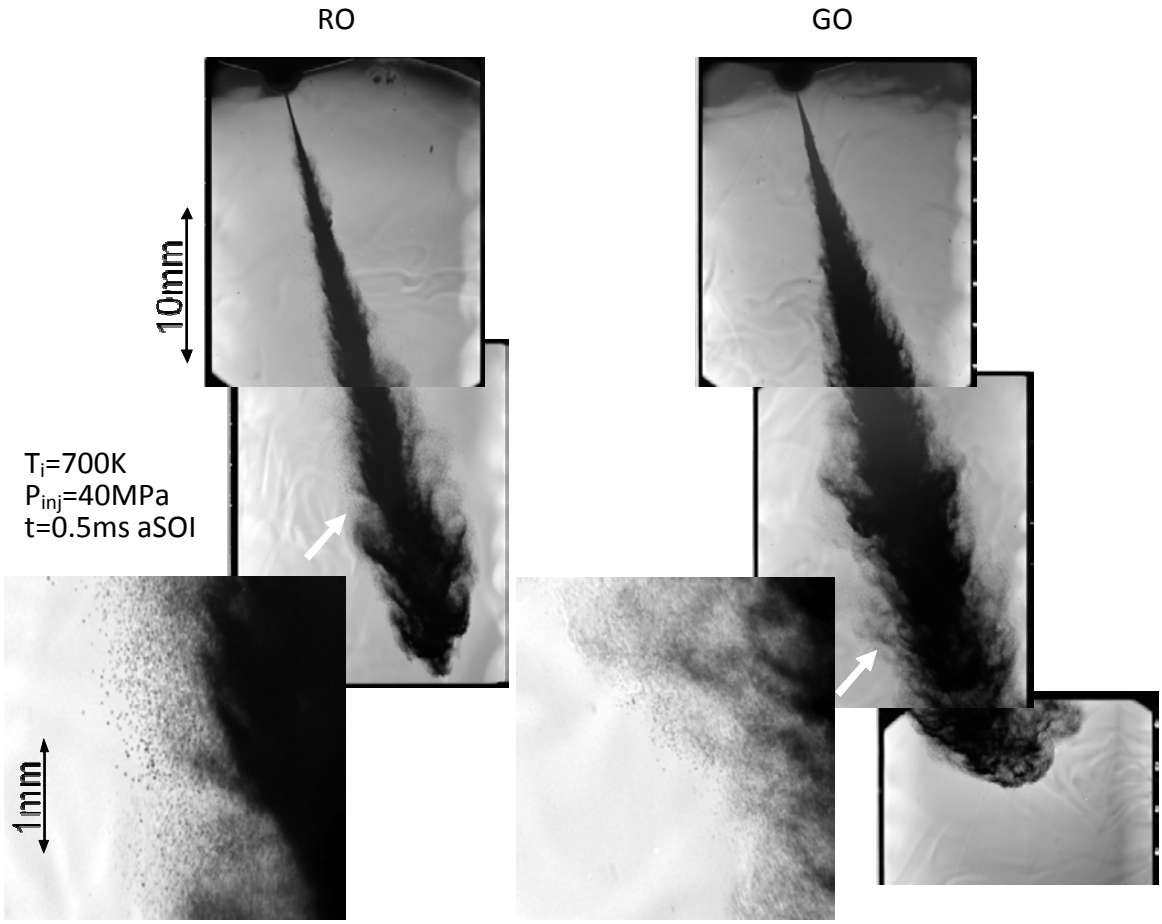

Fig.4-3 Comparison of spray structure and droplets between rape-seed oil and gas oil sprays (T_i=700K, P_{inj}=40MPa)

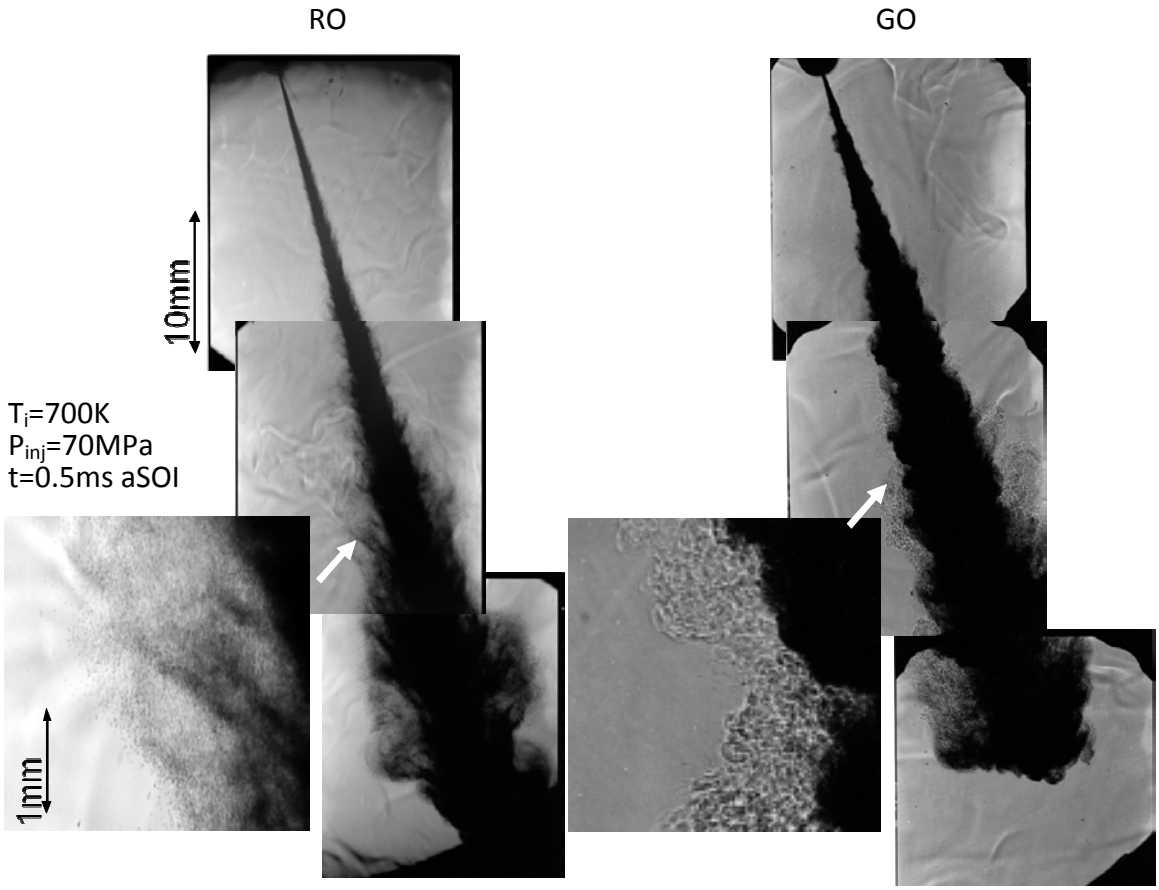

Fig.4-4 Comparison of spray structure and droplets between rape-seed oil and gas oil sprays (T_i=700K, P_{inj}=70MPa)

4.3 Droplet Distribution

To investigate further the atomization process of RO spray, droplets distribution captured by magnified images in Fig.4-1 to Fig.4-4 was quantified. Fig.4-5 to Fig.4-6 show the droplets size distribution. The analysis first divides spray length into 4 sections, 0-25%, 25-50%, 50-75% and 75-100% of spray length, then counts all droplets size D and number of droplets N at each section. All droplets diameters are characterized by representative grouping in every 5μm; for example, droplets with diameter from 15 to 20μm are arranged into group D=17.5μm and with diameter from 20 to 25μm into group D=22.5μm. Probability density distribution (PDF) of droplets diameter is calculated as the ratio of number of droplets in each diameter-group to total number of droplets along the spray.

Fig.4-5 compares PDF of droplets size between RO and GO sprays at condition of T_i=298K and P_{inj}=40MPa corresponding to Fig.4-1. GO spray shows similar PDF profiles from upstream (0-25% length) to spray tip region (75-100 length) with peak PDF at D=18μm. In contrast, droplets size distribution of RO spray is different at each section and droplets size is greater than that of GO spray. At section 0-25% length, most detected size of RO spray droplets is about 22μm. The peak PDF diameter is greater at 25-50% and 50-75% length. At spray tip region of 75-100% length, highest PDF is at about 37μm. This result suggests inferior atomization of RO spray. Poor spray development and atomization just after start of injection, which is shown in Fig.4-1, produce large size droplets at 0.5ms, in particular at downstream of the spray. It is important to reduce large-size droplets produced at early stage of injection because these droplets may have a bad influence on combustion and emission formation.

Fig.4-6(a) investigates effect of injection pressure on droplets distribution of RO spray at ambient temperature T_i=298K. As injection pressure increases, droplets size at upstream region of 0-25% length becomes smaller. Considering that droplets at early stage of atomization are formed at this region, high pressure injection improves initial atomization of RO spray to some extent. The droplets size at spray tip region of 75-100% length gets also smaller. Peak diameter of PDF at this region changes from 37μm at P_{inj}=40MPa to 25μm at P_{inj}=70MPa. However, RO spray droplets diameter is still larger than GO spray shown in Fig.4-5, and there remains a tendency that droplets diameter at peak PDF shifts larger size from upstream to downstream of the spray. It seems to be difficult to obtain enough atomization using high pressure injection only at low ambient temperature.

Fig.4-6(b) shows similar analysis as Fig.4-6(a) at high ambient temperature T_i=700K.

High ambient temperature promotes better atomization especially at downstream of the spray. Combination of high-pressure injection and high ambient temperature produces small droplets at peak PDF diameter less than 20μm along the whole spray boundary. Droplets diameter distribution of RO spray at T_i=700K and P_{inj}=70MPa is similar to that of GO spray at T_i=298K and P_{inj}=40MPa shown in Fig.4-5.

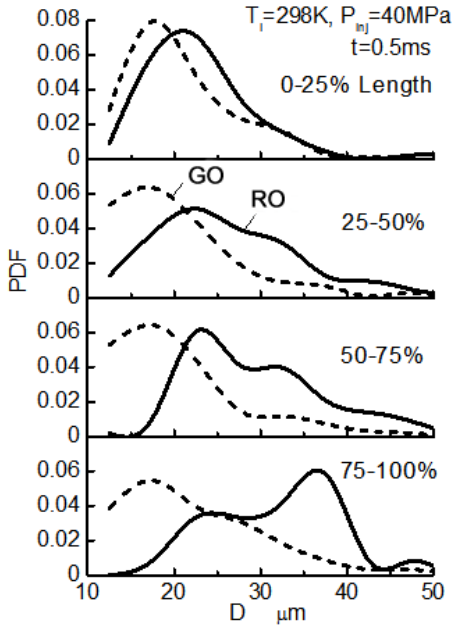

Fig.4-5 Comparison of droplets distribution between rape-seed oil and gas oil sprays (T_i=298K, P_{inj}=40MPa)

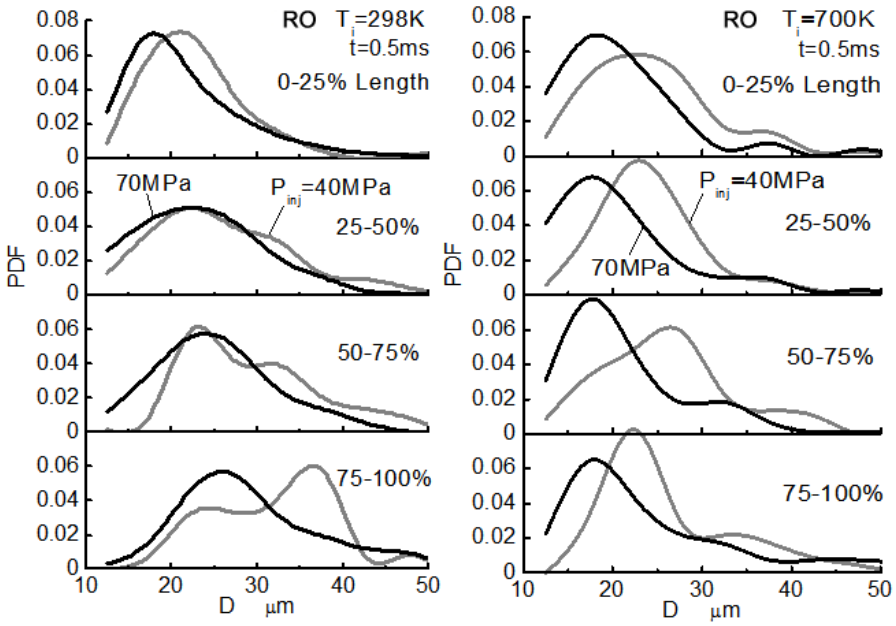

(a) T_i=298K (b) T_i=700K

Fig.4-6 Effect of injection pressure on droplets size distribution of rapeseed oil spray

4.4 Dynamic Behaviors of Evaporative Spray

Dynamic behavior of each fuel was also studied by using dual nano-spark method that takes succession pictures of the same spray by using different camera. The basic concept is equal to that of single nano-spark shadowgraphy. However, by using two nano-spark sources and two cameras, succession images of a single, same spray can be taken. Special optical arrangement and very precise setting was required; thus consume much time and great work. However, this enables the observation of droplets movement by comparing image from camera 1 to camera 2. Furthermore, the velocity and trajectory of the droplets can be calculated thus making the study of spray dynamic behavior possible. In addition, by using a custom made algorithm on image analysis software, the high density phase (liquid core region) and vapor phase can be extracted and observed. As many other researches only use high speed camera with low image resolution to study spray dynamic behavior, these results certainly will help deeper understanding on diesel engine spray dynamic behavior for the test fuel, GO and RO. In addition, the high density phase and vapor phase analysis can provide details insight on the atomization and vaporization process.

4.4.1 Diesel Spray

Fig.4-7 shows GO spray image and its analysis at T_i=298K, P_{inj}=70MPa, t=0.50ms aSOI (after start of injection), taken by dual nano-spark shadowgraphy and time interval between nano-spark 1 to 2 is Δt=25μs. Fig.4-7(a) shows the original images, (b) shows the droplet vector calculated by comparing the image from camera 1 to camera 2, (c) shows the averaged droplet flying velocity and (d) shows the averaged droplet flying angle. Fig.4-7(b) y axis shows the spray travel distance with Z_{sp}=0 equal to nozzle tip. The analysis first divides spray length into 4 sections, 0-25% (upper), 25-50% (middle), 50-75% (lower) and 75-100% (tip) of spray length for notation purpose. In Fig.4-7(c) and (d), for Z_{sp}=0 to 60mm, each 10mm is divided into individual sections, with the averaged value is calculated for each section. The flying angle is considered to be 0° along the x axis, with positive value clock-wise. Error bar shows the standard deviation.

From the vector line shown in Fig.4-7(b), it can be seen that the droplets in the middle and lower section of the spray moving outward from the spray boundary, meanwhile the droplets in the upper section is moving inside toward the spray body. This can be confirmed by observing the droplet flying angle graph in Fig.4-7(d), as the section of Z_{sp}=0~20mm shows negative value. Droplets of the upper section, which subjected to atomization for a longer duration, has smaller diameter and easier to be influence by air

entrainment due to small kinetic energy compared to droplets of the medium and lower section. This made the upper section droplets seem to be sucked into, or entrained into the spray body. In comparison, the middle and lower section droplets formed after the formation of spray body thus having a bigger kinetic energy fly outward.

Fig.4-8 shows image analysis of high density liquid phase and vapor phase taken by dual nano-spark photography at T_i=500K, P_{inj}=70MPa and t=0.50ms (aSOI). The 4 lines shows high density liquid phase and vapor phase with the former dictated by red line and the later by blue line. Furthermore, the darker color represent analysis image from camera 1 (1^{st} spark) and the lighter color for camera 2 (2^{nd} spark). From the figure, it can be observe that the vapor phase become large at spray tip section. This characteristic cannot be seen in the upper and middle spray section. It is believed that compared to the upper section, larger spray droplets at the spray tip section with relatively high velocity that is continuously formed and then vaporized, made the vapor phase in this section become larger.

Fig.4-9 shows the condition at T_i=700K, P_{inj}=70MPa and t=0.50ms (aSOI), similar to Fig.4-8 with different on the temperature. When compared to T_i=500K, it can be observed that the vapor phase on the spray tip region become more large. In addition, the high density liquid phase that existed in the spray tip region at T_i=500K can be seen quickly vaporized, making the spray penetration shorter.

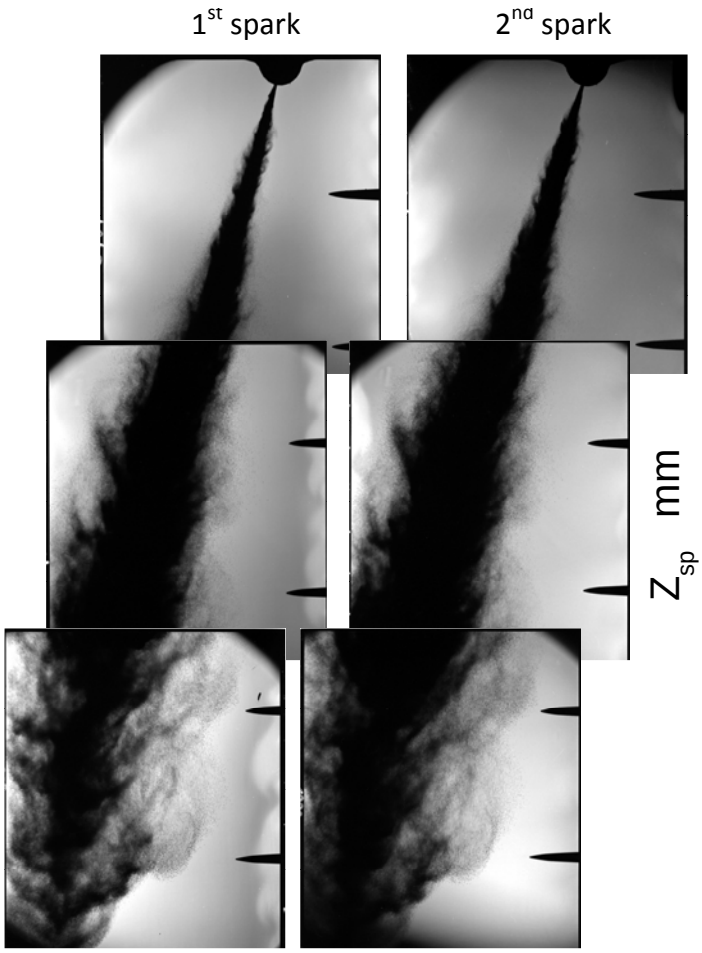

(a) Original spray image

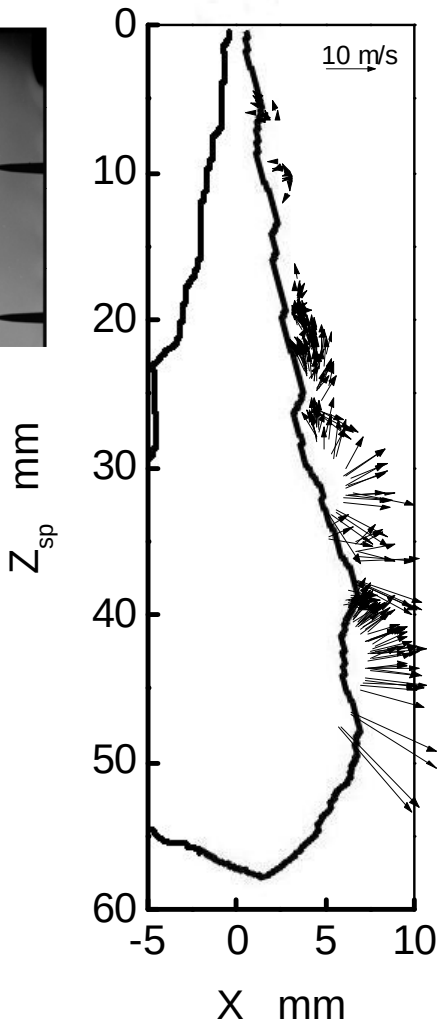

(b) Droplets vector

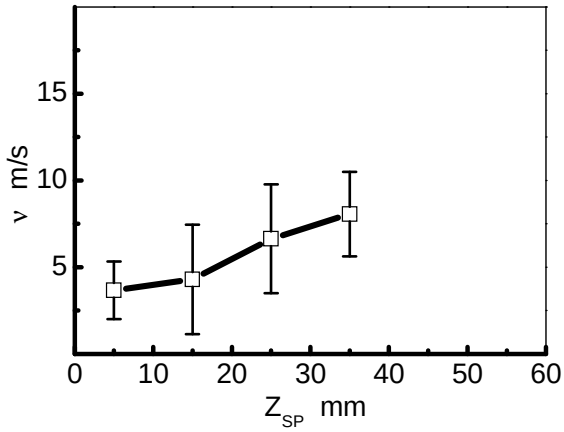

(c) Droplets flying velocity

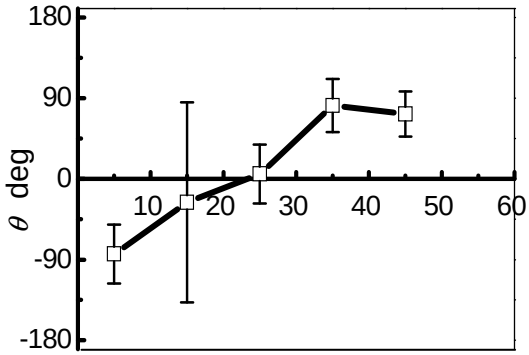

(d) Droplets flying angle

Fig.4-7 Gas oil spray images and droplets velocity (T_i=298K, P_{inj}=70MPa, t=0.50ms)

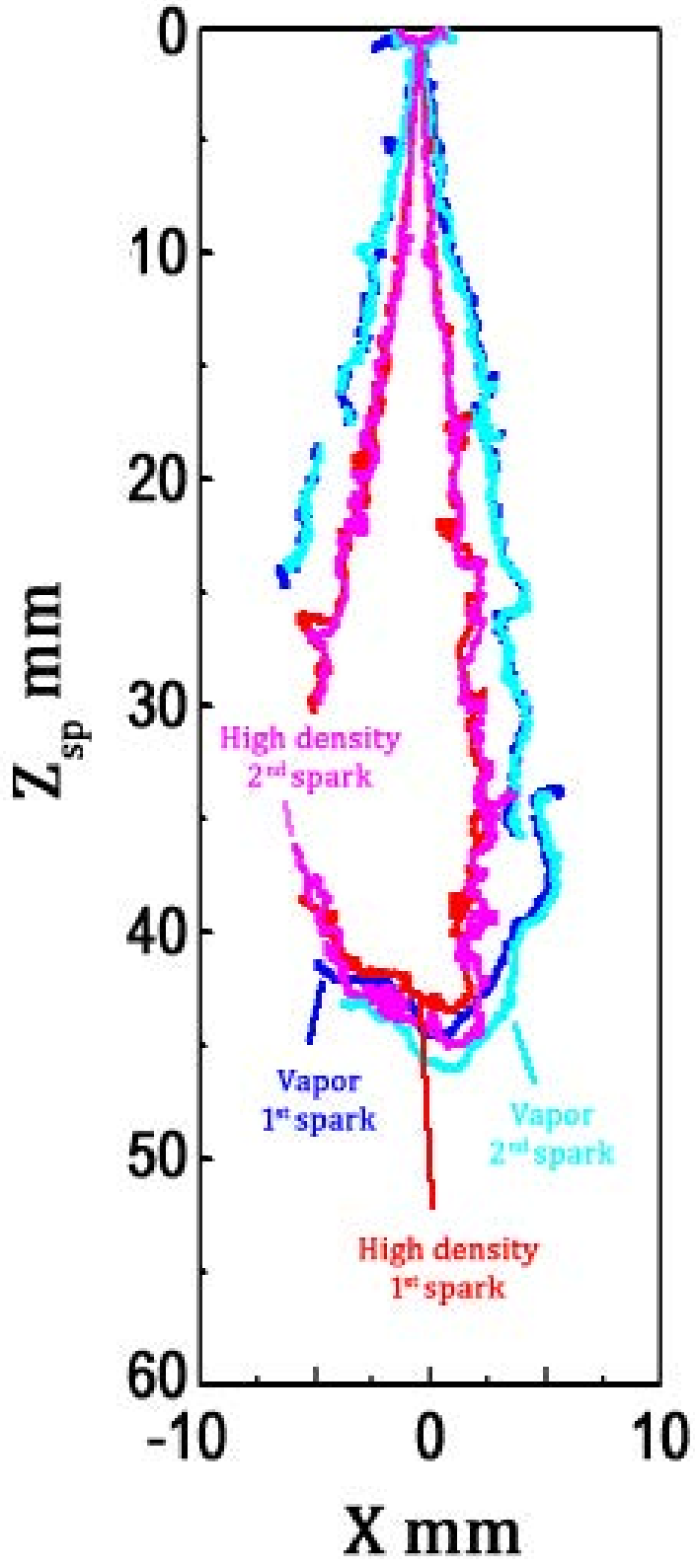

Fig.4-8 Progression of high density region and vapor boundary in gas oil spray
(T_i=500K, P_{inj}=70MPa, Δt=25μs, t=0.50ms)

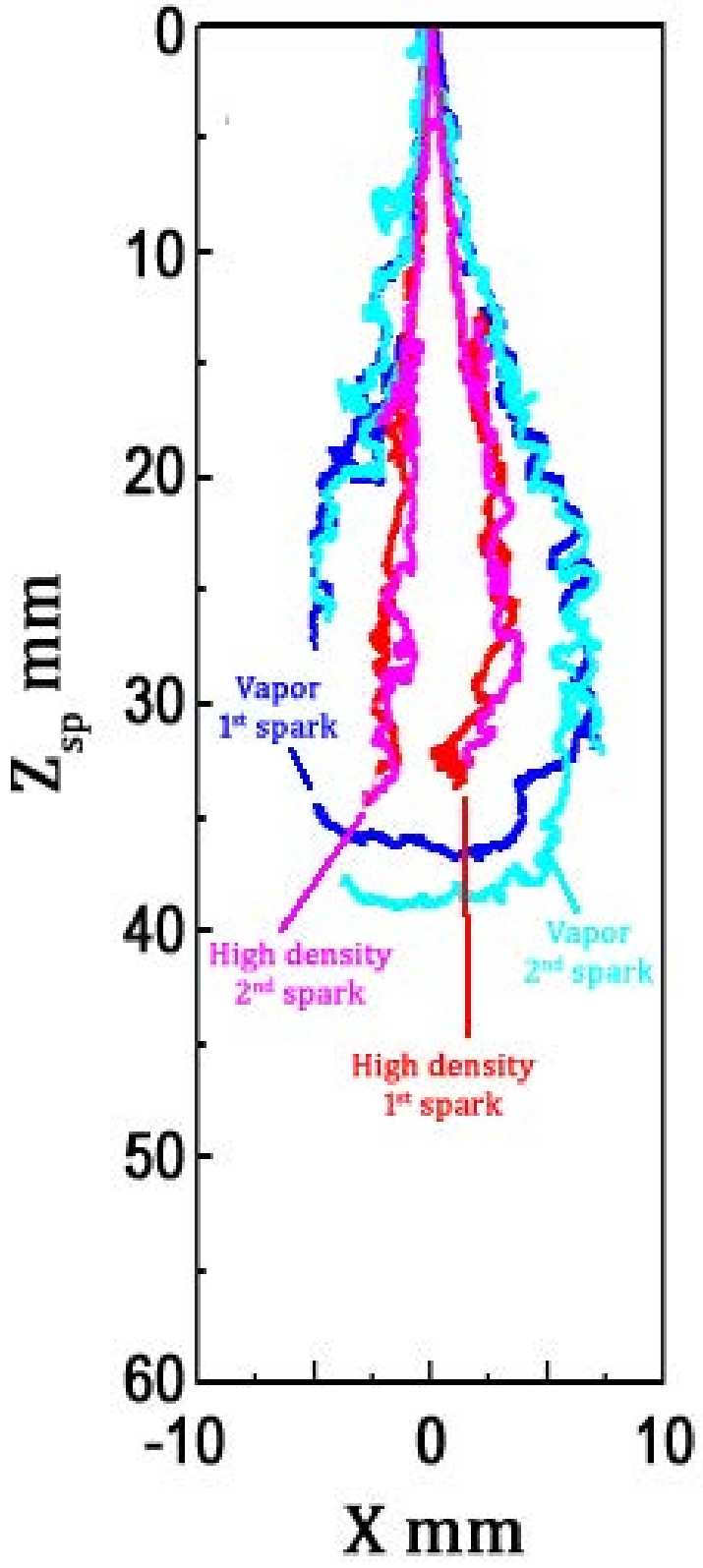

Fig.4-9 Progression of high density region and vapor boundary in gas oil spray
(T_i=700K, P_{inj}=70MPa, Δt=25μs, t=0.50ms)

4.4.2 Rapeseed Oil Spray

Fig.4-10 shows RO spray image and its analysis at T_i=298K, P_{inj}=70MPa, t=0.50ms aSOI (after start of injection) taken by dual nano-spark shadowgraphy and time interval between nano-spark 1 to 2 is Δt=25μs, similar to Fig.4-7. Fig.4-10(a) shows the original images, (b) shows the droplet vector calculated by comparing the image from camera 1 to camera 2, (c) shows the averaged droplet flying velocity and (d) shows the averaged droplet flying angle. Fig.4-10(b) y axis shows the spray travel distance with Z_{sp}=0 equal to nozzle tip. The analysis first divides spray length into 4 sections, 0-25% (upper), 25-50% (middle), 50-75% (lower) and 75-100% (tip) of spray length for notation purpose. In Fig.4-10(c) and (d), for Z_{sp}=0 to 60mm, each 10mm is divided into individual sections, with the averaged value is calculated for each section. The flying angle is considered to be 0° along the x axis, with positive value clock-wise. Error bar shows the standard deviation.

It can be observed from Fig.4-10(b), droplets vector in the upper section especially at Z_{sp}=0~20mm is small, similar to that of the GO. Air entrainment influence also can be seen as the droplets are moving toward the spray body. By observing the section of Z_{sp}=0~20mm of Fig.4-10(c) and (d), which has similar value to GO, it is understood that the RO spray upper section droplets dynamic is similar to GO. In contrast, at Z_{sp}=20~40mm, the droplets move along the spray axis, with smaller entrainment effect. The same tendency can be observed when Z_{sp}=40mm and larger. This flying angle tendency of RO spray droplets at middle and lower section is different from GO. It is believed that the different in droplet size, with the larger droplets of RO have bigger kinetic energy and the not easily affected by air entrainment. This made the droplets move along the spray axis with little deviation and believed to the one of the reason that made RO spray cone angle smaller when compared to GO. In addition, careful inspection on the branching structure on Fig.4-10 and also Fig.4-1 show RO spray has smaller branching structure when compared to GO spray. Fuel droplets on the spray tip is continuously under surrounding gas aerodynamic forces, decreasing its velocity, and at the same time, the droplets that came after that pushes forward and replace the exiting droplets on the spray tip. The droplets with low kinetic energy are pushed aside and form the outer spray region. This mechanism can be seen on the GO and RO spray. RO spray has high viscosity which made the droplets (quantity) that were pushed aside due to aerodynamic forces was small in numbers. This in turn made the spray cone angle smaller than of the GO and also the branching structure was not well developed. The final result is poor atomization for RO spray. In contrast, as the RO spray droplets kinetic energy is greater

than of the GO, the spray penetration length is longer.

Fig.4-11 shows RO spray image and its analysis at T_i=700K, P_{inj}=70MPa, t=0.50ms aSOI taken by dual nano-spark shadowgraphy, similar to Fig.4-10. It can be observed that with the increase in ambient temperature, RO spray cone angle become larger. The high ambient temperature decrease RO spray viscosity and this can be confirmed with the increase of spray cone angle. Clear branching structure also can be observed. In addition when compared to Fig.4-10(b) at T_i=298K where air entrainment effect can be clearly seen especially at the middle and lower section, it can be observed that droplets fly inward to the spray body exhibiting the influence of air entrainment. In addition, Fig.4-11(c) and (d) shows that the droplets velocity vector becomes small and at the lower section can be seen to fly outward of spray body. Decrease in the droplets size due to lower viscosity of RO spray is believed to be the reasons of these results. Based on these findings, it is clear that high ambient temperature improves atomization of RO spray. However, it should also be noted that even at T_i=700K, evaporation of RO spray can little be seen, and vapor region almost cannot be detected. This characteristic poses a problem to engine with low ambient temperature and running at low load, as it can be the cause of SOF increase.

Fig.4-11 show image of RO spray taken at T_i=850K, P_{inj}=70MPa, t=0.50ms, with a magnified section located on the right side. The magnified image represents area from the full spray image marked with red boundary. From the magnified image it can be seen that at T_i=850K, the formation of vapor phase at spray boundary can be observed. This is very interesting as it is known from Fig.4-4, even at T_i=700K, vapor phase is difficult to be observed. This result shows that in the condition of very high ambient temperature, even of RO spray (middle and lower section) undergoes atomization which eventually leads to vaporization.

Fig.4-13 shows the high density liquid and vapor phase analysis of the image, with the former dictated by red line and the later by blue line. The result shows that large area of vapor phase in the middle section. In contrast, high density liquid phase can be observed advancing at the spray tip. This is similar to Fig.4-8 which shows GO spray at T_i=500K. It is believed that in order to promote faster vaporization at the spray tip section, higher ambient temperature is required.

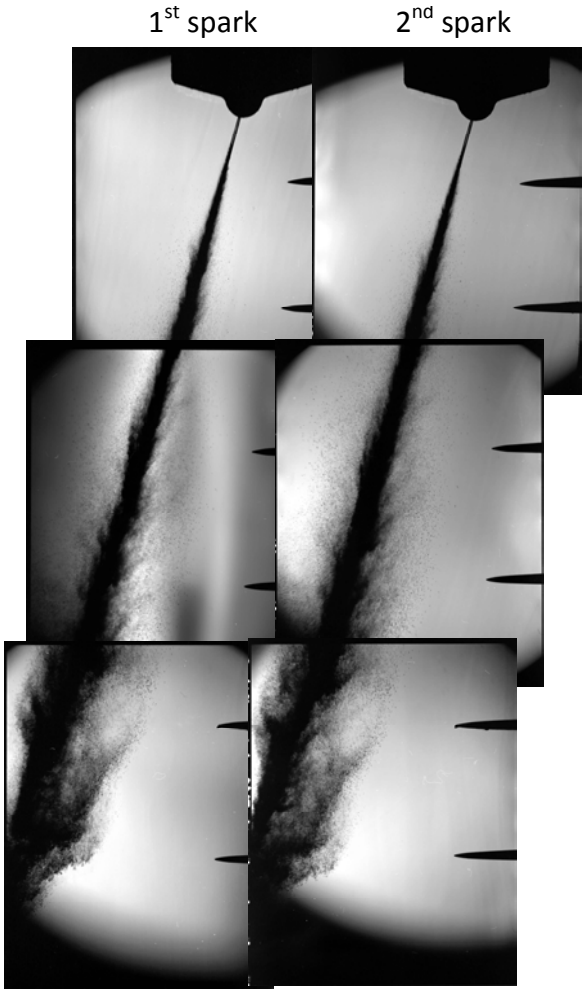

(a) Original spray image

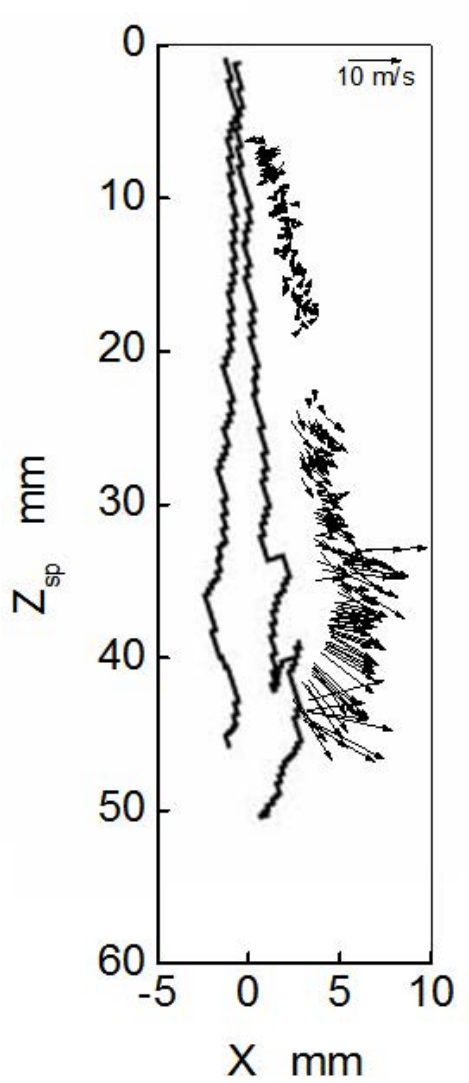

(b) Droplets vector

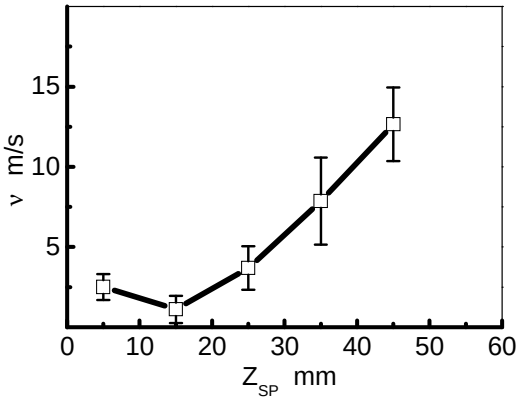

(c) Droplets flying velocity

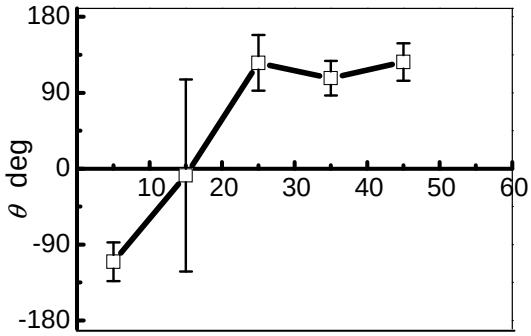

(d) Droplets flying angle

Fig.4-10 Rapeseed oil spray images and droplets velocity (T_i=298K, P_{inj}=70MPa, t=0.50ms)

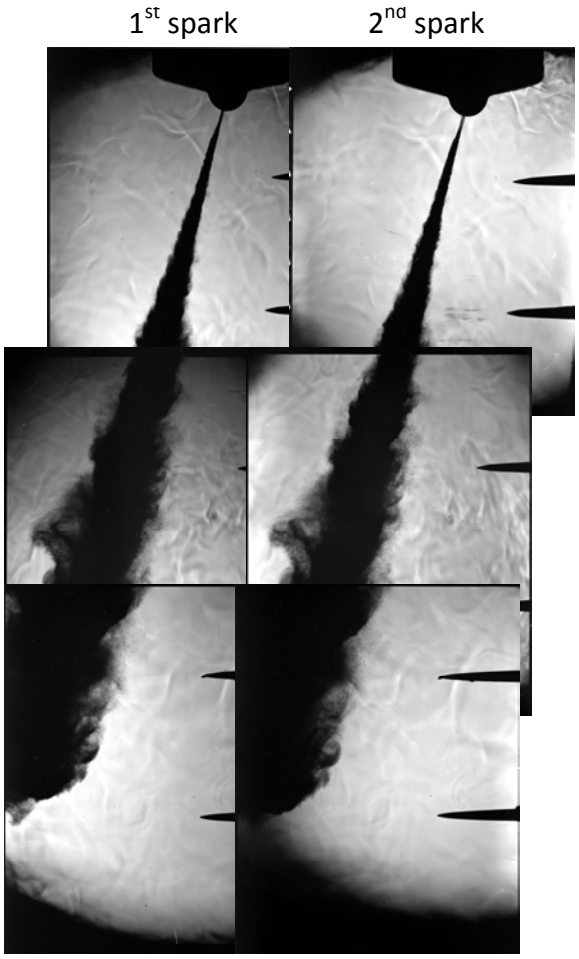

(a) Original spray image

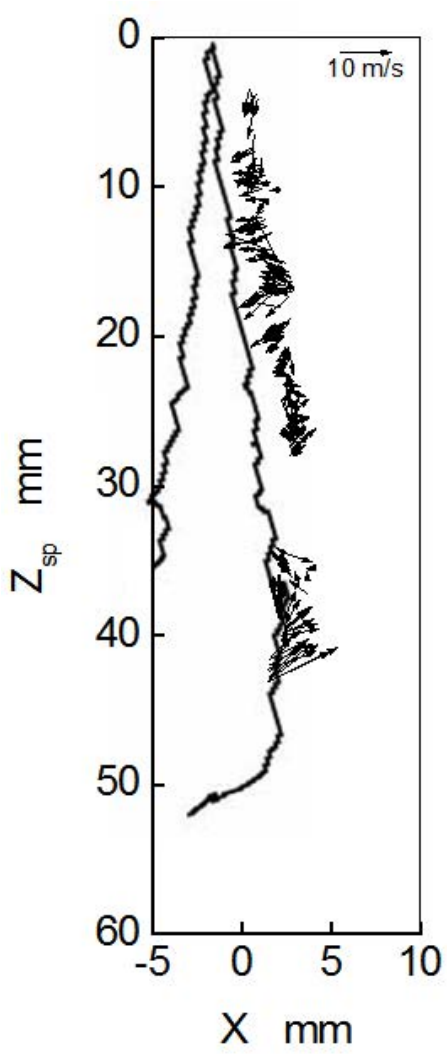

(b) Droplets vector

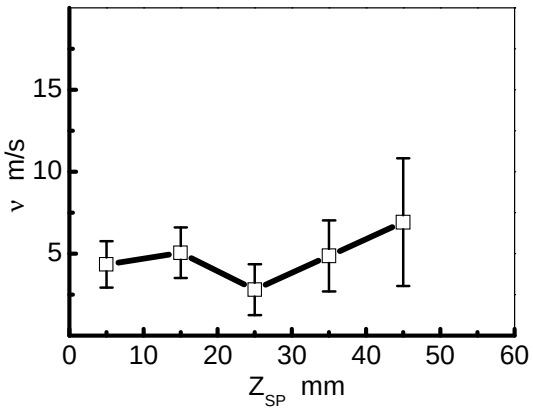

(c) Droplets flying velocity

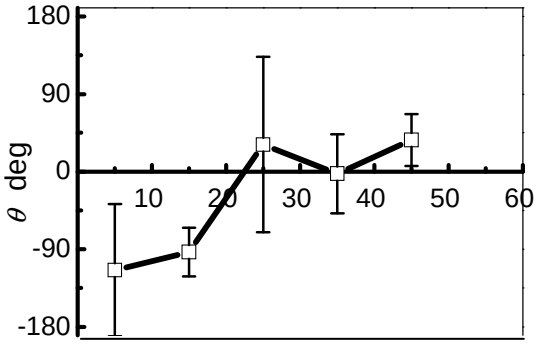

(d) Droplets flying angle

Fig.4-11 Rapeseed oil spray images and droplets velocity (T_i=700K, P_{inj}=70MPa, t=0.50ms)

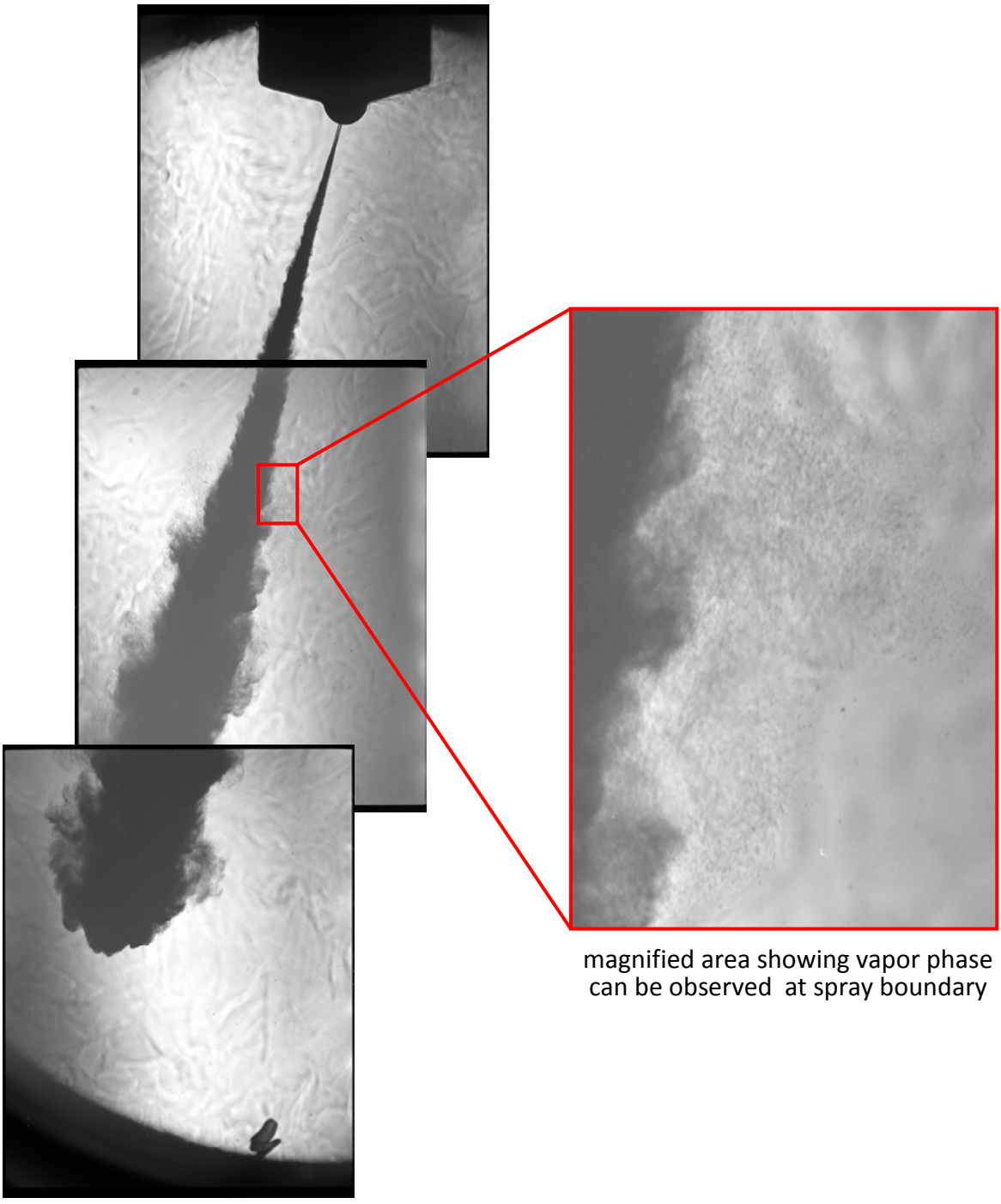

Fig.4-12 Vaporization of rapeseed oil spray (T_i=850K, P_{inj}=70MPa, t=0.50ms)

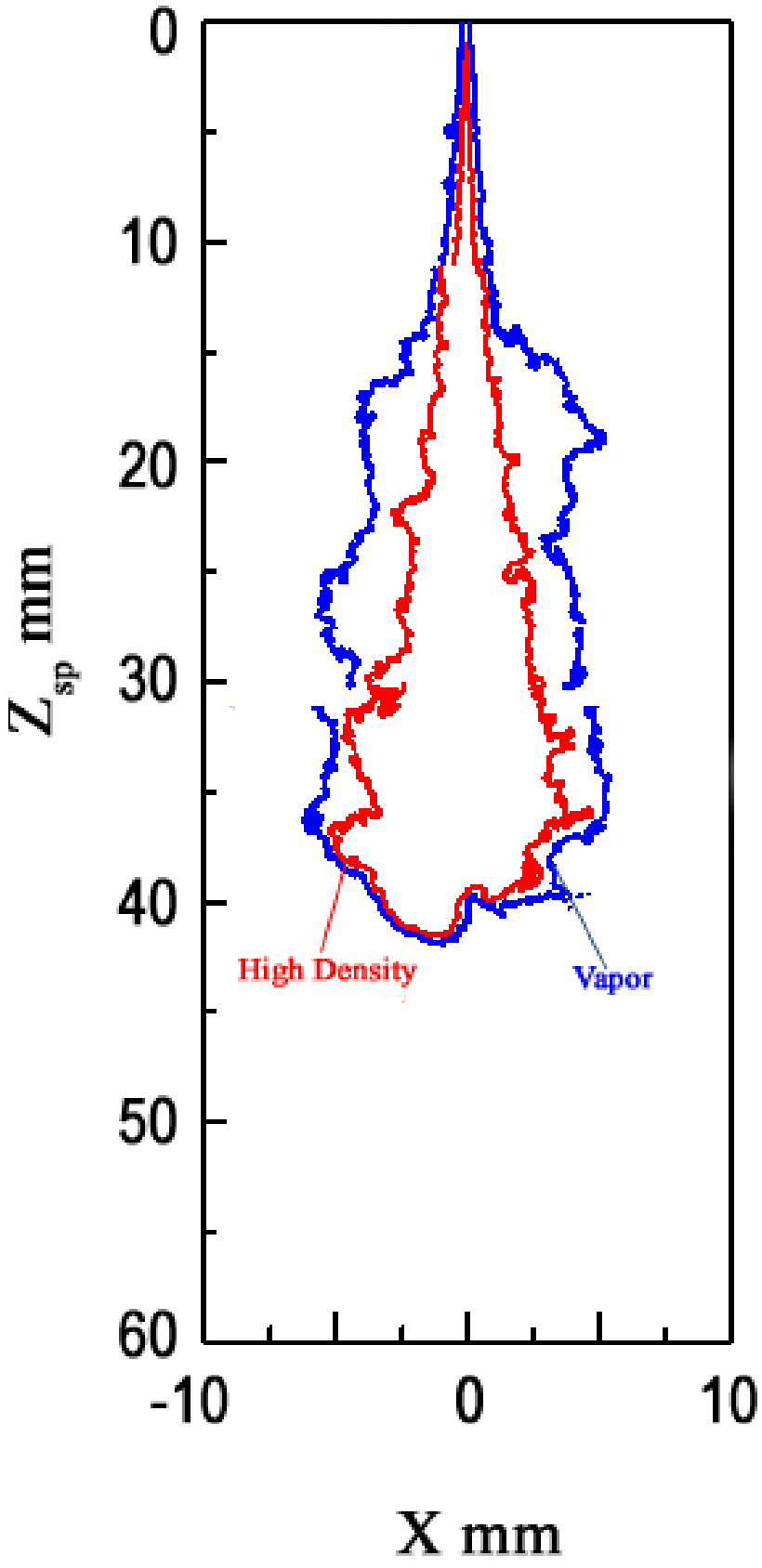

Fig.4-13 Rapeseed oil spray high density region and vapor boundary
(P_{inj}=70MPa, T_i=850K, t=0.5ms)

Chapter 5 Effect of Nozzle Geometry on Spray Development of Multi-hole Rapeseed Oil Spray

5.1 Introduction

As the characteristics of RO and GO free jet spray has been discussed earlier on the previous chapter; next, we will try to study the effect of nozzle geometry on spray development of RO fuel in a multi-hole nozzle. As the emission standard becomes more stringer than ever, the need for a more controllable combustion where pollution emission is reduced is a must. The use of multi-hole nozzle injector provide the fuel to be atomize in a wider area inside the piston cavity (multiple jet spray), while creating a favorable spray pattern with a separated spray jets, which can be independently directed at desired locations, achieving improved matching between the injector and the combustion chamber designs; that could assist for a better effective combustion. This is especially beneficial in HSDI (High Speed Diesel Engine), which also included diesel engine used in regular passenger automobile, that has high engine RPM (revolution per minute) while usually having a small combustion chamber. Conversely, as the multi-hole injector nozzle hole diameter generally has small hole diameter, the need of a relatively high-pressure injection system (which can be complicated and costly) is required to force the fuel into the small nozzle hole and to penetrate into the compressed air inside the engine combustion chamber. However, even with the disadvantage in term of system complexity and cost, multi-hole injector has proven to improve diesel engine combustion and emission, and could certainly be a viable candidate for alternative fuel injection delivery system.

It is proven in previous chapter that RO spray has a problem of poor atomization especially at initial stage of injection. It also widely known that nozzle geometry and configuration could affect combustion process in diesel engine. This is closely related to the spray characteristics of fuel injected by the nozzle. Thus, this chapter tries to investigate effect of sac-volume and nozzle scaling of multi-hole injector on RO spray characteristics, aiming to find measures to improve emissions when using RO in DI diesel engines.

Spray development for RO and GO was directly observed from the bottom view using high speed digital video camera. Spray penetration and spray cone angle was then calculated for comparison. In addition, spray structure was also taken from side view using shadowgraph photography. The high resolution image from still camera then analyzed to characterize the spray structure.

5.2 Nozzle Specification

Multiple type of nozzles were used in this experiment. Table 5-1 shows each nozzle specification. Fig.5-1 shows nozzle schematics with d_i is the nozzle inlet hole diameter and d_o is the nozzle outlet hole diameter. Nozzle P57 and P28 are four-hole nozzle with same hole-diameter of 0.25mm and different sac-volume. The sac-volume of P57 is 0.57mm^3. P28 is a mini-sac nozzle with sac-volume of 0.28mm^3. P57 and P28 were used to investigate effect of sac-volume on RO spray development.

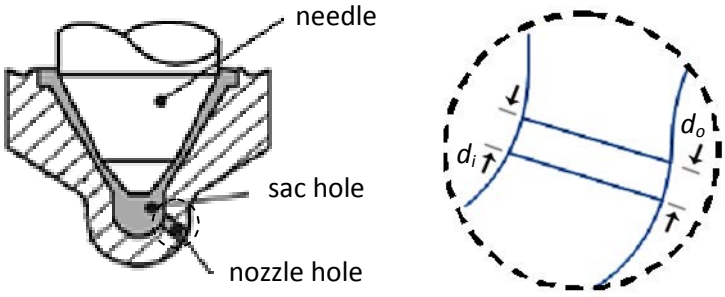

Fig.5-1 Schematic diagram for direct injection diesel engine spray nozzle

Nozzle PS, PE and PN are five-hole nozzles with same inlet hole-diameter and different outlet hole-diameter. PS has straight hole of 0.25mm in diameter. PE is enlarging hole with inlet diameter of 0.25mm and outlet diameter of 0.27mm. PN is narrowing hole with inlet diameter of 0.25mm and outlet diameter of 0.23mm. The three nozzles are mini-sac nozzles with sac-volume of 0.28mm^3 and flow rate is identical. Comparing RO spray characteristics injected by these nozzles can reveal effect of scaling of nozzle hole on RO spray development. Furthermore, the different sac-volume between nozzle P57 and P28 believe to affect the spray characteristics.

Table 5-1 Nozzle specification

Nozzle Type	Nozzle Designation	Symbol	Number of holes	Nozzle hole diameter		Sac volume [mm^3]	Flow rate [g/min]
				inlet d_i [mm]	outlet d_o [mm]		
DI engine multi-hole nozzle	Large sac vol	P57	4	0.25		0.57	1360
	Smaller sac vol	P28				0.28	
	Straight hole	PS	5	0.25	0.25	0.28	
	Enlarge hole	PE			0.27	0.28	
	Narrowing hole	PN			0.23	0.28	

5.3 Comparison of Spray Development between Rapeseed Oil Spray and Diesel Spray on Multi-hole Nozzle

First, spray development of RO spray was compared with GO spray. Multi-hole nozzle P57 that has four holes with hole-diameter of d_n=0.25mm was used in this analysis. The spray development was directly observed from the bottom view using high speed digital video camera. This is to make general comparison on the spray development between RO and GO spray when using multihole nozzle.

Fig.5-3 shows spray development at different injection pressure of (a)P_{inj}=40MPa and (b)P_{inj}=70MPa at ambient temperature of T_i=298K. As seen in the images of lower injection pressure P_{inj}=40MPa in Fig.5-3(a), GO spray clearly penetrates at early stage of injection of t=0.2ms aSOI. At t=0.6ms, tip of GO spray reaches the chamber wall at distance 30mm from nozzle outlet; while, RO spray develops very slowly at 0.2ms. This is because high viscosity may prevent RO injection at start of injection. This has an influence of spray development at initial stage of injection, resulting in short penetration length at 0.6ms with RO spray.

In the case of higher injection pressure of P_{inj}=70MPa in Fig.5-3(b), RO spray can develop greater at t=0.2ms and 0.6ms. High pressure injection supports injection of high viscosity fuel at initial stage of injection. The spray structure of RO becomes similar to that of GO at 0.6ms. However, the greater part of RO spray seems to stick to wall surface although GO spray image shows reflecting spray caused by wall impingement at 0.6ms and 1.0ms. Poor atomization of RO spray produces this kind of characteristics of wall impingement.

Fig.5-2 Spray cone angle analysis example.
Measurement were made for each hole spray jet

Fig.5-4 analyzes spray development as shown in Fig.5-3 quantitatively. Fig.5-4(a) is time history of penetration of each spray and Fig.5-4(b) is variation of spray cone angle. The cone angle is measured as follows. First, a circle with the center consistent with the center of injection holes is drawn in the images. The circle has a diameter of 20mm that is a third of the chamber diameter. Next, two intersection points between the circle and spray boundary are specified. Finally, two lines that connect each point to the center of the circle are drawn. The angle formed by the two lines is defined as spray cone angle.

Lower diagram in Fig.5-4(a) illustrates that GO sprays reach chamber wall at about 0.3ms aSOI at P_{inj}=40MPa. RO sprays develop slowly and every spray reaches the wall at about 0.8ms. When injection pressure increases as shown in upper diagram, penetration of RO spray is improved. RO spray impinges on the wall at 0.5ms that is earlier than 0.8ms at P_{inj}=40MPa. In contrast, spray penetration itself changes little in GO spray with changed injection pressure from 40MPa to 70MPa. Effect of injection pressure on spray penetration is greater for RO rather than GO.

From the lower diagram in Fig.5-4(b), it can be seen that spray cone angle differs between RO and GO sprays at time earlier than 0.5ms. It is notable that RO spray produces very small cone angle at initial stage of injection, which is expected by imaged in Fig.5-3(a). The small cone angle is disappeared at high injection pressure in upper diagram. The variation of cone angle at time later than 0.5ms is almost same level between RO and GO sprays regardless of injection pressure.

These results suggest that, at very initial stage of injection with low injection pressure, atomization of RO spray seems to be extremely poor. Considering that injection duration is about 0.5ms at light load condition with a real DI diesel engine, poor atomization characteristics at initial stage of injection may be a potential of SOF emission.

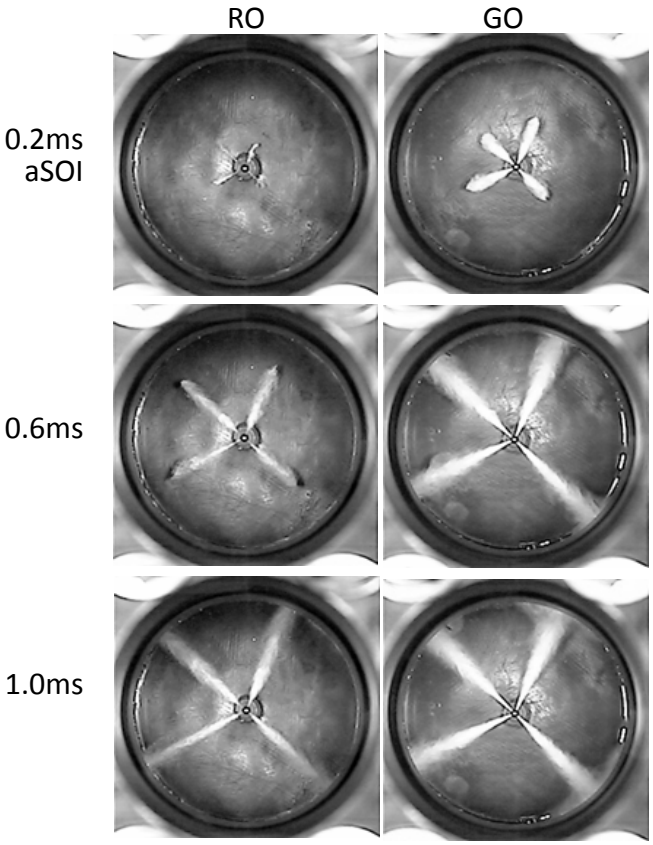

(a) P_{inj}=40MPa

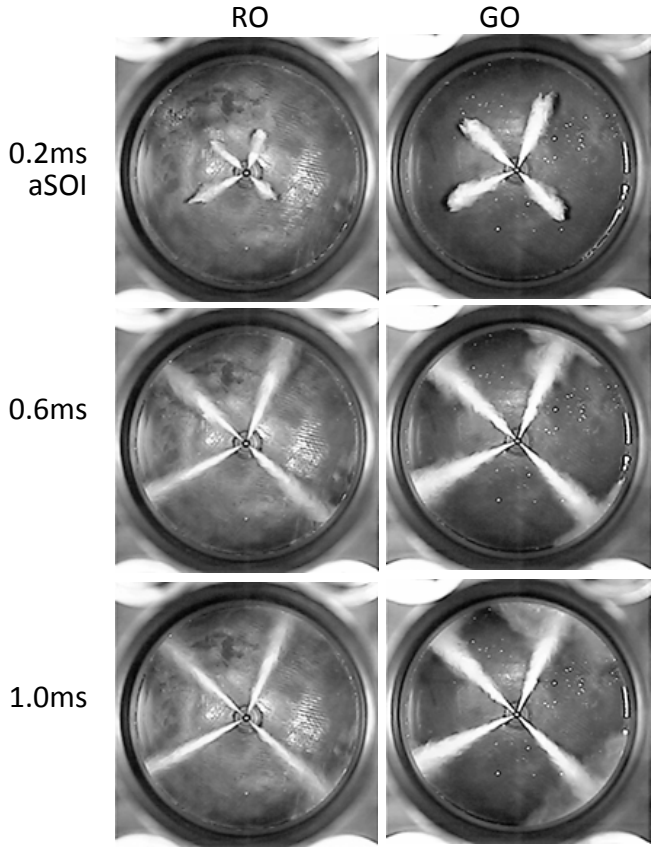

(b) P_{inj}=70MPa

Fig.5-3 Comparison of multi-hole spray development at initial stage of injection (T_i=298K)

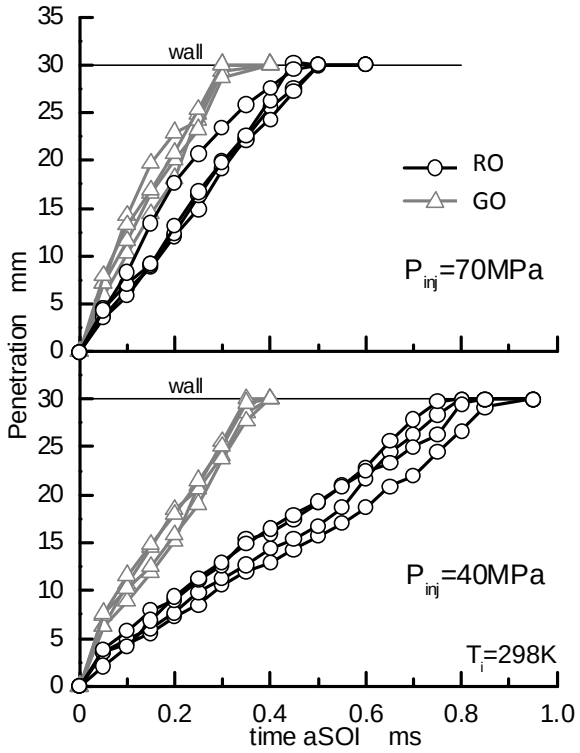

(a) Spray penetration

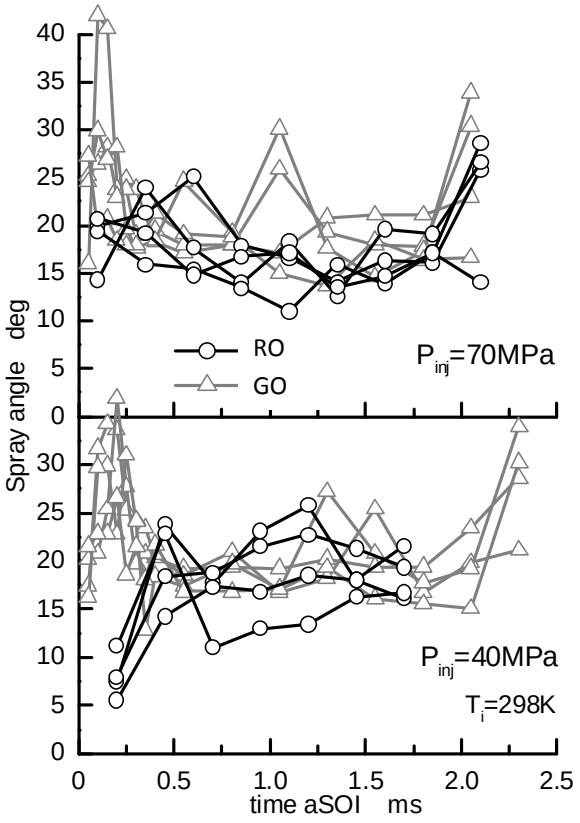

(b) Spray cone angle

Fig.5-4 Variation of spray penetration and cone angle

5.4 Effect of Nozzle Sac-volume

To improve spray atomization, one of useful method as well as high-pressure injection is using mini-sac nozzle. This section investigates effect of nozzle sac-volume on characteristics of RO spray. P57 and P28 nozzles are used in this study. Both are four-hole nozzles with hole diameter d_n=0.25mm as shown in Table 5-1. They have different sac-volumes of 0.57mm^3 for P57 and 0.28mm^3 for P28.

Fig.5-5 shows spray development of RO spray at ambient temperature of T_i=298K and T_i=700K using P57 and P28 nozzle. At injection pressure P_{inj}=40MPa, spray development just after start of injection at 0.2ms is sufficiently improved using mini-sac nozzle of P28 as compared with P57 nozzle. Significant increase in penetration length can be observed. The same is also true when P_{inj}=70MPa. This suggest that nozzle with mini-sac geometry can emit fuel quickly from the injector. In addition, should this type of nozzle is paired with common-rail injection system; the high injection pressure can be kept constant from the start of injection and throughout the process.

In the other hand, even though RO spray penetration at 0.6ms becomes longer by using mini-sac nozzle P28 in place of P57 when P_{inj}=40MPa, the effect of mini-sac nozzle on spray development is hardly seen when injection pressure increases to P_{inj}=70MPa. It can be suggested that mini-sac nozzle has a significant effect on spray development especially during the initial period of injection.

Fig.5-6 compares variation of penetration and spray cone angle of RO spray between P57 and P28 nozzles. Penetration history in Fig.5-6(a) indicates that mini-sac nozzle has an effect on improving spray penetration particularly at time longer than 0.4ms aSOI and lower injection pressure of P_{inj}=40MPa. As seen from spray cone angle variation in Fig.5-6(b), mini-sac nozzle can solve the problem of very small cone angle at initial stage of injection.

From the result, it is believed that RO spray development at early stage of injection can be improved the best by using mini-sac nozzle accompanied with high injection pressure. It also actually improves the spray condition on lower injection pressure. This can be helpful should high injection pressure system in not applicable or not practical for the purposed engine. However, from the images, there is less effect on fully developed spray as compared with initial period just after start of injection when using mini-sac nozzle. Although this fact seem insignificant, it has to be said that it is also important for the developed RO spray to reduce influence of poor atomization characteristics produced at early stage of injection.

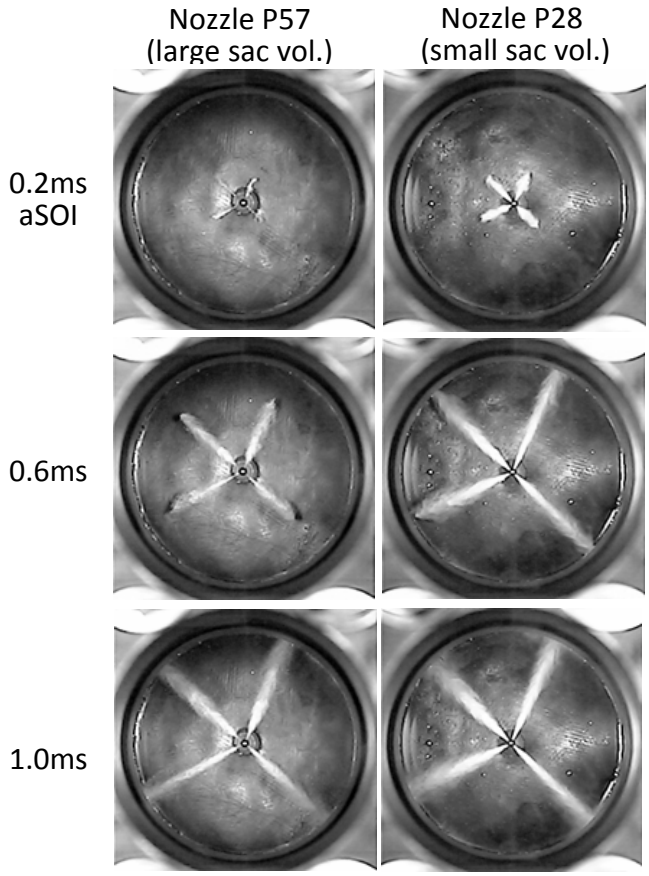

(a)P_{inj}=40MPa

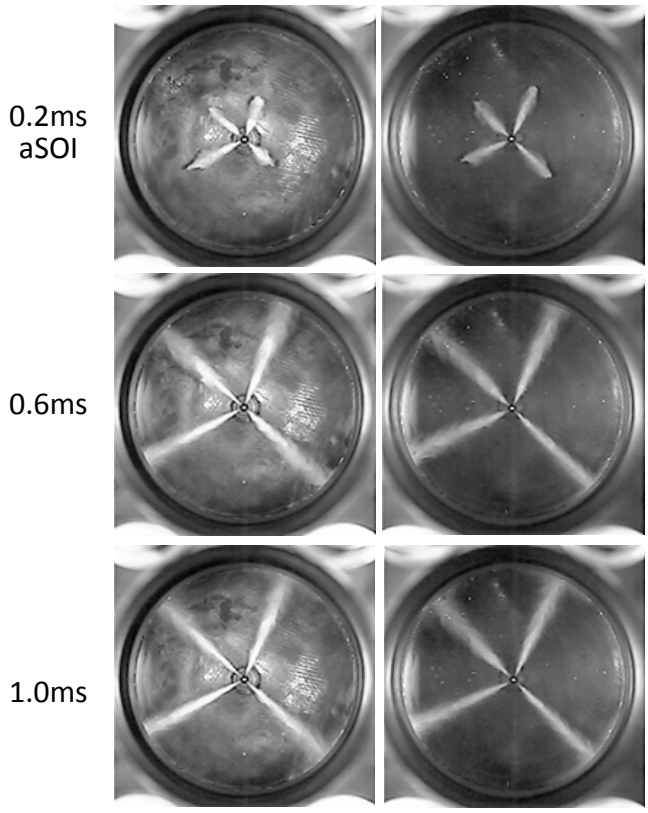

(b)P_{inj}=70MPa

Fig.5-5 Rapeseed spray development of rapeseed oil with different injection pressure and different volume-sac nozzle (T_i=298K)

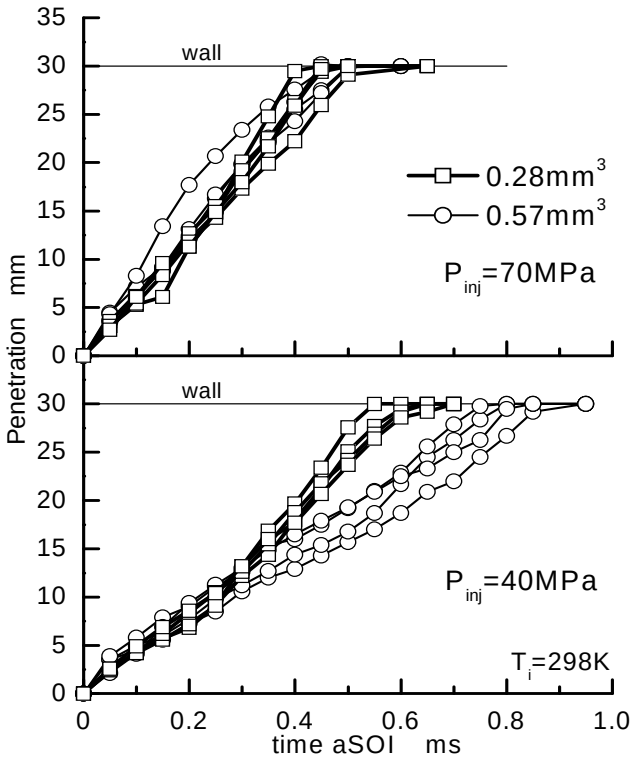

(a) Spray penetration

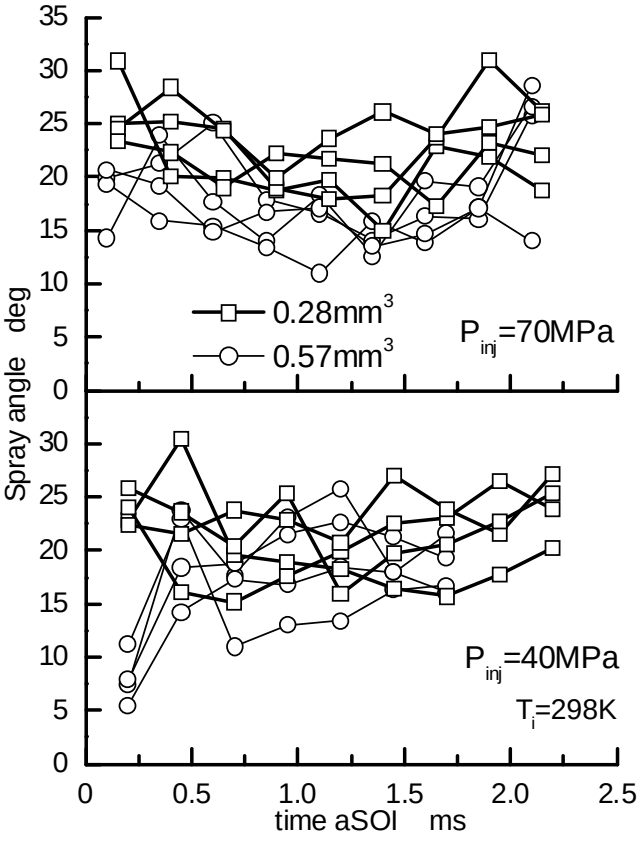

(b) Spray cone angle

Fig.5-6 Effect of nozzle sac-volume on variation of spray penetration and cone angle

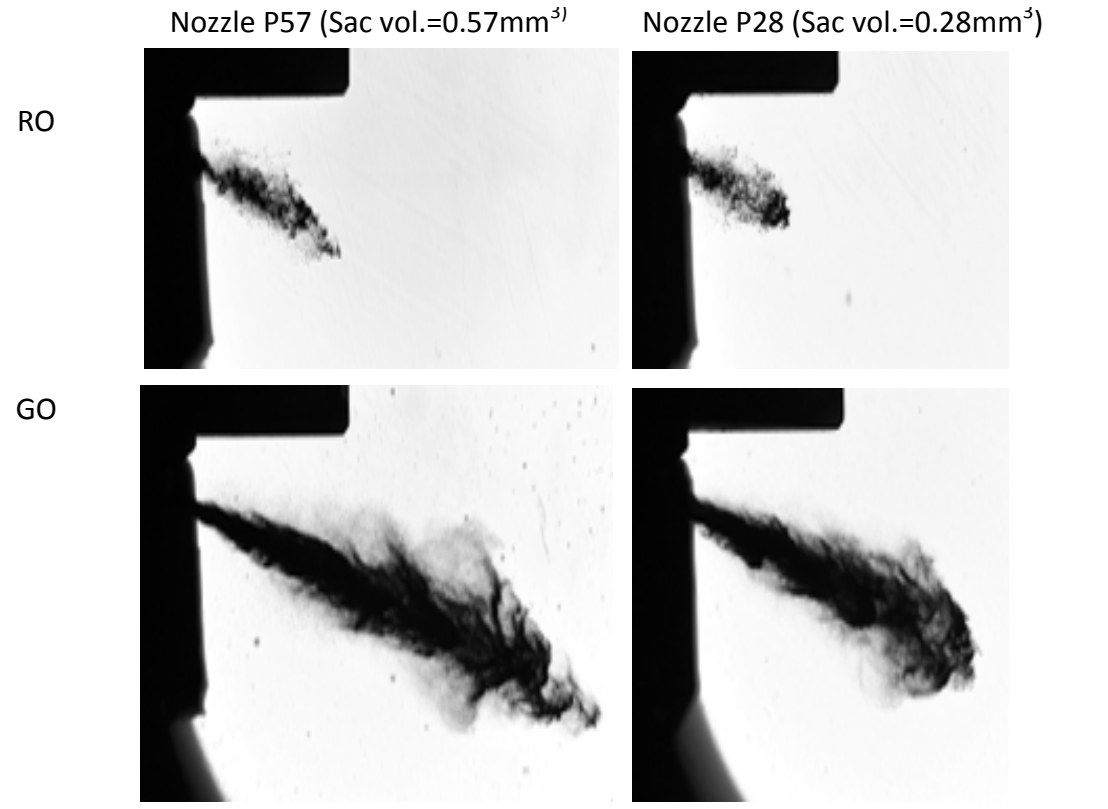

(a) P_{inj}=40MPa

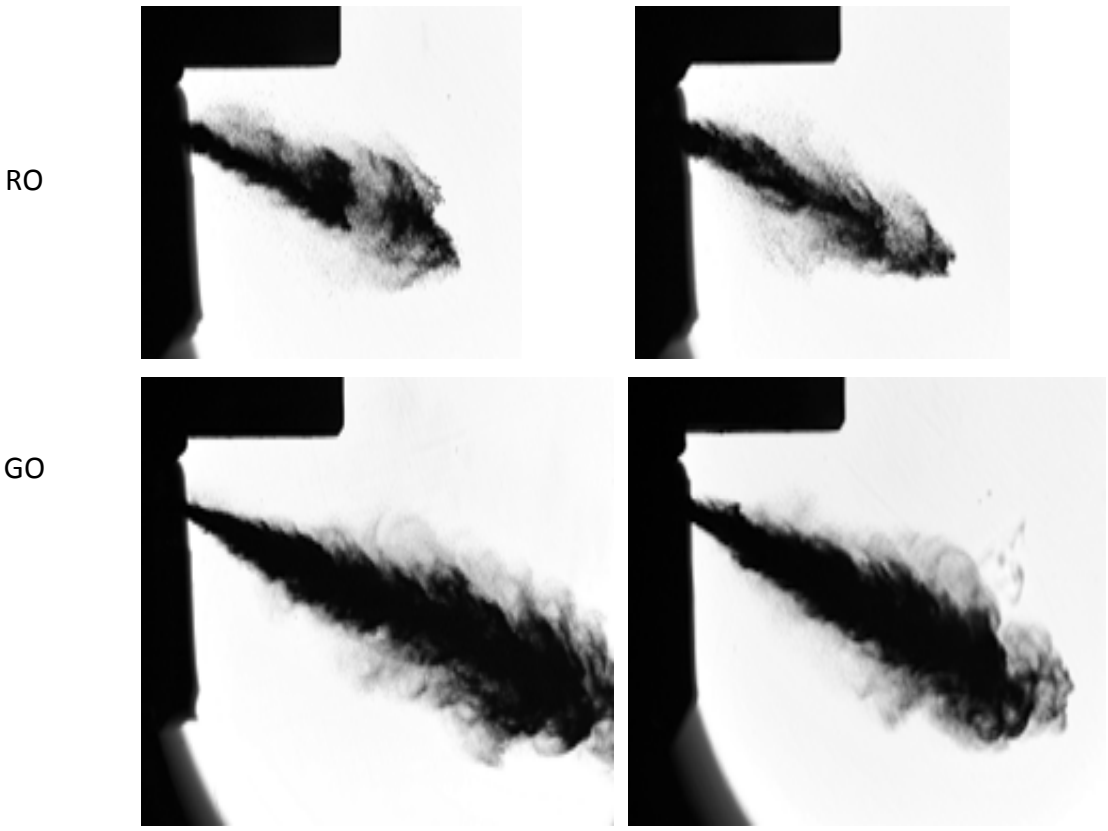

(b) P_{inj}=70MPa

Fig.5-7 Effect of nozzle sac-volume on spray structure at initial stage of injection (t=0.5ms aSOI)

Next, to study the effect of sac-volume on spray structure, macro-scale image of one of four-hole sprays is taken by shadowgraph photography technique. The multihole nozzle is configured in such a manner that only spray image from one of the nozzle holes was taken. Caution has been taken to confirm that even though only one nozzle was available for picture taking, the jet sprays from other nozzles were not obstructed in which can negatively affect the results. The image was taken from the side, different from the bottom view image from the high-speed camera.

Fig.5-7 shows spray structures of RO and GO fuels at t=0.5ms aSOI using two nozzles with different sac-volumes. At low injection pressure condition of P_{inj}=40MPa in Fig.5-7(a), images of RO spray have heterogeneous density for both sac-volumes. In contrast, GO sprays show distinct main stream like a liquid column with thick density at spray centerline and branching structures are already formed at this time. When injection pressure increases to P_{inj}=70MPa as shown in Fig.5-7(b), even RO spray narrowly forms main stream, although GO spray is fully developed. Mini-sac nozzle has more uniform density at spray centerline than larger sac-volume one. However, stick-like structure of RO spray is still formed using mini-sac nozzle.

5.5 Effect of Scaling of Nozzle Hole

Study on the effect of scaling of nozzle hole-diameter on RO spray is investigated. This section uses three types of mini-sac nozzles shown in Table 5-1. Every nozzle has the same inlet hole-diameter of 0.25mm with different outlet diameter. First is straight-hole nozzle named PS, 0.25mm in hole-diameter. Second is enlarging-hole nozzle named PE, 0.27mm in outlet hole-diameter, and third is narrowing-hole nozzle named PN, 0.23mm in outlet hole-diameter.

Fig.5-8 compares spray development of RO spray at room temperature of T_i=298K using three nozzles. As shown in the Fig.5-8(a) of P_{inj}=40MPa, penetration is in order of PN>PS>PE. One reason of long penetration of PN (Narrowing) nozzle is that this nozzle has smaller outlet hole-diameter as compared with other nozzles. There is little difference in spread of spray represented by spray cone angle. Figure Fig.5-8(b) shows the case of higher injection pressure of P_{inj}=70MPa, the difference with penetration gets little. According to these results, small hole-diameter is effective to improve penetration of RO spray at initial stage of injection with low injection pressure. Narrowing-hole nozzle is a piece of method to reduce outlet hole-diameter. However, small diameter tends to be blockaded by deposit. It is necessary to pay attention to deposit formed by long time engine operation.

Fig.5-9 compares spray structures taken by shadowgraph photography method. At P_{inj}=40MPa in Fig.5-9(a), spray structures are similar among three nozzles. Each spray has heterogeneous density distribution at spray centerline and distinct liquid column is invisible. When injection pressure increases to P_{inj}=70MPa shown in Fig.5-9(b), high density region can be observed. Droplets formed around spray boundary become smaller size and the number of droplets increases by increased injection pressure from 40MPa to 70MPa. Narrowing nozzle PN has main stream with thickest density and longest penetration. Larger number of droplets is formed at spray tip region for PN nozzle. However, stick-like structure of RO spray can be little improved by scaling of nozzle hole under room temperature atmosphere.

For reference and comparison, Fig.5-10 shows the spray development of GO spray at room temperature of T_i=298K using same three nozzles. At P_{inj}=40MPa, PE has the longest penetration, while at P_{inj}=70MPa, it seem that there is not much different in each nozzle spray penetration length. Meanwhile, Fig.5-11 shows the GO spray structure of taken by shadowgraph photography. The spray structure is definitely different from that of RO, where GO has a more homogenous density distribution with distinguish liquid core and branching structure at the boundary region.

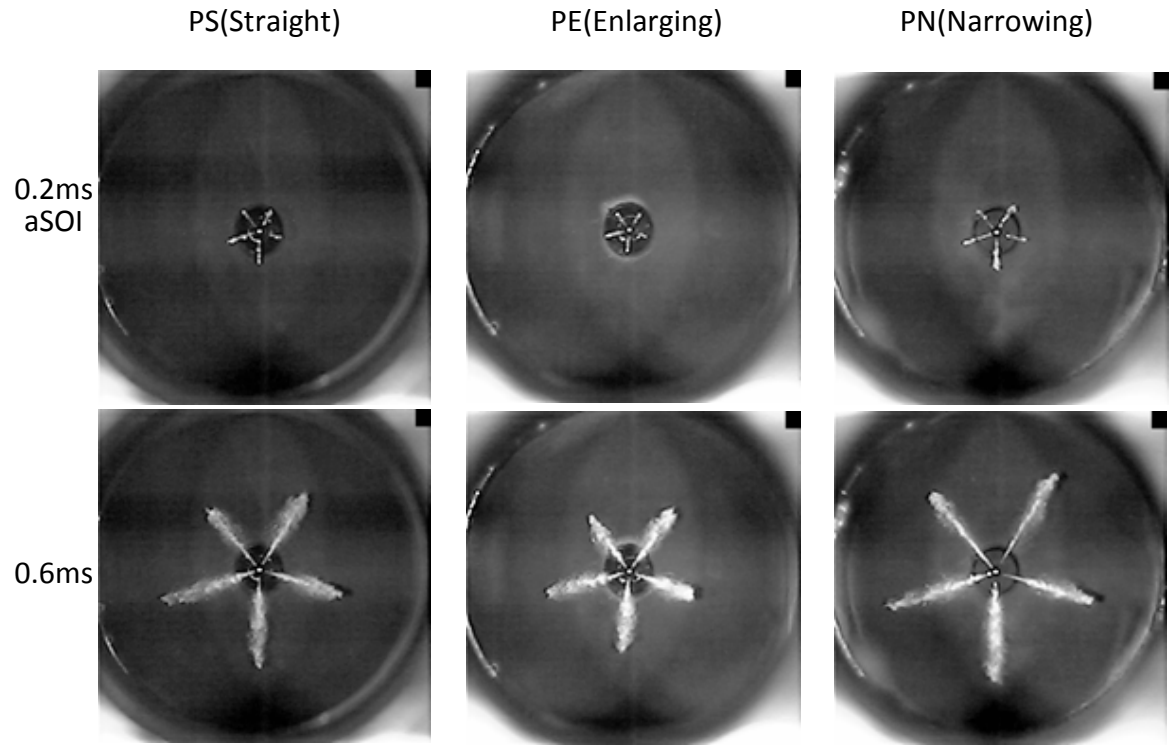

(a) P_{inj}=40MPa

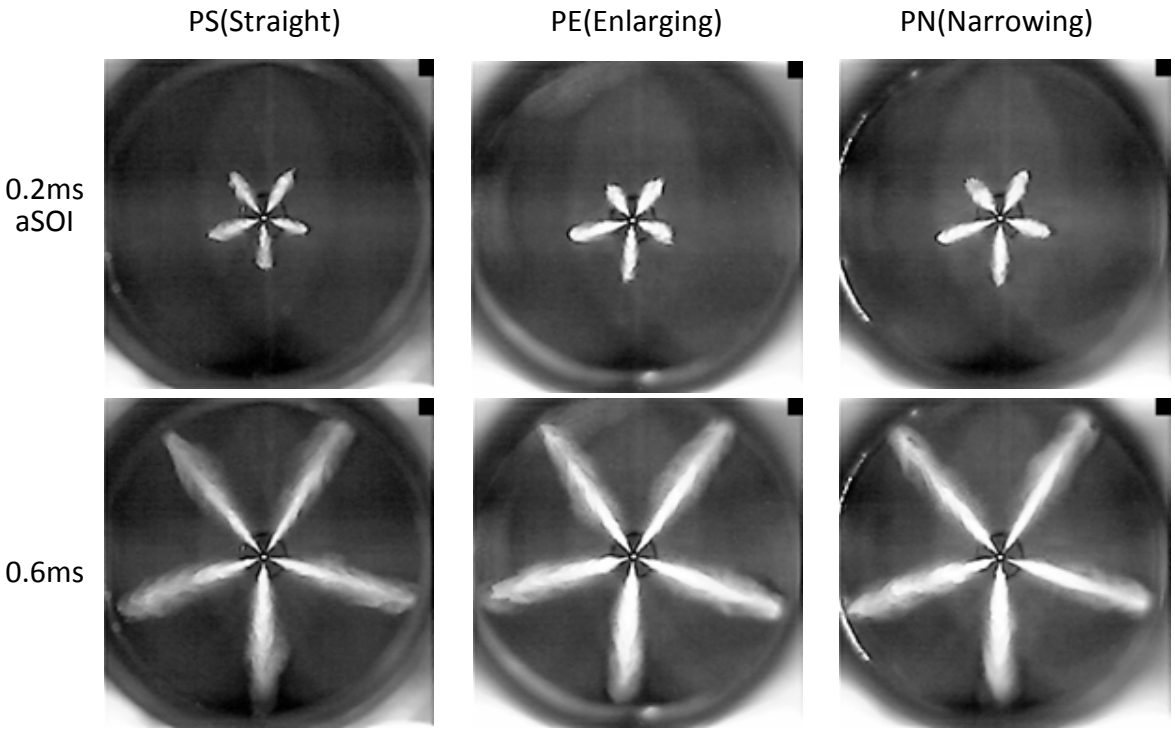

(b) P_{inj}=70MPa

Fig.5-8 Rapeseed oil spray developments of three types of nozzle hole configuration

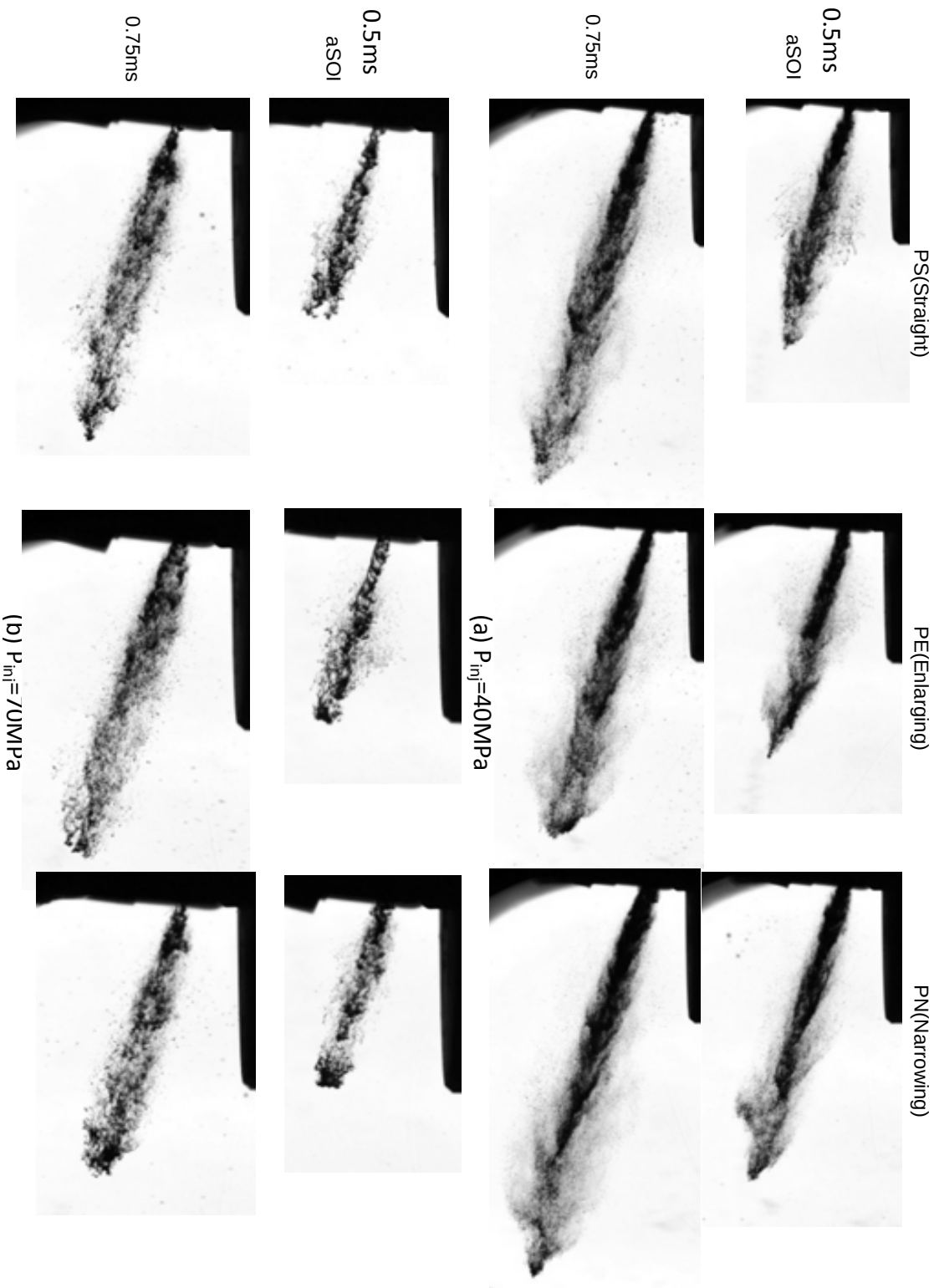

Fig.5-9 Characteristics of rapeseed oil spray structure at initial stage of injection

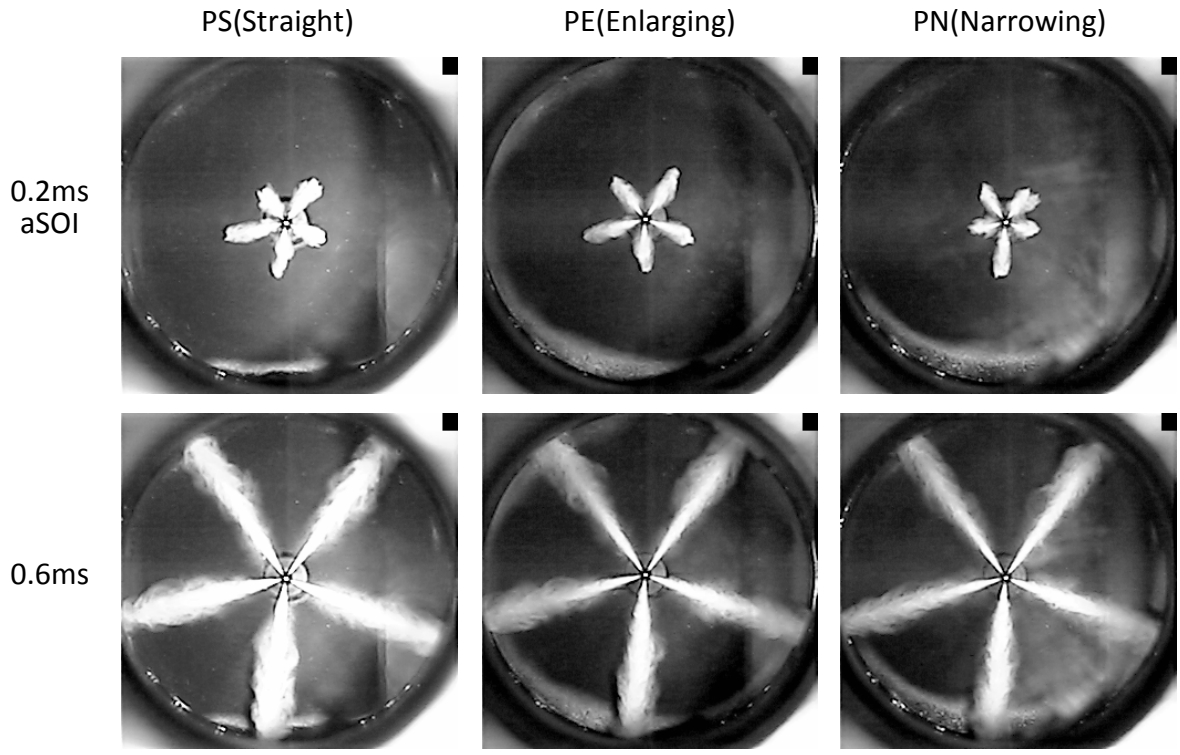

(a) P_{inj}=40MPa

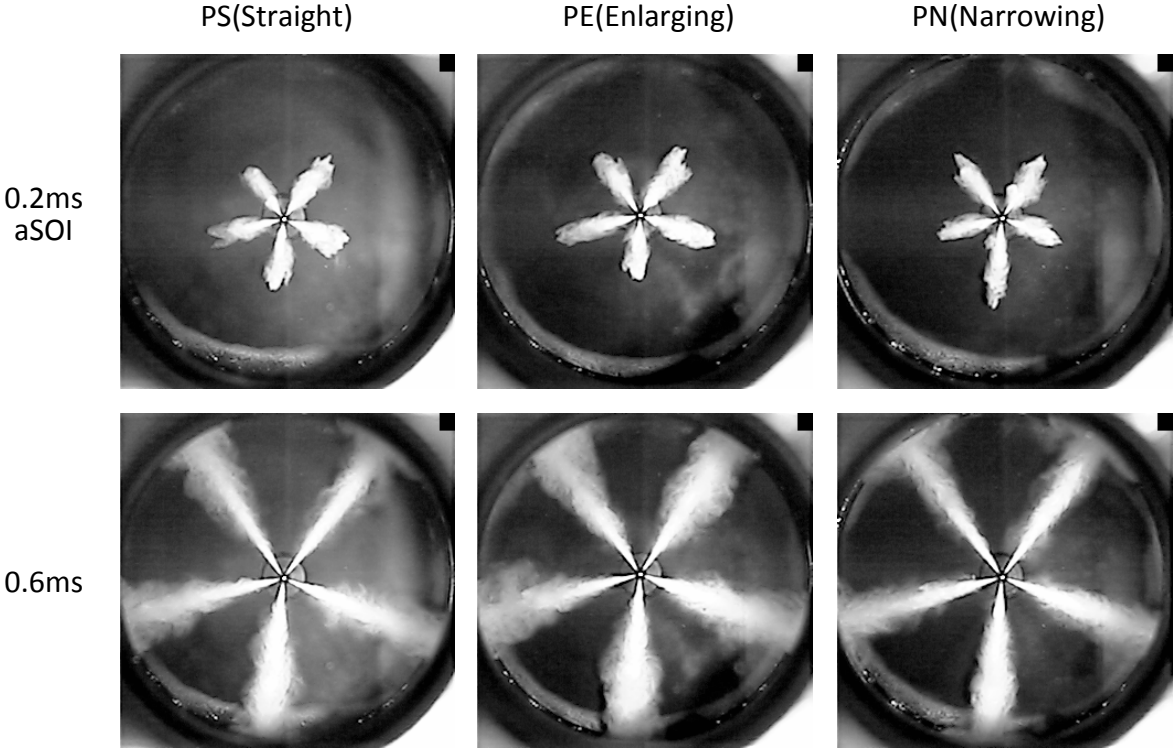

(b) P_{inj}=70MPa

Fig.5-10 Gas oil spray developments of three types of nozzle hole configuration

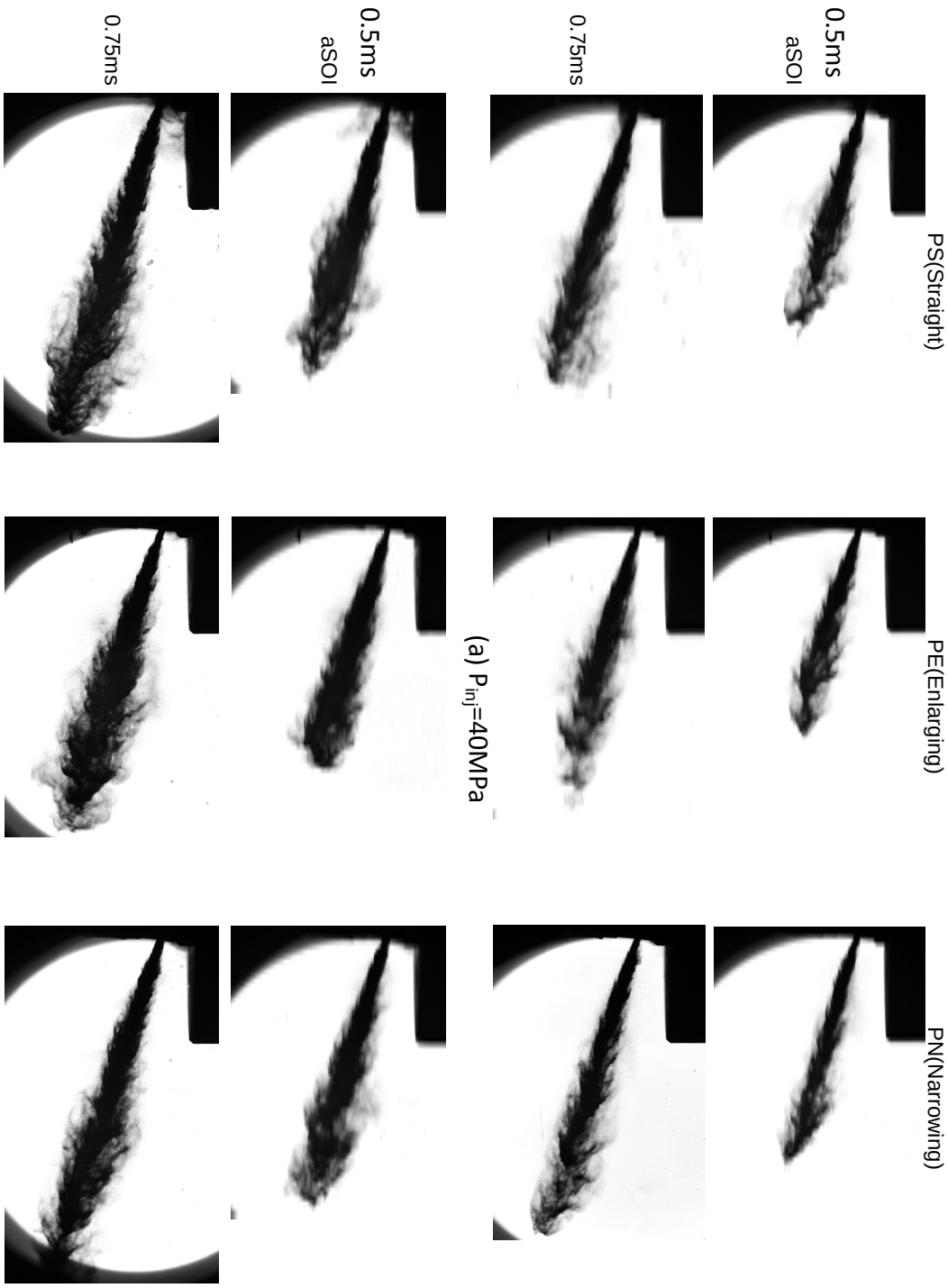

Fig.5-11 Characteristics of gas oil spray structure at initial stage of injection

Chapter 6 Effect of Wall Configuration on Wall Impingement of Rapeseed Oil Spray

6.1 Introduction

From previous chapter, it is known that application of high-pressure injection and high ambient temperature could promote better spray atomization and fuel-air mixing. This has been proven true and many strategies to improve atomization were based on this finding. But it is known also that RO spray atomization is very slow. Even with the high injection pressure strategy, which in practice can be achieved by today equipment, this will limit the engine design and force the usage of high pressure injection system which sometimes is not required to start with. Thus, the need to search for other plausible strategy is required to improve RO spray atomization and one of the more practical methods is wall impingement

Though wall impingement is actually not a favorable condition in the case of GO as many problems are attributed to it. Especially in small DI diesel engines a major part of the injected fuel impinges on the cavity walls (combustion chamber). This causes the formation of a fuel film on the cavity wall when the wall temperature is low and forms rich mixtures near the cavity wall when operating loads are high, giving a significant effect on unburnt HC and soot emissions. Of course the wall impingement can be avoided with multi-hole nozzles of smaller hole area and larger diameter of the combustion chamber. But, with this system the air movements like swirl and squish are weak and the combustion duration is long causing a deterioration of the smoke quality. So, many researchers have suggested to use impinging spray more actively.

RO spray on the other hand might benefits by the interaction of the fuel and the wall, also the air movement generated by wall impingement. Thus, this chapter tries to explore the possibility of wall impingement strategy to improve RO spray atomization, and also study the effect of wall configuration to RO spray. The spray chamber was modified to provide access for a shaped metal to be inserted inside the chamber, simulating the wall configuration for fuel impingement. Images were taken by direct photography using high-speed camera and also by using nano-spark shadowgraphy technique.

6.2 Wall Configuration

The spray chamber was fitted with shaped metal insert to act as the wall impingement surface. The walls that simulate piston cavity shape are shown in Fig.6-1. Wall 1 is toroidal type cavity (afterward will also be referred as “Toroidal”). Wall 2 is re-entrant type cavity that has squish-lip on the top and it has flat bottom (afterward will also be referred as “Flat Bottom”). Wall 3 is standard re-entrant type cavity (afterward will also be referred as “Squish”). In Fig.6-1 spray directions in this study are also shown. The positional relation between each wall and spray corresponds to the position at TDC with a real engine. Fuels were injected using a single-hole nozzle with hole-diameter of d_n=0.18mm at an orientation angle of 15°,to simulate nozzle hole angle of 159° to the shaped metal insert.

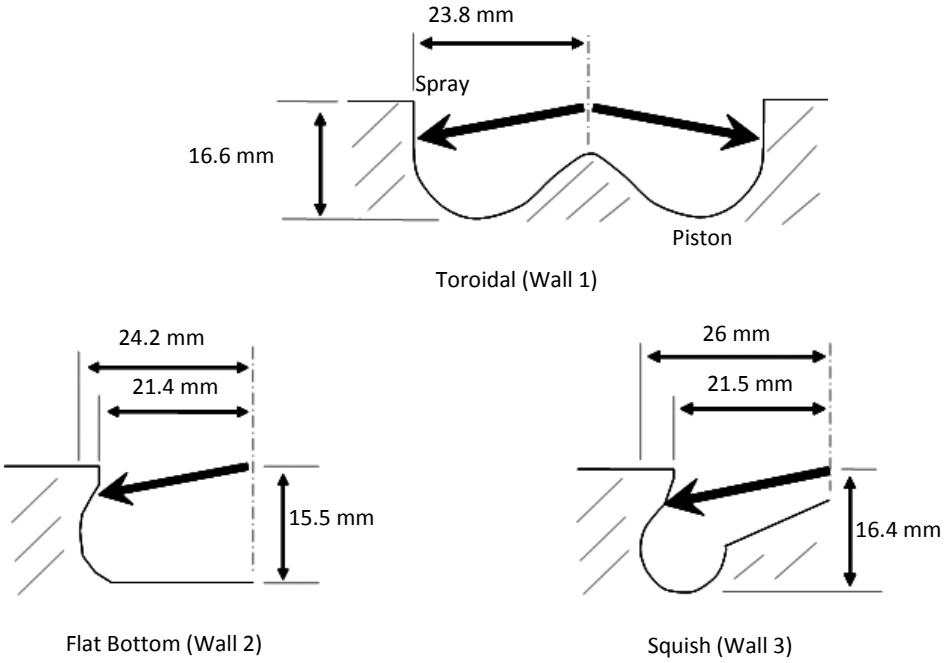

Fig.6-1 Geometry of impinging wall

As the chamber is configured such a manner where the injector is located in the upper section, and the spray chamber itself fixed to rapid compression machine at one end (refer Fig. 2-5), the metal insert can only be inserted using the other end. This forced the metal insert to be fixed in a confusing direction, as can be seen later in the images taken. While some of the images has already been rotated due requirement during image analysis, other were left untouched and remain in its original condition. In either case, all images represent the parameter required in the study as per stated in each image description.

6.3 Wall Impingement At Room Temperature

Fig.6-2 compares images of RO and GO spray wall impingement under ambient temperature of T_i=298K with fuel injection pressure P_{inj}=40MPa or 70MPa. The spray was set to collide with the wall equivalent to orientation angle of 159° from injector centerline. The image was capture at 0.5ms after the spray impingement on the wall. Every image is a combination of two photos, for better resolution and wider observation area.

Generally, it can be observed in all wall configurations that, after impingement, the main spray is divided into two wall jets (afterward will also referred as “wall spray”). One is going upward to the upper section and the other is going downward to the lower section. Regarding RO spray with P_{inj}=40MPa in Fig.6-2(a), the wall jet tends to develop with high density liquid film after impingement for every all wall configuration. It can be observed that the jet develops along the lower section greater than upper section. When injection pressure increases to P_{inj}=70MPa in Fig.6-2(b), the upper and lower section spray path length increase and numbers of droplet also increase. Atomization is improved by wall impingement with high injection pressure. However, liquid film is still observed at T_i=298K. Regarding Toroidal, the upper section spray clearly exceeds the wall height. It can be expected in the engine that the fuel will not fully evaporate and eventually impinge on the lower part of the cylinder head. Impingement of non-evaporation fuel on engine wall is believed to be source of SOF emission at low load operation.

In contrast, spray developments to the upper section are limited with Flat Bottom and Squish shape. The squish-lip shape can effectively prevent spray development toward upper direction. In Flat Bottom, increasing injection pressure lengthens wall jet penetration and produces fine droplet around the spray tip region. The spray reaches the flat stage area in the bottom of the wall. Spray atomization is most improved with Flat Bottom. Spray penetration of Squish is shorter than that of Flat Bottom. Squish has round shape floor in the bottom, which seems to prevent wall jet penetration. Moreover, Squish has wider impinging angle than Flat Bottom. Wider impinging angle has less effect of wall impingement on atomization. Fig.6-2(b) also shows GO spray at P_{inj}=70MPa for reference. Effect of wall impingement is great with GO spray. Squish that has wide impinging angle and short spray penetration can produce lots of fine droplets as well as Toroidal and Flat Bottom in the case of GO spray. Atomization is more sensitive to wall configuration for RO spray than GO spray.

Fig.6-3 compares the droplets size distribution of RO spray wall impingement at T_i=298K by analyzing images in Fig.6-2. In this analysis, droplets are grouped by every 5μm. D

denotes representative droplets-diameter of each group and N is number of droplets in each group. At P_{inj}=40MPa in Fig.6-3(a), number of droplets is largest for Flat Bottom, followed by Toroidal wall and Squish. Most of the droplet size is under 30μm, with maximum frequency of 20-25μm for Flat Bottom. Increase in injection pressure P_{inj}=70MPa in Fig.6-3(b) indicates improvement of atomization showing increase of number of droplets. In particular, Flat Bottom produces large number of droplets in diameter under 20μm. Considering the images in Fig.6-2(b), long spray path penetration with Flat Bottom produces relatively wider spray boundary area for atomization, resulting in large number of small size droplets. This suggests that for RO spray impingement, it is desirable for spray atomization to improve spray penetration after impingement.

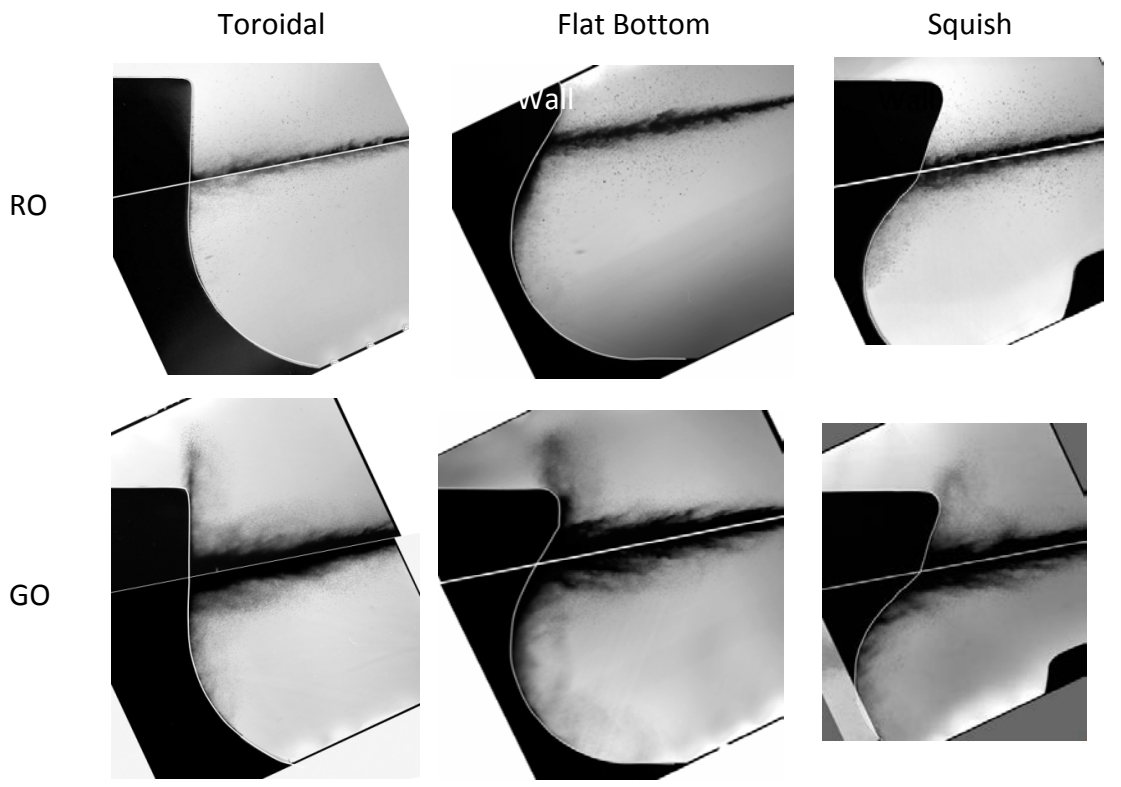

(a) P_{inj}=40MPa

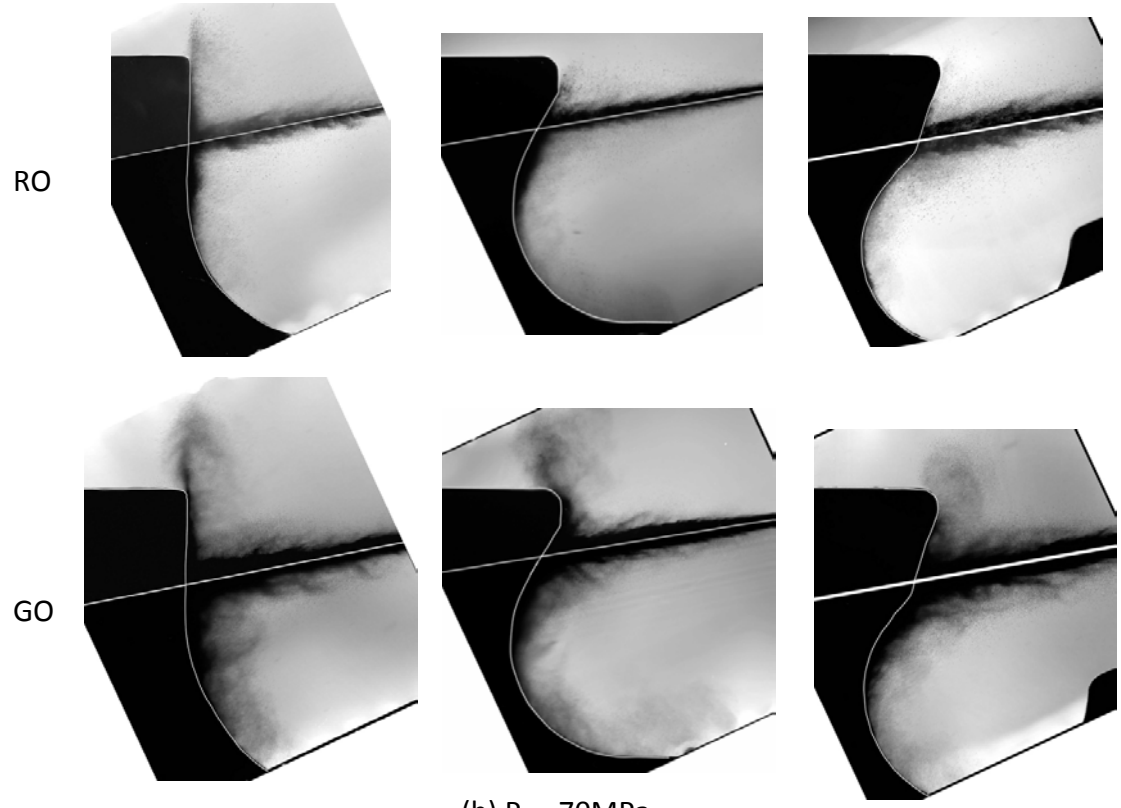

(b) P_{inj}=70MPa

Fig.6-2 Wall impingement spray comparison between rapeseed oil and gas oil (T_i=298K, 0.5ms after impingement)

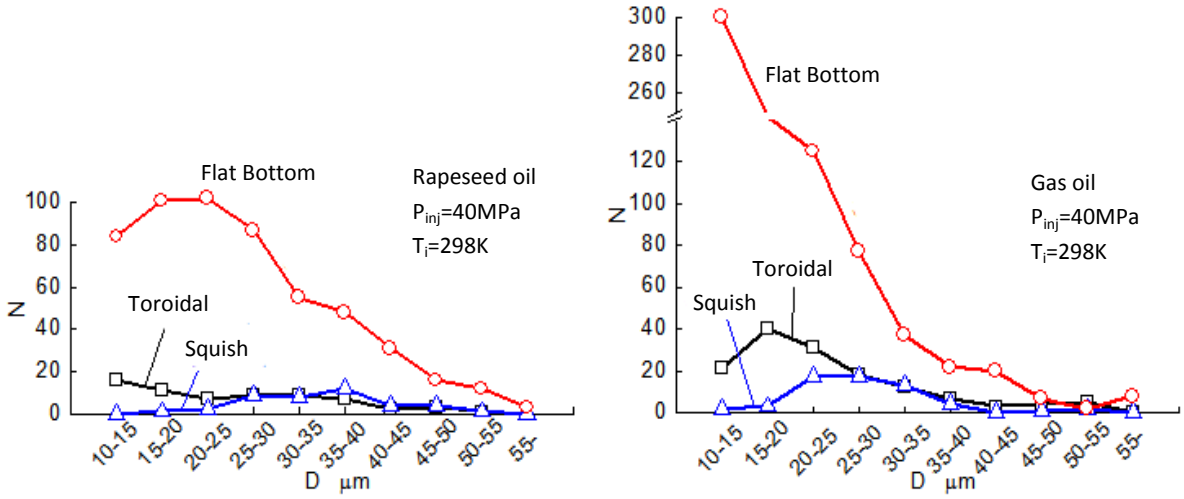

(b) P_{inj}=40MPa

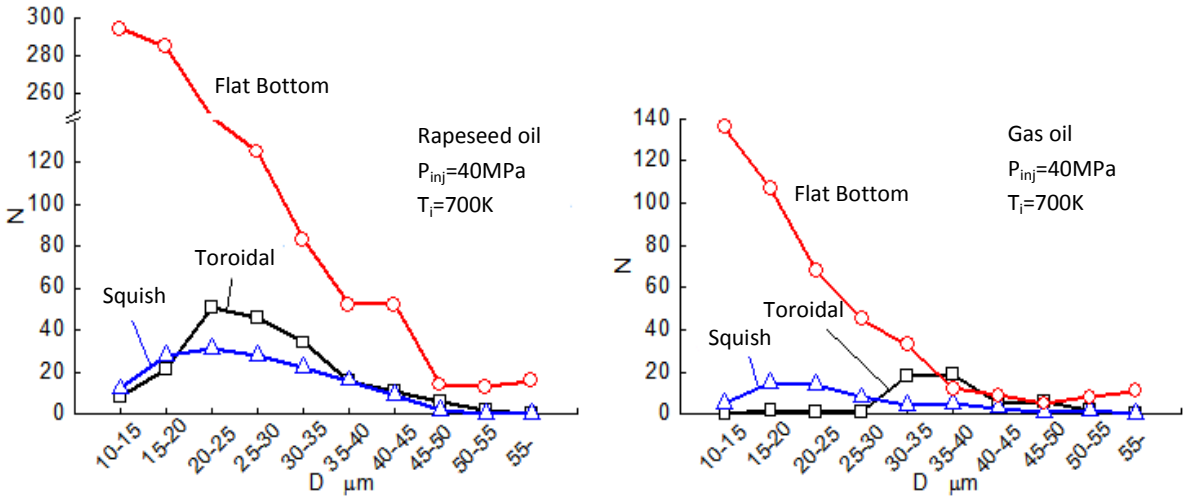

(b) P_{inj}=70MPa

Fig.6-3 Droplet distribution comparison between rapeseed oil and gas oil for wall impingement (T_i=298K, 0.5ms after impingement)

6.4 Wall Impingement At High Ambient Temperature

Fig.6-4 shows the wall impingement images for RO spray with ambient temperature increased to T_i=700K. In the case of high ambient temperature, high droplets-density region covers wide area. These characteristics are remarkable at high injection pressure and can be seen clearly. In addition, high ambient temperature condition comparatively reduces the region of high density liquid core. Result in Fig.6-2 shows that Flat Bottom has the longest spray path length with fine droplets can be seen around the spray tip. In contrast, it can also be observed that the liquid film formation was reduced when compared to room ambient temperature. This in turn proposes that at high ambient temperature, the ratio of RO spray that impinges the bottom side of cylinder head while in liquid state is reduced.

Similar to room temperature, Squish limit the progression of wall spray toward the upper section, which mean that the spray spillage from piston cavity also limited and reduce the spray impingement to cylinder head lower section. As for Toroidal, with increase of temperature, the spray fuel spillage from piston cavity become worse. This is especially true for RO as atomization for RO is slow when compared to GO.

Interestingly, when referring to Fig.4-4, where even at high ambient temperature and high injection pressure condition, little droplets evaporate for free-spray of RO fuel and vapor phase is not visible. However, impinging spray images in Fig.6-4 shows that even at lower injection pressure, P_{inj}=40MPa, vapor phase can be clearly seen formed at the spray tips area along the wall lower section. At higher injection pressure, the vapor phase is significantly larger and prominent. Thus, it can be said that wall impingement considerably promotes droplet evaporation, especially at high ambient temperature.

Fig.6-5 shows the droplet size distribution obtained by the images in Fig.6-4 when T_i=700K. In this analysis, droplets are grouped by every 5μm. D denotes representative droplets-diameter of each group and N is number of droplets in each group. At lower injection pressure, results shows that Flat Bottom has significant larger droplet number count, when compared to Squish and Toroidal. Average droplet diameter is also smaller, whit highest frequency around 20~25μm, which suggest that atomization, can be achieved quickly by using Flat Bottom wall configuration. Interestingly, when compared to room temperature condition in Fig.6-3, the droplet number decrease is significant. This is believed that the decrease in droplet number was due high ambient temperature condition which promotes atomization process and made the droplet to evaporate faster.

In addition, with increase of injection pressure, results show that number of

droplets becomes even smaller. This suggests a large number of droplets evaporate at high temperature with high injection pressure. The results again show Flat Bottom still has the largest droplet numbers, but when compared to the lower injection pressure condition, the decrease is rather significant. This result reinforce the finding that with higher injection pressure, faster atomization can be archived, and while this is largely known, in this particular case, Flat Bottom wall configuration is believed to promote atomization process better than Squish and Toroidal.

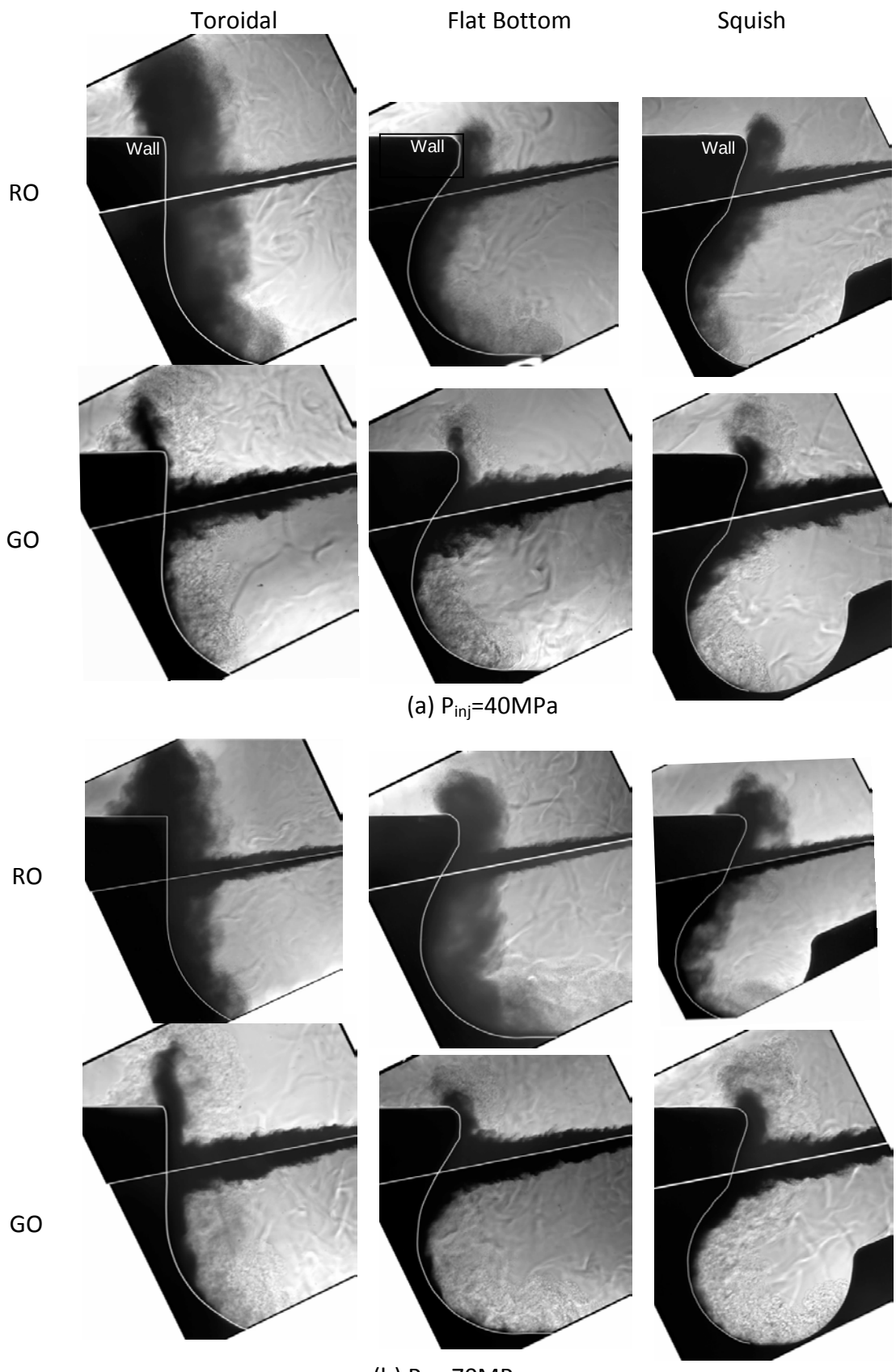

(a) P_{inj}=40MPa

(b) P_{inj}=70MPa

Fig.6-4 Wall impingement spray comparison between rapeseed oil and gas oil (T_i=700K, 0.5ms after impingement)

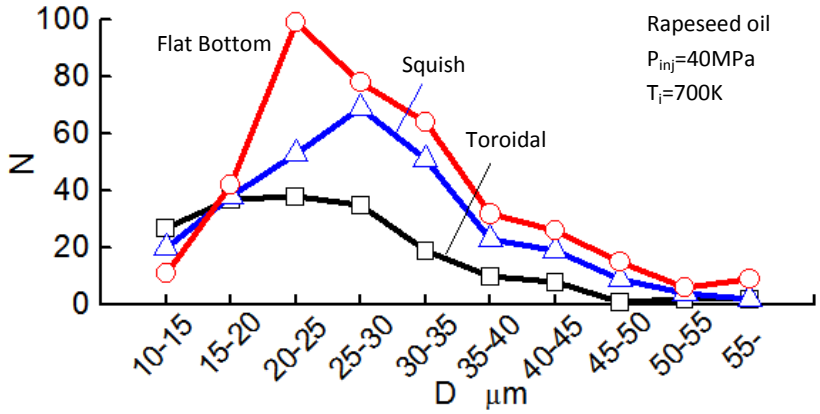

(a) P_{inj}=40MPa

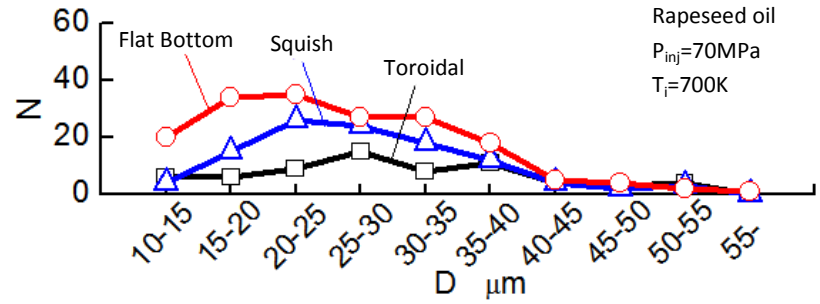

(b) P_{inj}=70MPa

Fig.6-5 Droplets distribution of rapeseed oil spray at high temperature atmosphere (T_i=700K, 0.5ms after impingement)

6.5 Effect of Nozzle Hole Angle

It is known from the previous section that spray to wall impingent angle during spray impingement has an effect to the spray atomization. In addition, it was also shown that the spray development after impingement and atomization (droplet generation) were influenced by the wall configuration. This section will try to study the spray development of spray impingement between spray with nozzle hole orientation angle of 159° and spray with nozzle hole orientation angle of 145°.

The same wall configuration known as Toroidal, Flat Bottom, and Squish were used. Ambient temperature was kept at room temperature of T_i=298K, with injection pressure P_{inj}=40MPa and 70MPa. Spray duration was kept at 2ms. Images were taken by direct photography method using high-speed video, for spray development observation.

First, previous experiment results from a high-speed video imaging will be summarized and explained. RO spray with injection pressure of P_{inj}=40MPa, at 0.6ms after impingement, spray fuel spill over from the piston cavity (piston bowl) can be seen for Toroidal with each nozzle hole angle of 145° and 159°. In contrast, Flat Bottom and Squish wall configuration, there is no spray fuel spillage from the piston cavity. This result shows that Flat Bottom and Squish wall configuration can be effective in limiting the fuel spray spillage out from the piston cavity for RO spray. When the injection pressure increase to P_{inj}=70MPa, as expected RO spray can be seen spilling out from the cavity chamber of Toroidal wall configuration. Interestingly, for Flat Bottom and Squish wall configuration, fuel spray spillage from the piston cavity can be observed for the nozzle hole angle of 159°. Thus, these results indicate that to limit the spray fuel spillage out from the piston cavity due to wall impingement, in the case of wall configuration used in this study, nozzle hole angle of 145° was beneficial, paired with the Flat Bottom and Squish can prove effective and provide good result. However, this result only evaluate the macroscopic spray development characteristics, especially regarding spray fuel spillage due to the limitation on the image resolution, other parameter were not measured.

For a more details study, nano-spark shadowgraphy method was used to observe microscopic characteristics, with each spray taken 2 times at different section and then combined together (better resolution and wider observation area) for each wall impingement. The same nozzles, nozzle angle hole of 159° and 145° were used paired with Toroidal wall configuration.

Fig.6-6 shows comparison of wall impingement for these two nozzle for RO spray

and GO spray, with P_{inj}=40MPa and T_i=298K, 0.5ms after wall impingement. In either case, fuel injected at orientation of 145° develops a larger spray tip, and the wall spray path has longer length. This is believed maybe due to the fact that when compared to 159° which spray impingement angle was more perpendicular, while with the 145° spray orientation was more parallel to the wall, thus making the wall spray spread more readily after impingement. In addition, droplet generation after wall impingement of RO spray at 145° spray orientation seemed to be slow when compared to 159°. In contrast, in the case of GO spray, it can be observed that droplet generation of 145° spray orientation is much faster with larger droplet number count.

To confirm the observation especially on the droplet generation after wall impingement, using image from Fig.6-6, droplet distribution comparison between the 2 nozzle for RO spray and GO spray was made as shown in Fig.6-7. As can be seen, the results shows that for each fuel type, nozzle hole angle of 145° has a greater droplet number counts. Especially in the case of GO spray, nozzle hole angle of 145° provide significant droplet number count increase (greater droplet generation) when compared to 159°. In contrast, this is different for the case of RO spray where the droplet count is not drastically different and the increase on droplet number count with the use of 145° is little.

To shortly conclude the results in this chapter, it can be suggested that wall impingement could improve RO spray atomization, especially with the help of high ambient temperature and high injection pressure. In addition, suitable piston cavity design can help in mitigating the negative impact of wall impingement, particularly to prevent spray fuel spillage from piston cavity where it has high probability to impinge and form deposit at the lower section of the cylinder head. Design such a squish-lip shaped cavity can be very useful in this case. Moreover, the piston design such as Flat Bottom that has flat bottom shape also can help to improve RO spray by eliminating any obstacle for the wall spray to penetrate longer, thus generating larger spray area that will help to promote atomization. Lastly, as interaction of spray wall impingement also affected by impingement angle, nozzle design which in this particular case, related to the nozzle hole angle also should be take into consideration.

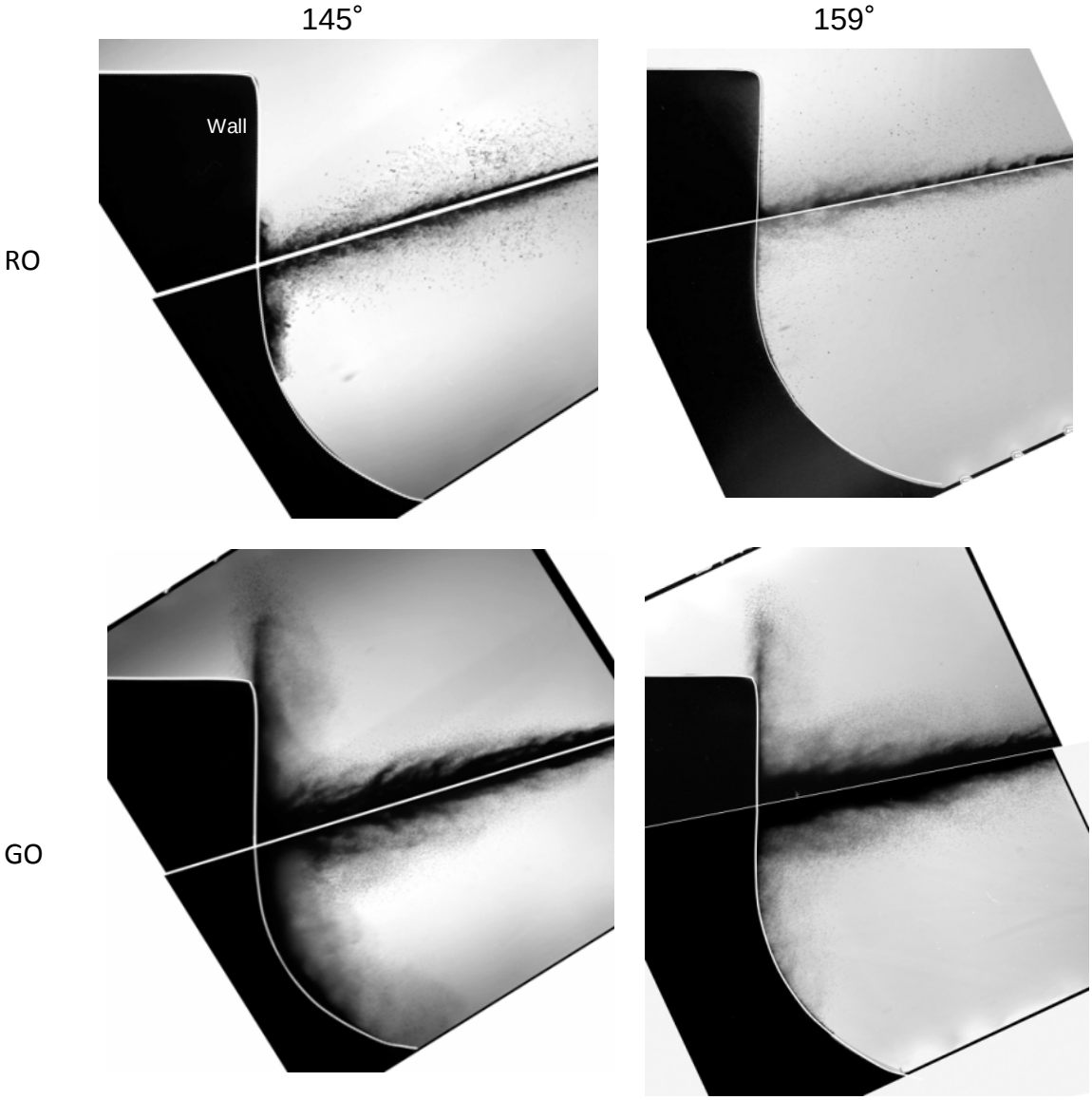

Fig.6-6 Comparison on the effect of spray nozzle angle to wall impingement
(P_{inj}=40MPa T_i=298K, 0.5ms aSOI)

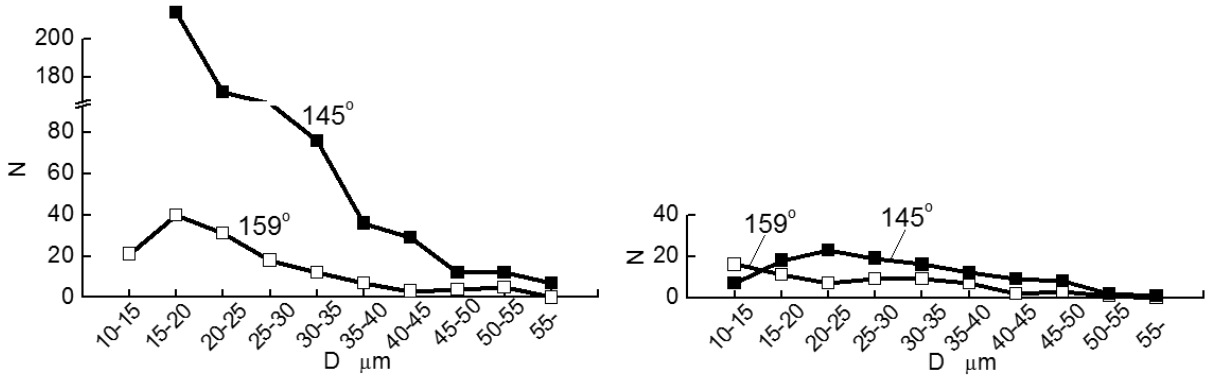

Fig.6-7 Droplet distribution comparison of spray nozzle angle
(Toroidal, P_{inj}=40MPa T_i=298K, 0.5ms aSOI)

Chapter 7 Effect of Air Movement to Spray Development of Rapeseed Oil Spray

7.1 Introduction

In has been proven from the results from Chapter 4 to 6 that RO spray has very slow atomization due to its high viscosity nature. Although high injection pressure, high ambient temperature and combination of nozzle geometry with piston cavity design and suitable injection strategy can promote faster atomization of RO spray, another factor that was not discussed is the effect air movement that could positively influence RO spray development.

It should also be stated that the diesel spray injector used in all the experiments done in Chapter 4 to 6 is for the use of DI diesel engine, which generally use the concept of fast fuel – slow air mixing. This is due to the fact that DI diesel engine has to force the fuel to highly compressed air, the fuel need to be of high velocity. In contrast, as the fuel in injected directly to the spray chamber, air movement is relatively slow and quite limited.

On the other hand, IDI diesel engine uses a different air mixing strategy, which is slow fuel – fast air mixing. IDI diesel engine usually designed to have a prechamber (small space to initiate air fuel mixing) that the spray is injected into. Air movement inside the combustion chamber is amplified as it move through the prechamber where it will mix with the fuel before making it way to the main combustion chamber. This process made effective fuel air mixing possible. The fast movement of air mitigates the need of high velocity spray jet, which make IDI diesel engine not requiring high injection pressure fuel delivery system.

Although this study focuses on the use of RO in DI diesel engine, it would be intriguing to study the characteristic of RO spray beyond the limitation of DI diesel engine usage. As the usage of alternative fuel (in this case, RO) is not limited to one type of engine only, the study of any viable condition that could help to improve the spray atomization is commendable. In addition, the usage of RO in IDI diesel engine was suggested to be actually more suitable then DI especially when considering the possibility of injector choking which can be a major problem when using RO to DI diesel engine. As IDI diesel engine spray use the pintle-type nozzle, this risk is largely reduced.

7.2 Experimental Apparatus and Swirl Generation

To study the effect of air movement, in particular to generate the swirl (air movement inside the chamber), a swirler was used. This swirler is fixed inside the chamber as shown in Fig.7-1, just after the stop ring. It functions by carefully guiding the inert gas that is propelled by the rapid compression machine to move into the chamber in an angle (α) which will produce fast air movement (swirl). At the same time, as inert gas is being compressed inside the chamber, high ambient temperature also is generated.

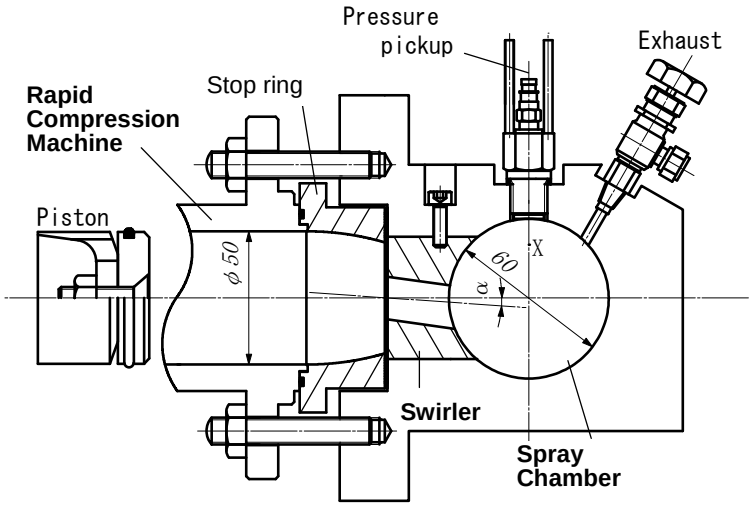

Fig.7-1 Chamber cross section with swirler

To confirm the swirl speed, trial experiment by using tracer particle inserted in the chamber was done. Fig.7-2(a) shows the swirl speed distribution when measured from chamber center at Ti=700K. It can be seen that the swirl speed, V_s become big when further from the center, with the highest velocity about V_s=60m/s measured at location of 2/3 of the chamber radius. This is approximately around r=15~20mm. In contrast, when the swirl is located near the outside spray wall chamber, the swirl speed decrease and become little.

Fig.7-2(b) shows swirl speed and the changes in chamber ambient temperature, T_i versus time. Time is calculated starting when the piston hit and immobilized onto the stopper, t_0=0ms. As shown in the figure, swirl speed and ambient temperature decrease with time, and V_s=60m/s is achieved around T_0=8ms. In this study, experiment parameters are chamber ambient temperature to be at T_i=700K and swirl speed is V_s=60m/s. This require the spray to be injected on T_0=9ms.

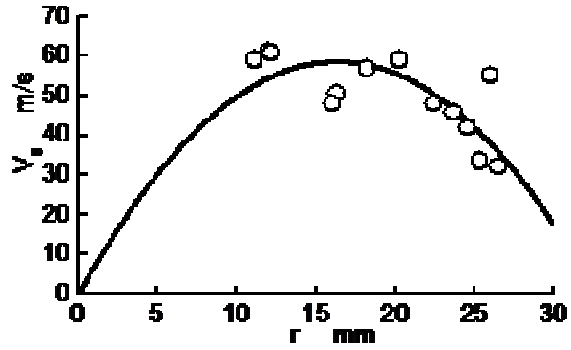

(a) Swirl speed distribution measured from center during Injection

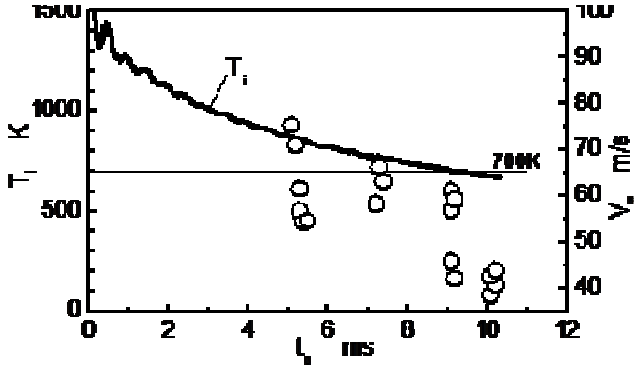

(b) Swirl speed and average ambient temperature versus time

Fig.7-2 Swirl inside the spray chamber

It should be stated as this experiment was a joint research with a commercial company, the specification on the IDI nozzle is not available for publication due to legal issue. However, the result theoretically should reflect the characteristic of RO spray development when injected using IDI nozzle that available for commercial use.

Other apparatus were as per explained in Chapter 2. In addition, a few alterations was also done particularly on the optical arrangement and the light source to accommodate shadowgraph high speed video camera imaging, to capture a more visible cloud-like dense droplet region as the current direct photography high speed video produce low contrast image; making this region difficult to identify.

7.3 Comparison of Spray Development between Rapeseed Oil Spray and Diesel Spray in IDI Nozzle

Fig.7-3 and Fig.7-4 shows comparison between RO and GO spray development in IDI nozzle, at P_{inj}=40MPa.. The former is at T_i=298K or room temperature while the later is at high ambient temperature of T_i=700K. Spray picture was taken using shadowgraph photography technique which provide very high resolution image. As RO has very slow initial spray development, RO spray images were taken at t=1ms and 2ms. Meanwhile, GO is spray images were taken at t=0.3ms and 0.5ms.

In Fig.7-3, it can be seen that RO spray form a stick like appearance through out the spray formation. This is similar to results obtain from Chapter 4, where RO characteristics were studied using DI nozzle. This particular characteristic also made atomization process to be retarded for RO spray. In addition, the spray liquid core has a heterogeneous liquid distribution, making the confirmation of spray main jet to be difficult. Referring to the magnified image, it can be observed that spray droplet form along the spray boundary from upper to lower section. However, the droplet size is big when compared to that of GO. In contrast, GO spray for IDI nozzle is very similar to DI nozzle in Fig.4-1. Spray development and droplet size seem to be the same. The only noticeably different is that DI nozzle seems to form a slightly larger spray angle especially at the nozzle exit.

With high ambient temperature, shown in Fig.7-4, It can be observed that RO penetrate easier. When compared to T_i=298K at t=1ms, the penetration length shows significant increase, and also droplet formation can be seen at the boundary region, which is not existed before. However, when refer to the magnified image, droplet size still relatively big. When carefully observed especially at the lower section, the droplet count is still not as much as GO, which at this condition has formed region with high density of droplet, especially at the spray tip. Also, the stick like appearance still visible in IDI nozzle RO spray and while branching structure similar to GO can be observed, the branching structure is premature and not as refined as GO. This suggests slow atomization even with high ambient temperature condition. As for reference, when compared to DI nozzle spray at the same condition in Fig.4-3, DI nozzle spray has a smaller droplet, suggesting IDI nozzle has a slower atomization rate compared to DI nozzle.

To study more of spray development characteristics of RO, the images in Fig.7-3 and Fig.7-4 were analyze by in-house image analysis system, explained in detain on Chapter 3. The result is shown in Fig.7-5 and Fig.7-6. This result shows the spray boundary outline and

spray liquid core progression. In addition, the same analysis was done to DI nozzle spray, and the result is shown in Fig.7-7, for reference purpose.

Fig.7-5 shows that RO has very narrow region of high density liquid core when compared to GO. With progression in time, the spray outline seems to expand further from the center axis. However, the high density liquid core region still remains narrow and in certain location, can be seen to be detached. In addition, the spray outline analysis is influence by the large droplet that formed along the boundary region, such making the spray outline to appear expanding. This characteristic is similar to DI nozzle spray in Fig.7-7(a).

In Fig.7-6, with increase in ambient temperature, the high density liquid core region seems to become larger, but still narrow when compared to GO. The outer spray outline also expands further outward from the nozzle center axis. This suggest high ambient temperature promote atomization. The same effect can be seen in GO spray. In general, the spray penetration length also becomes shorter, suggesting higher atomization rate. When compared IDI nozzle to DI nozzle spray development at high ambient temperature in Fig.7-7(b), the different of high density liquid core region is significant. DI nozzle can be seen to have a bigger area high density liquid core region, which is also continuous without any detachment. In addition, DI nozzle forms a bigger spray tips.

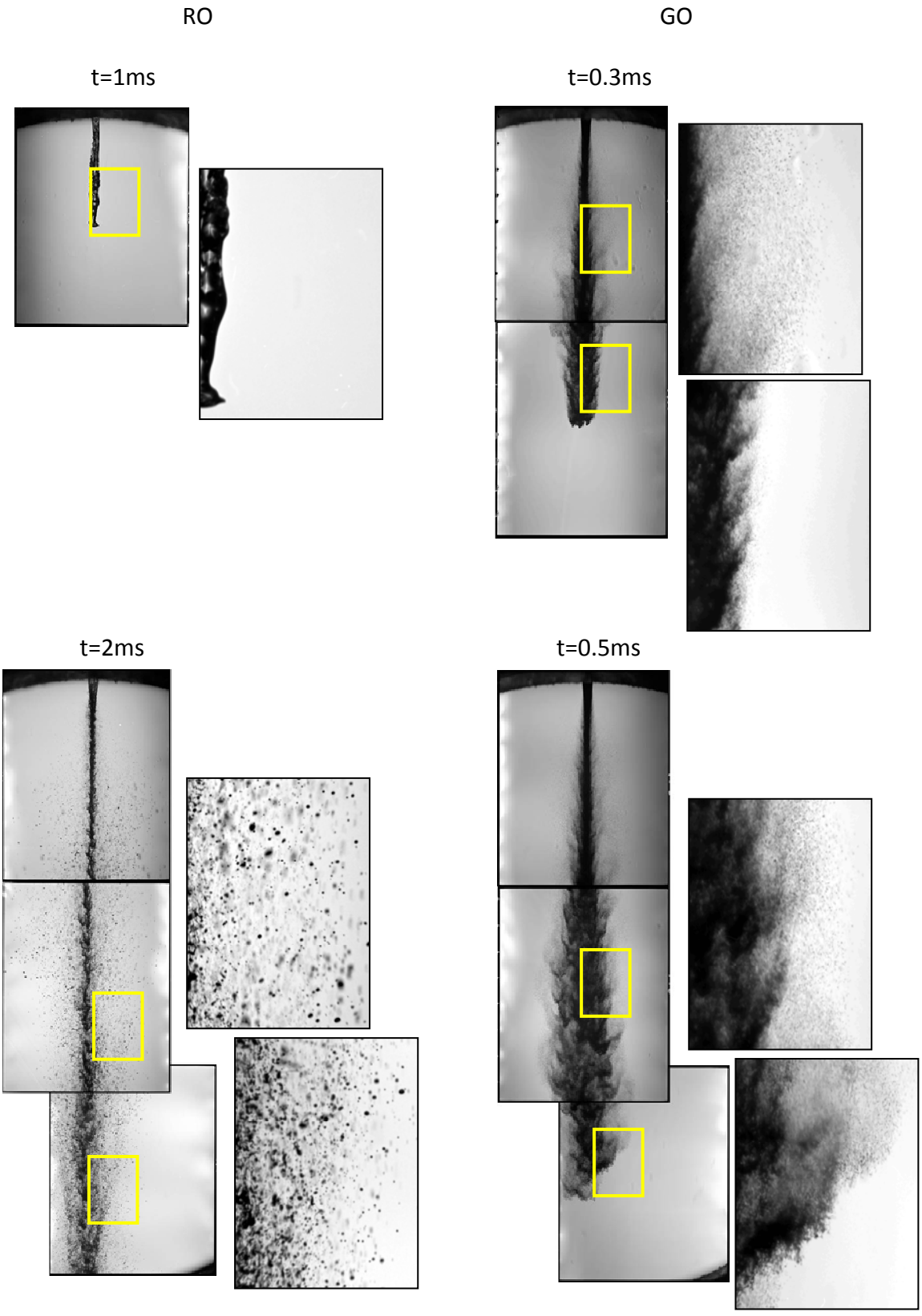

Fig.7-3 Comparison between rapeseed oil to gas oil spray development
(IDI nozzle, P_{inj}=40MPa, T_i=298K)

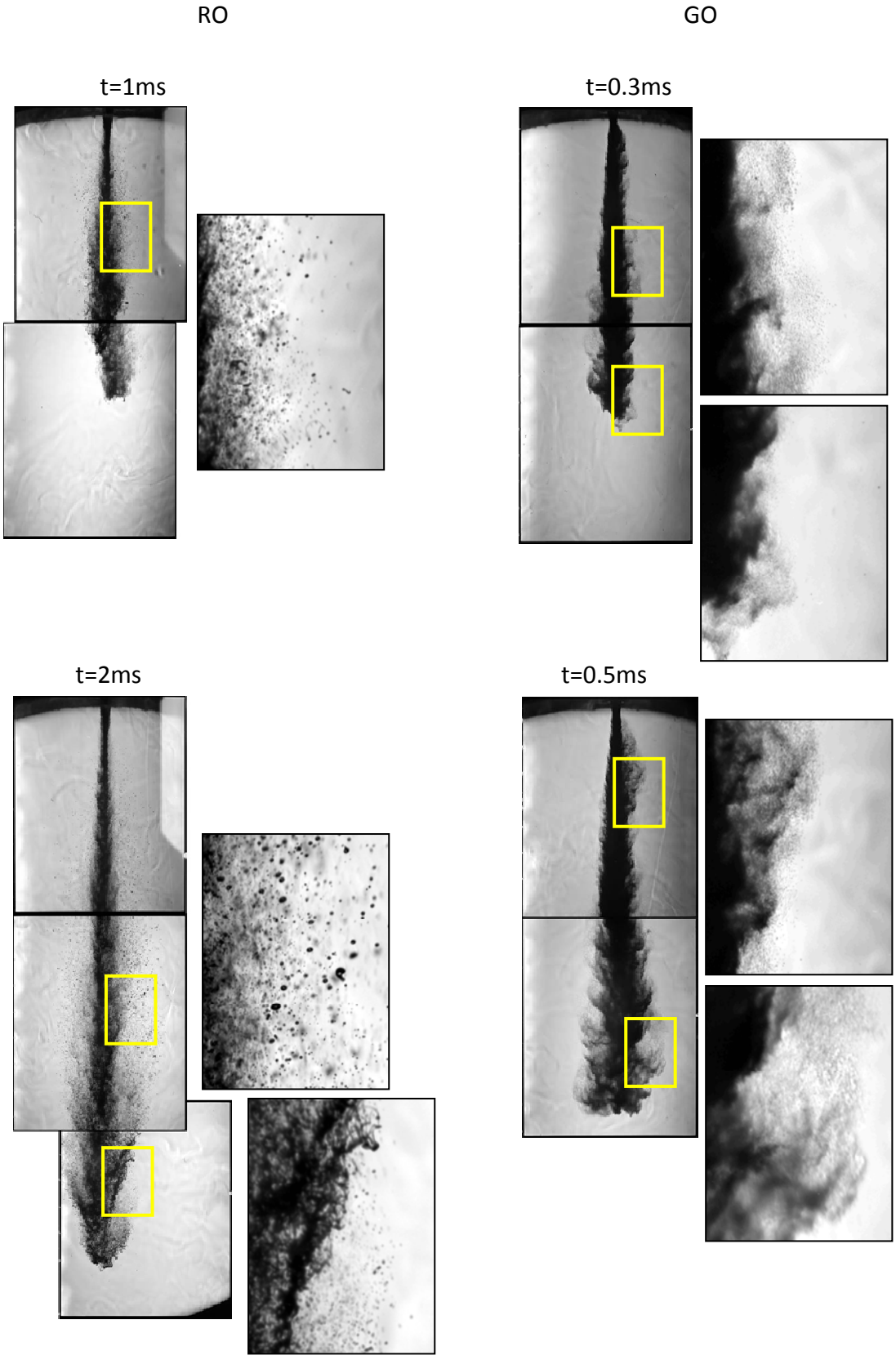

Fig.7-4 Comparison between rapeseed oil to gas oil spray development
(IDI nozzle, P_{inj}=40MPa, T_i=700K)

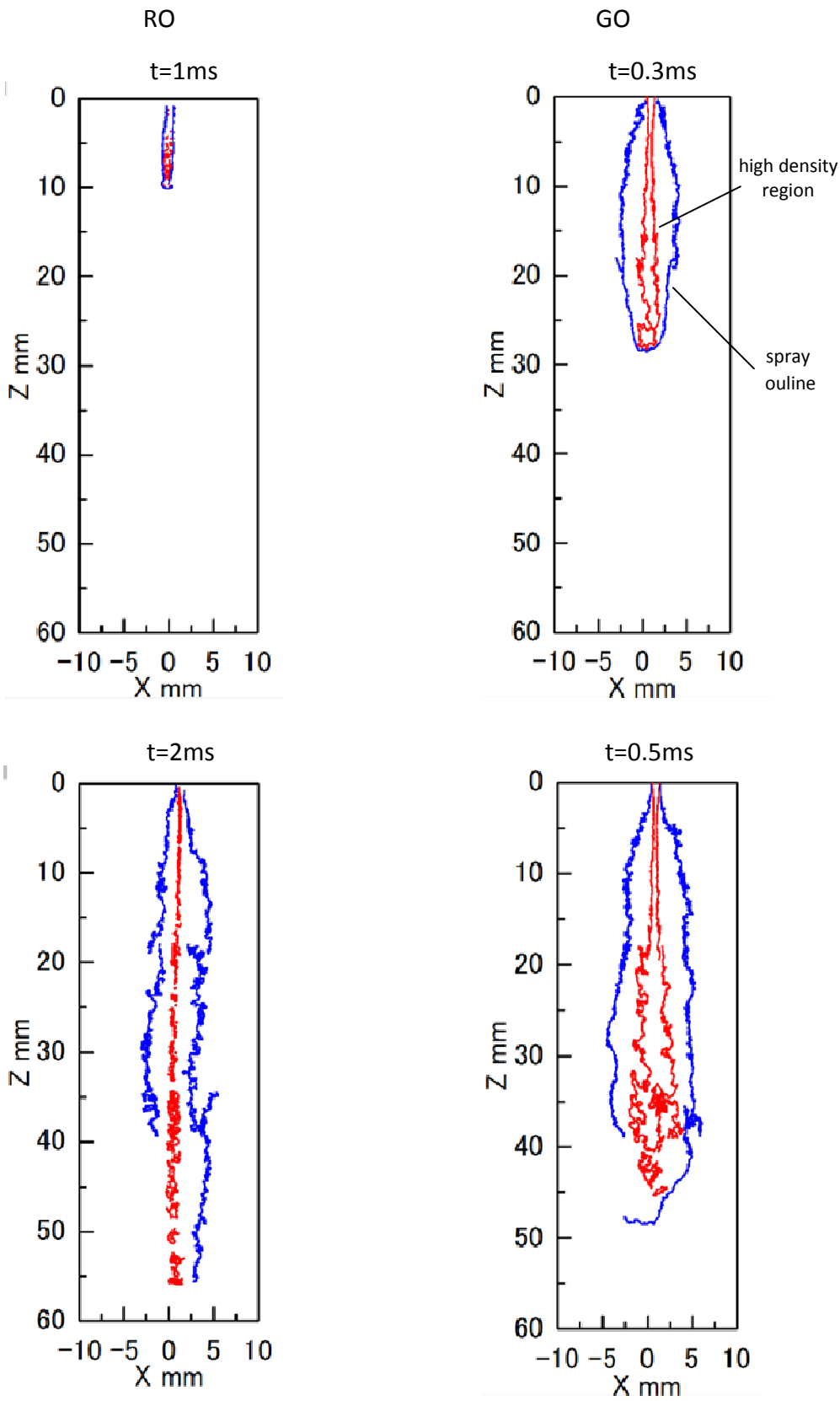

Fig.7-5 Spray development outline and progression of liquid core in IDI nozzle (P_{inj}=40MPa, T_i=298K)

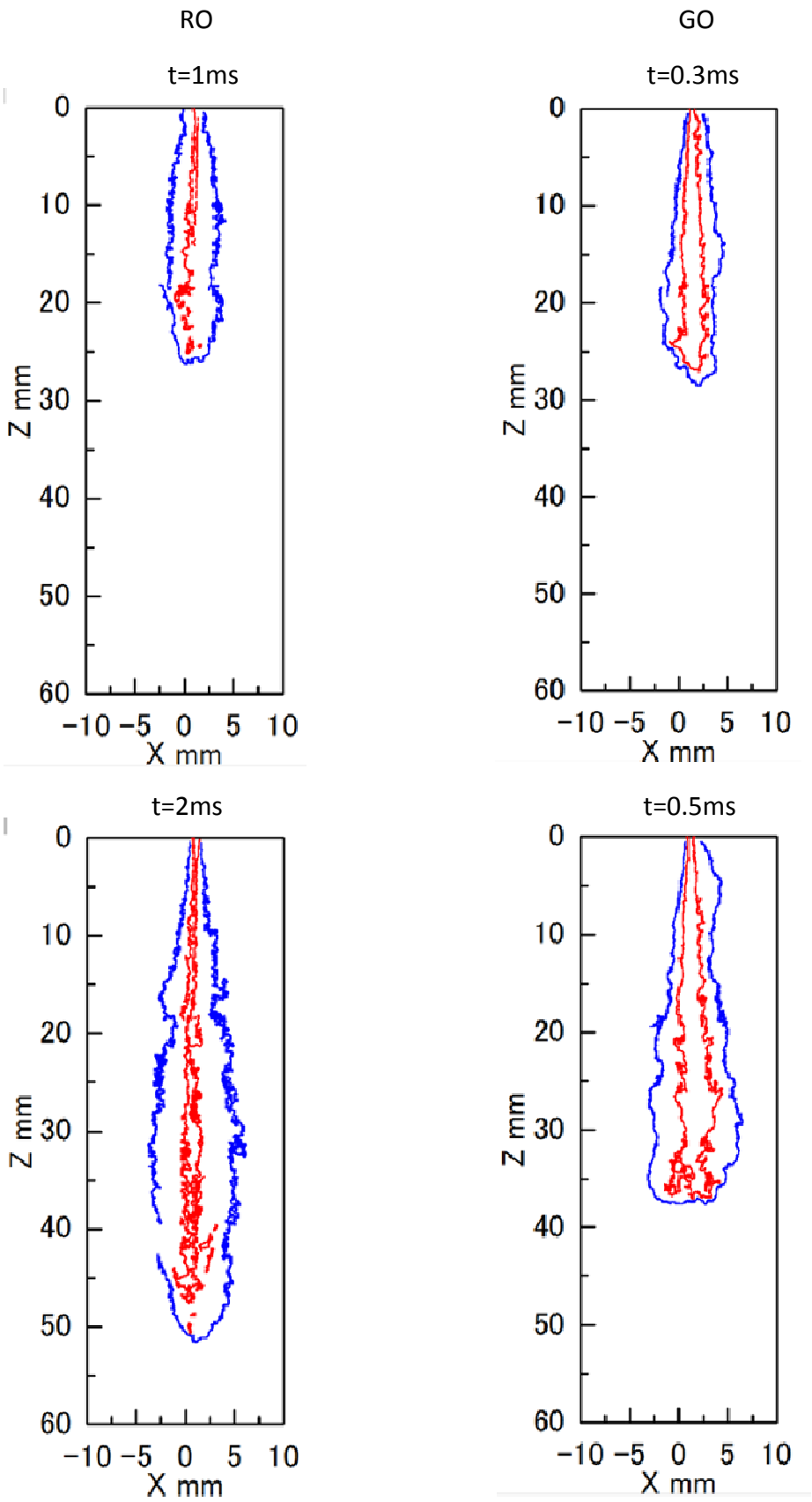

Fig.7-6 Spray development outline and progression of liquid core in IDI nozzle (P_{inj}=40MPa, T_i=700K)

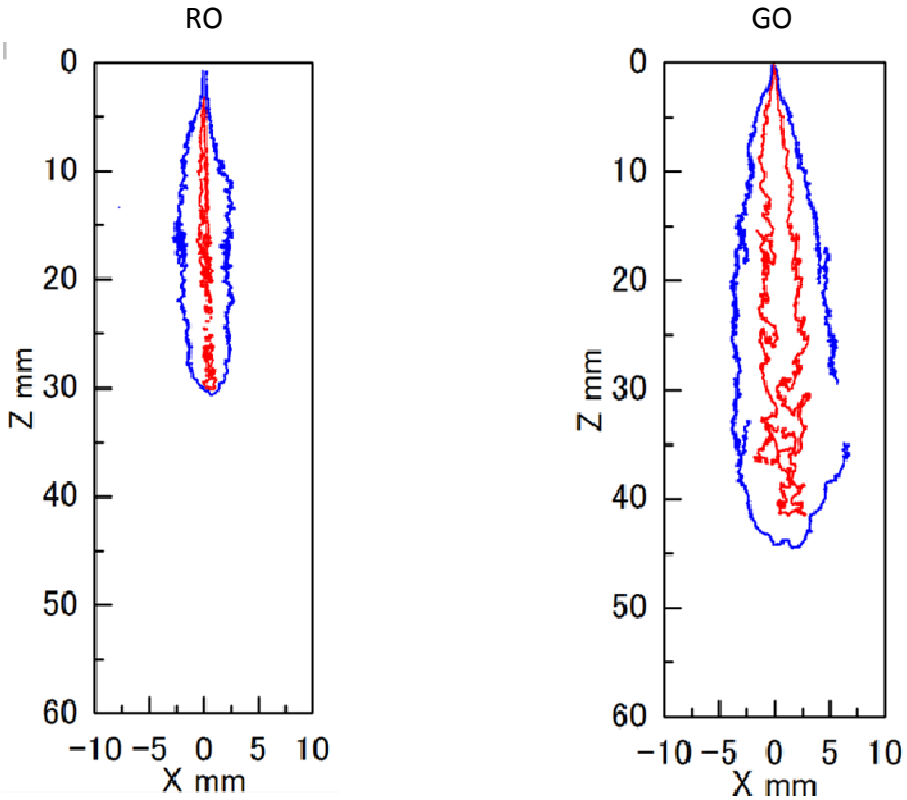

(a) P_{inj}=40MPa, T_i=298K, t=0.5ms

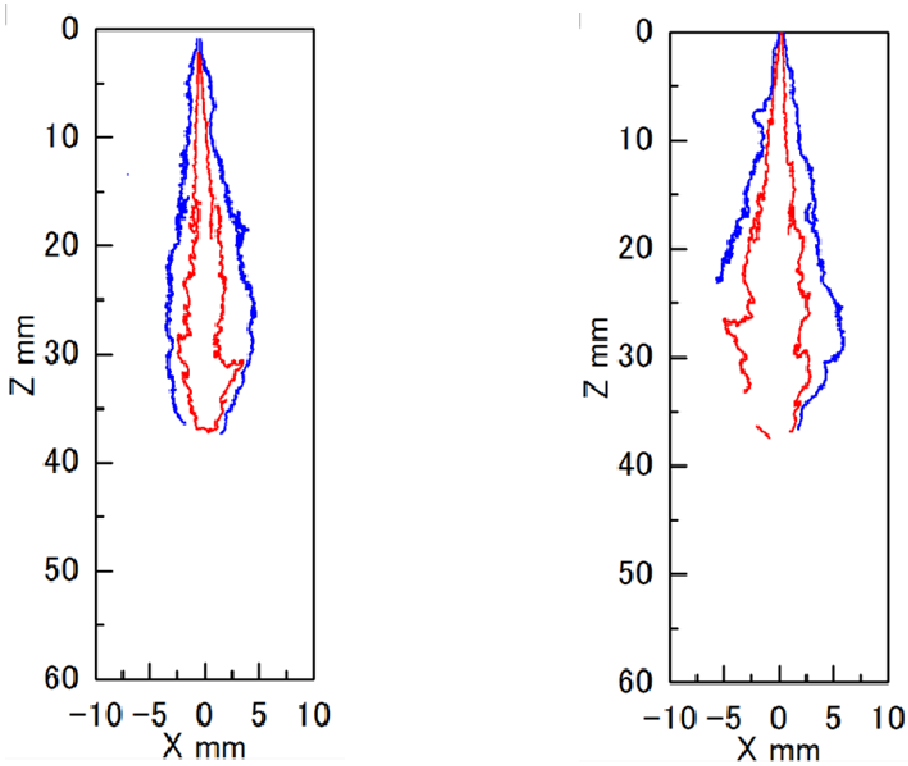

(b) P_{inj}=40MPa, T_i=700K, t=0.5ms

Fig.7-7 Spray development outline and progression of liquid core in DI nozzle

7.4 Droplet Distribution

Using the images taken, image analysis for droplet sizing and distribution was done. Similar to method used in previous chapter, the spray is divided into section, in this case, into 3 sections, namely upper, middle and lower. All droplets diameters, D are characterized by representative grouping in every 5µm and N is the droplet count number.

Fig.7-8 shows IDI nozzle RO spray droplet distribution. As shown in Fig.7-8(a), at P_{inj}=40MPa, T_i=298K and t=2.0ms, the spray upper and middle section has a large droplet size with average of 20-25µm at middle section. When compared this with GO spray in Fig.7-9, it can be seen that GO spray has a smaller average droplet size with highest frequency of 10-15µm in middle section when t=0.5ms. In addition, when compared the number of droplet between RO and GO spray, GO clearly has bigger number of droplet especially at the upper section. At middle section, the number seem to be comparable with the smaller average droplet size while at lower section, GO spray has smaller droplet number, which suggest that GO spray lower section droplet is undergoing rapid vaporization. This indicates that even with longer injection time, RO spray still have problem to produce small diameter size droplet.In the other hand, Fig.7-8(b) shows droplet distribution of IDI nozzle RO spray at high ambient temperature of T_i=700K. When compared T_i=298K, the total droplet number count was reduced. This suggests atomization is faster with higher ambient temperature. In particular, the middle section average droplet size was reduced with the highest frequency of 15-20µm. It also can be observed that at lower section, very little number of droplet visible for sizing.

For comparison, it should be stated that referring to Fig.4.6 which so RO spray DI nozzle droplet distribution, it can be seen that IDI has larger droplet size throughout the spray length. It can be suggested that IDI nozzle produce slower atomization of RO spray than of DI.

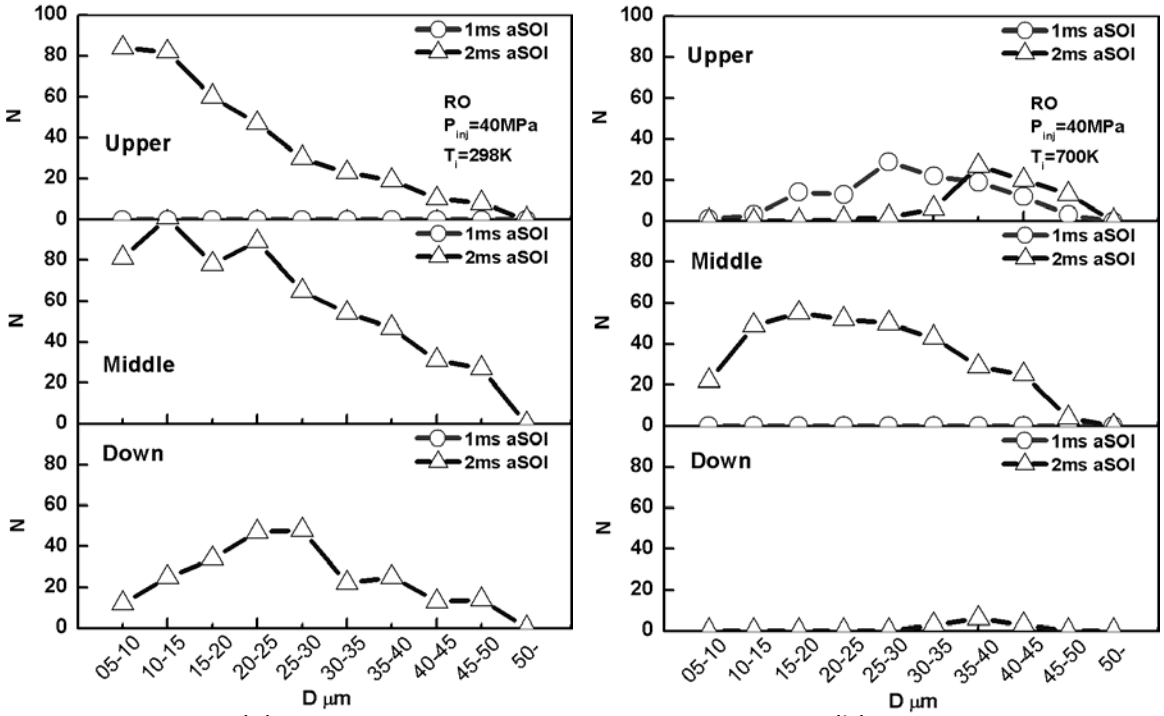

(a) T_i=298K (b) T_i=700K

Fig.7-8 Droplet distribution of rapeseed oil (P_{inj}=40MPa)

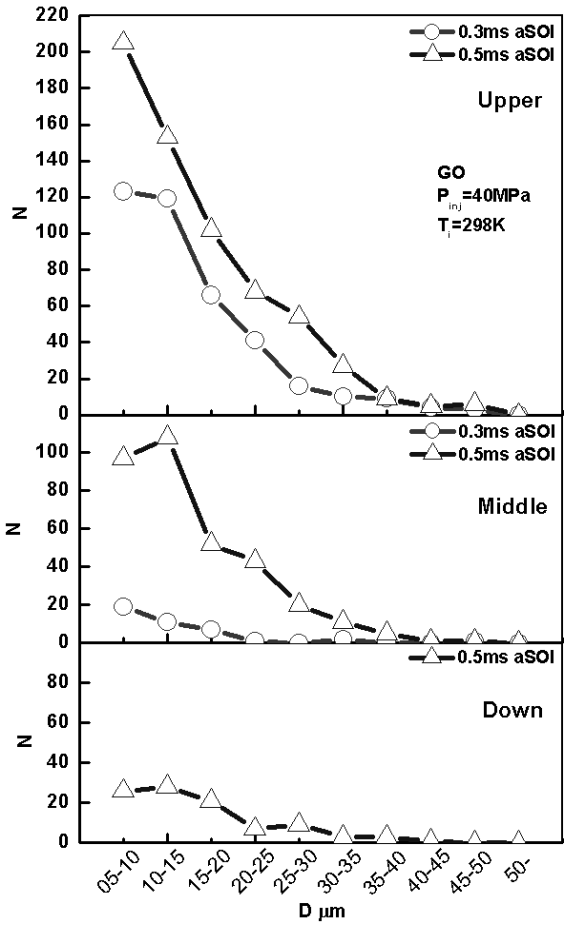

Fig.7-9 Droplet distribution of gas oil (P_{inj}=40MPa, T_i=298K)

7.5 Air Movement Effect to Rapeseed Oil Spray Development

Next, we will study the effect of high speed swirl to the spray development process in IDI nozzle spray, for RO and GO. The experiment parameter were done at injection pressure of P_{inj}=40MPa and also at P_{inj}=70MPa, with the ambient temperature of T_i=700K. The swirl speed is V_s=60m/s around the vicinity of 20mm, which translate to 2/3 distance from the chamber center and move counter clock wise. The spray was injected downward to the chamber with the spray injector located straight above the chamber center.

Fig.7-10 shows the spray development of RO spray for IDI and DI nozzle. Injection pressure was P_{inj}=40MPa and ambient temperature was T_i=700K, with IDI nozzle spray on the left and DI nozzle spray on the right It is obvious that from the image, DI nozzle spray has greater penetration length which suggest higher injection rate, and form a circular spray path similar to IDI nozzle but with the spray main body retaining the downward direction more. The spray also seems to expand outward from the main body spray through the whole spray length, which suggests fuel dispersion due to swirl. At t=2.0ms, it can be seen that DI nozzle has completed the injection with the main body is now not visible, and the spray tip has made a full circle and converging at the nozzle tip. At t=3.0, almost all the dense droplet region vanish and not visible in the image which suggested that the spray is currently being vaporized; and at t=5.0ms, the spray has fully vaporized.

In contrast, RO spray IDI nozzle result is consistence with the previous experiment which was taken using direct photography high speed camera method. The spray has relatively slow penetration rate especially at initial injection period, and significantly affected by the swirl and has circular spray path. At t=2.0ms, the spray tip reach the chamber bottom, having made a ½ circle. Only until t=4.0ms, the spray tips made a full circle; with the spray injection is completed and the main spray body was now not visible; while at t=5.0ms, most of the droplet dense region is now not visible. The result suggests that IDI nozzle has slower atomization rate than DI nozzle for RO spray.

Similar trend can be seen in GO spray in Fig.7-11. IDI nozzle GO spray was easier to be influenced when compared to DI; where the spray progress nearer along the wall and the spray boundary expand greatly suggesting fuel dispersion due to swirl. At t=2.0ms, spray injection in either nozzle has completed and the spray body is not visible. Interestingly, the dense droplet region that left visible show approximately the same size, which suggest that atomization rate of IDI and DI nozzle for GO spray is comparable.

Further comparison on the effect of air movement to RO spray can be made in the

form of comparison of free jet spray to spray under swirl condition. Results of DI and IDI nozzle under swirl condition, when compared to the previous free jet images in Chapter 4, clearly show the different of spray boundary fuel-air mixing. On free jet spray, RO spray form a very narrow cone angle, while under swirl condition, the spray expend outward from center axis due to the dispersion of fuel from air movement. This in turn, increases air entrainment inside the spray body, expand the spray boundary and eventually effect the spray atomization.

To conclude this chapter, a study was made to compare RO spray development between IDI and DI nozzle, for reference purpose. A comparison on RO spray under swirl condition and free jet spray was also made. The result here would like to note the possibility of DI engine injection system which incorporate high air movement strategy to be use for RO, which has been proven to have significantly better atomization than without the assistance of air movement, and the benefits is significantly greater in RO than GO.

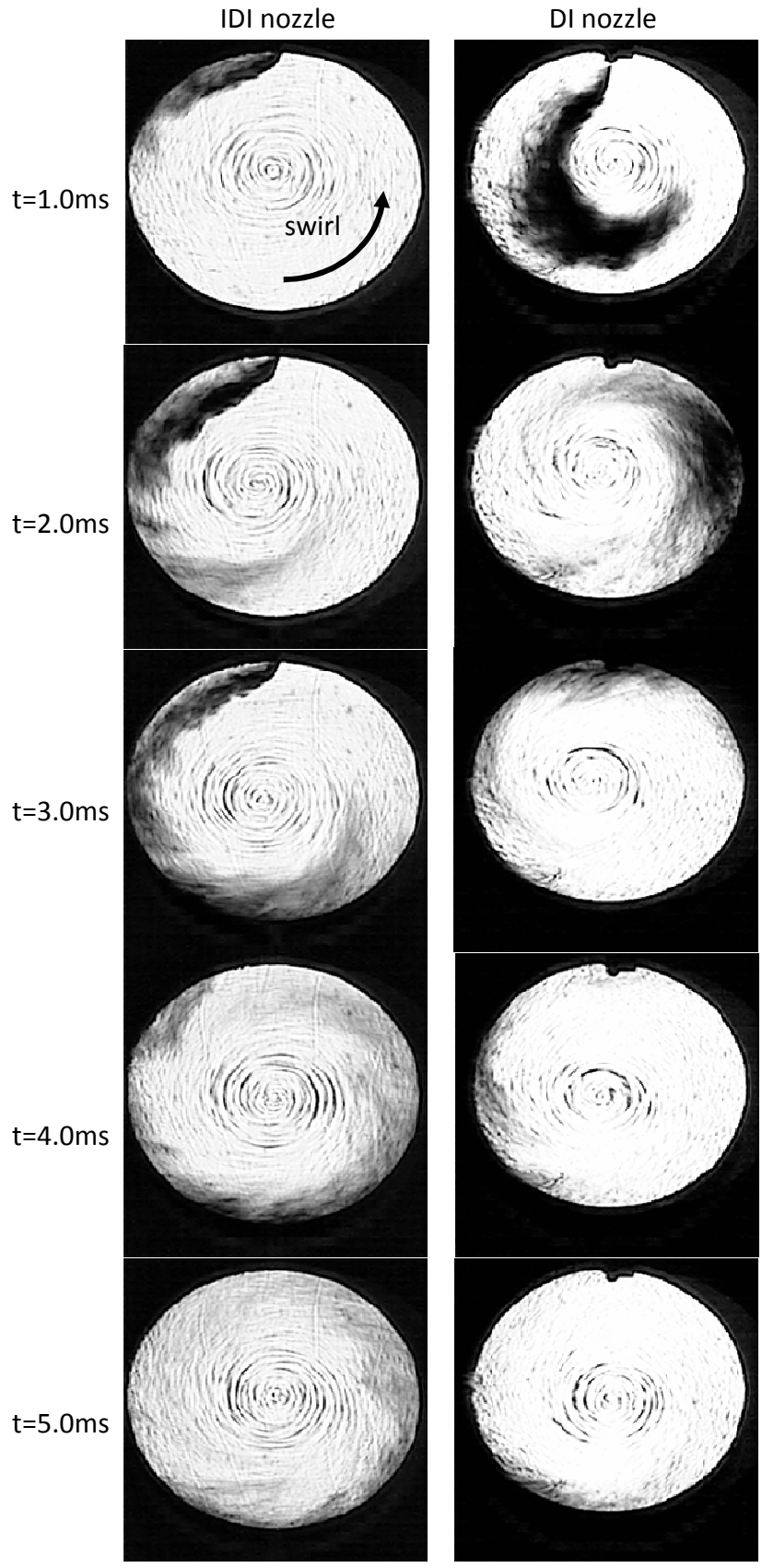

Fig.7-10 Comparison between IDI nozzle and DI nozzle rapeseed oil spray development under swirl influence (P_{inj}=40MPa, T_i=700K)

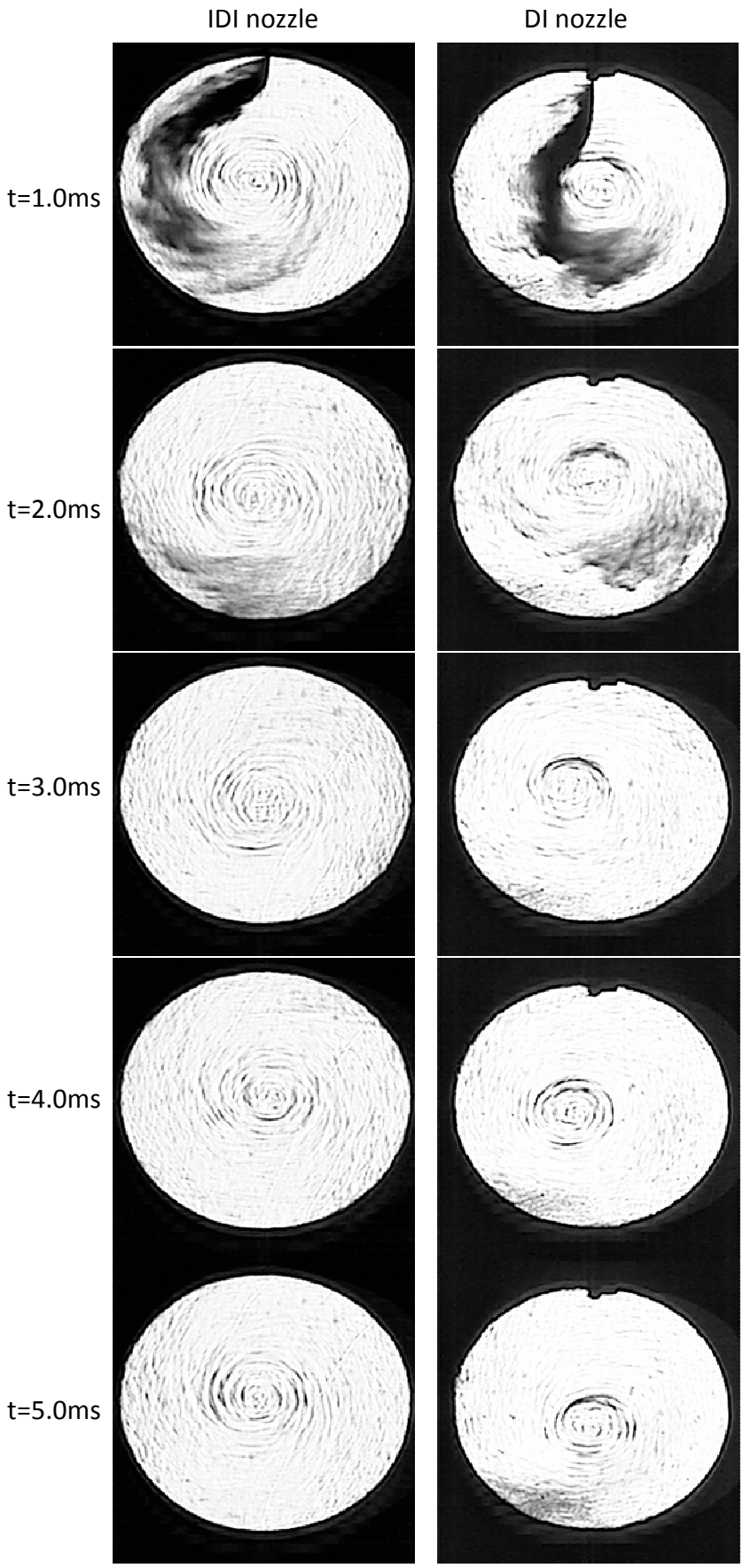

Fig.7-11 Comparison between IDI nozzle and DI nozzle gas oil spray development under swirl influence (P_{inj}=40MPa, T_i=700K)

Chapter 8 Conclusion

In this study, the spray characteristics of diesel also known as gas oil (GO) as a reference fuel and rapeseed oil (RO) including macroscopic and microscopic spray structure, spray development, fuel evaporation, and droplets atomization were studied. Dynamic behavior of each spray was also studied. A rapid compression machine was utilized to simulate the high pressure and high ambient temperature in actual diesel engine. Shadowgraphy that utilize nano-spark light source was used for high resolution still picture capture. High speed video camera was also use to capture spray development. Analysis of still picture is done by using image analysis software coupled with custom made algorithm that has been initially calibrated.

Result shows that RO spray has poor atomization and needs high temperature and high pressure to help atomization. The use of suitable nozzle geometry, in particular nozzle with mini-sac design and narrow outlet nozzle diameter can help atomization process especially at the initial stage. Wall impingement strategy, with suitable wall configuration (shape) and injection nozzle angle also can help atomization process of RO spray as it can promote longer wall spray jet (path) and create a wider spray boundary for droplet formation. Lastly, the effect of high speed swirl (air movement) was study and proven to be beneficial in improving RO spray atomization.

1. Poor atomization and evaporation characteristics of RO at early stage of injection may produce a source of SOF emission at light load engine operation that has short injection duration, low injection pressure and low ambient temperature. Improvement on atomization process is a necessary for RO to be use in diesel engine.

2. Atomization of RO spray is worse than that of GO spray, in particular at early stage of injection. RO spray forms a stick-like structure without branching structure at spray boundary as compared with GO spray. RO spray has heterogeneous density distribution in a liquid column at spray centerline. The droplets formed by RO spray are bigger size and the number of droplets is less than that of GO spray.

3. High viscosity characteristic prevents RO injection at initial stage of injection. RO spray hardly penetrates at less than 0.5ms after start of injection, in particular, at low injection pressure. Although high injection pressure lengthens penetration of RO spray, high

temperature atmosphere is further necessary to produce branching structure and fine droplets. High temperature is effective to promote atomization especially at downstream of RO spray.

4. At lower ambient temperature, droplets of the upper section of GO and RO, due to small kinetic energy, can be observed to be heavily affected by air entrainment and move toward the spray body. Droplets of the middle and lower section of GO and RO show different tendency from each other. GO spray droplet from these sections fly outside from the spray body, with some of them moving at 90° from the spray axis. In contrast, most of the RO spray droplets move along the spray axis without much deviation. This is believed due to the droplet size different between GO and RO spray droplets, with RO spray droplets has a larger droplet size and kinetic energy.

5. At T_i=700K, although droplet formation can be seen, vapor phase is not visible for the RO spray. This is due to the high vaporization temperature of RO. When ambient temperature increased to T_i=850K, vapor phase can be observed especially at the middle section.

6. Spray characteristics of RO can be improved by using mini-sac nozzle accompanied with high injection pressure. Even at lower injection pressure, mini-sac usage has longer penetration rate especially 0.4ms after start of injection and also improve the initial spray cone angle at initial injection period, which could improve atomization.

7. Narrowing-hole nozzle with small outlet hole-diameter increase spray penetration length at initial injection stage. This is believed due to the small outlet hole diameter. However, at high injection pressure, the penetration length difference to other nozzle design is little.

8. Wall impingement effectively promotes RO spray atomization. Regarding piston-wall configuration, squish-lip can prevent spray development toward upper direction, leading to prevention of liquid film impingement on the lower face of cylinder head in a real engine. Spray atomization is more sensitive to wall configuration for RO than GO. Better atomization results in quick evaporation of droplets at high temperature

atmosphere.

9. The piston-wall that has flat floor at the bottom can improve atomization followed by wall-impingement because this kind of wall configuration promotes spray penetration along the wall. It is necessary for RO spray that has stick-like structure to promote spray penetration after wall-impingement because long spray path offers wide spray boundary region to form droplets.

10. Image of high speed swirl with high ambient temperature effect to RO and GO spray for IDI nozzle was successfully taken by high speed video camera direct photography technique. From the result, high speed swirl significantly affected the spray development in which the spray progress in circular path. The image also shows that the fuel along the spray boundary, all throughout the spray jet from the upper section to the lower section dispersed and made the spray to enlarge promoting atomization.

11. Comparison of effect of high speed swirl between IDI nozzle and DI nozzle was made using high speed video camera shadowgraph technique. IDI nozzle has slower atomization rate than DI nozzle for RO spray. This is consistence with the result which shows IDI nozzle produce larger diameter size of droplet. In contrast, GO spray atomization rate for each nozzle seem to be comparable.

Acknowledgement

It is a great feeling to finally make it into this last part of my Doctoral Thesis. It has been a long journey, with ups and downs, a journey of joy while at the same time, a journey of test; which need another book for itself should I try to document it.

My deepest gratitude to my supervisor Professor Dr. Yoshiyuki Kidoguchi. co-supervisor Associate Professor Dr. Yuzuru Nada. Not forgetting Professor Emeritus Dr. Kei Miwa and also Professor Dr. Tomoaki Yatsufusa. Their involvement, supervision, support has guide me to be a better researcher, and given me the instrument to finish this thesis.

It is also a great pleasure to meet and work with the member of Power Engineering Lab, Tokushima University. It has to be said that most of the research results were the success of hard teamwork between spray team group members. Thank you to Dr. Adam Abdullah, Mr. Yasunari Tsuboi, Mr. Nagayasu Sho, Mr. Takashi Yano, Mr. Nakagiri Misato, and Mr. Uwa Naoya. Also, special thank to my lab friend, Dr. Amir Bin Khalid, Dr. Mas Fawzi Bin Mohd Ali and Mr. Aizam Shahroni Bin Mohd. Arshad. And also the best of luck to the newest spray member, Mr. Mohd. Al-Hafiz Bin Mohd. Nawi.

It would also be unfinished and incomplete without thanking my family, for their love and support. Lots of love to my wife, Nor Hazlin Binti Ramli for the companion, care, and patience during all these years. Also my three chubby and irresistible cuddly sons, Amirul Afiq, Adiel Ariq and Afnan Akid for their laughter and smile. I would also like to extend the greatest thank, to my mother Salmah Biti Haji Abdul Kadir, for the lasting love and confidence in her son. Also my brother, Syahmi Bin Sapit and sister, Hanani Binti Sapit, thank you for your support and care.

Lastly, I would like to thank the Ministery of Higher Education Malaysia and University Tun Hussein Onn Malaysia for the providing me the chance and scholarship to pursue my doctoral degree in The University of Tokushima.